MAGNETIC PROPERTIES

Norman M. Edelstein and Gerard H. Lander

20.1   INTRODUCTION

20.1.1   Magnetic measurements

The magnetic properties of actinide ions and compounds arise from the spin and orbital angular momenta of the unpaired electrons. The theoretical basis for understanding these properties was provided by Van Vleck in 1932 in his classic work *The Theory of Electric and Magnetic Susceptibilities* (Van Vleck, 1932). The Van Vleck equation is expressed as follows:

$$\chi_M = \frac{N \sum_i [(E_i^{(1)})^2/kT - 2E_i^{(2)}] \exp(-E_i^0/kT)}{\sum_i \exp(-E_i^0/kT)} \tag{20.1}$$

where χ_M is the molar susceptibility and E_i the energy of the ith energy level, which can be expanded as a power series in the magnetic field H:

$$E_i = E_i^0 + E_i^{(1)}H + E_i^{(2)}H^2 + \cdots \tag{20.2}$$

The material can possess no residual moment in the absence of a magnetic field, so that:

$$\sum_i E_i^{(1)}\exp(-E_i^0/kT)= 0 \tag{20.3}$$

The term in equation (20.1) involving $E^{(1)}$ is the first-order Zeeman interaction and the term involving $E^{(2)}$ is the second-order Zeeman interaction. If the ground crystal field (CF) state is a singlet and the next state is greater than kT away in a particular temperature range, the first-order term will be zero and only the second-order term will contribute to the paramagnetic susceptibility, which will be independent of temperature (temperature-independent paramagnetism, TIP).

If enough information is available about an ion or molecule (i.e. from optical spectroscopy) such that the properties of the energy levels in a magnetic field can be calculated, magnetic susceptibility measurements provide a good test for the eigenfunctions. Conversely, magnetic data can be used to determine information about energy levels and their eigenfunctions. Magnetic measurements usually are performed in the temperature range 2–300 K (energy range $\sim$1.5–200 cm^{-1}). From optical data, the crystal or ligand-field splittings of the ground state of some 5f^1 hexahalo compounds are shown in the second column of Table 20.1 and vary from 1730 cm^{-1} in Pa^{4+} to about 7500 cm^{-1} for Np^{6+}. For 5f^2 U^{4+} compounds, the total crystal-field splitting of the ground ^{3}H$_4$ term is about 2240 cm^{-1} in Cs$_2$UCl$_6$ (Johnston *et al.*, 1966), about 2000 cm^{-1} in Cs$_2$UBr$_6$ (Johnston *et al.*, 1966), about 2400 cm^{-1} in U(C$_5$H$_5$)$_4$ (Amberger, 1976b), and about 1800 cm^{-1} for U(BH$_4$)$_4$ diluted in Zr(BH$_4$)$_4$ (Bernstein and Keiderling, 1973). For the 5f^3 and 5f^4 ions, U^{3+} and Np^{3+} diluted in LaCl$_3$, the total crystal-field splitting of the ground terms are 451 and 465 cm^{-1}, respectively (Carnall, 1992). From the above data, it is clear that temperature-dependent magnetic susceptibility measurements provide information only about the ground crystal field state and possibly a few lower-lying states. Most susceptibility measurements are performed on polycrystalline samples that give only the average susceptibility. Magnetic susceptibility values can also be performed on liquid solutions of pure compounds by use of the Evans nuclear magnetic resonance (NMR) method (Evans, 1959).

Electron paramagnetic resonance (EPR) measurements for actinide ions are usually made at liquid-helium temperatures in order to lengthen the spin–lattice relaxation time (T_1) so that the resonance can be observed (Abragam and Bleaney, 1970; Boatner and Abraham, 1978). Consequently information is obtained only about the ground crystal field state and possibly the first excited state. The spectra are interpreted in terms of an effective spin Hamiltonian:

$$H = \mu_B(g_x H_x S_x + g_y H_y S_y + g_z H_z S_z) \tag{20.4}$$

where μ_B is the Bohr magneton, and g_i, H_i, and S_i ($i = x, y, z$) are the components of the g-tensor, the magnetic field, and the spin operator along the principal axes of the crystal field. For a crystal or molecule with the highest-symmetry rotation axis (the z-axis by definition) of three-fold symmetry or greater, $g_x = g_y = g_\perp$ and $g_z = g_\parallel$. For T$_d$ or O$_h$ symmetry, the g-value is isotropic (except when a Γ_8 state is lowest). For this review, hyperfine and quadrupole effects usually are not considered.

Table 20.1 *Optical transitions, g-values, and the best-fit parameters to the Eisenstein–Pryce theory for some $5f^1$ hexahalo compounds (Eichberger and Lux, 1980).*

Compound	Electronic transitions and ground state g-value					Best-fit parameters				
	$\Gamma_7\text{–}\Gamma_8$ (cm^{-1})	$\Gamma_7\text{–}\Gamma_{7'}$ (cm^{-1})	$\Gamma_7\text{–}\Gamma_{8'}$ (cm^{-1})	$\Gamma_7\text{–}\Gamma_6$ (cm^{-1})	$|g|$	ζ (cm^{-1})	θ (cm^{-1})	φ (cm^{-1})	k	k'
$((C_2H_5)_4N)_2PaCl_6$[a]	1730	5330	7140	8011	1.141	1689	600	3525	0.83	0.46
$CsUF_6$	5363	7400	13800	15900	0.708	2206	3335	8050	0.84	0.61
$RbUCl_6$	3800	6794	10137	11520	1.12	2219	826	5794	0.78	0.45
$CsUBr_6$	3700	6830	9761	10706	1.21	2190	99	5746	0.79	0.32
NpF_6	7543	9348	24000	27000	0.605	2697	4775	16921	0.85	0.60

[a] See Piehler *et al.* (1991) for more accurate optical data on Pa^{4+} diluted in Cs$_2$ZrCl$_6$.

An electron configuration with an odd number of electrons ($f^1, f^3, \ldots.,$ etc.) has a Kramers degeneracy that can be lifted by a magnetic field but not by a crystal field. However, it is possible that the pair of states that lies lowest will not have an EPR signal because the selection rule $\Delta J_z = \pm 1$ will be violated. For example, consider a $J = 5/2$ term in a purely axial crystal field. This term will be split into three doublets: $J_z = \pm 1/2, \pm 3/2$, and $\pm 5/2$. If the crystal field is such that the $J_z = \pm 3/2$ or $J_z = \pm 5/2$ state is lowest, there will be no EPR transitions allowed.

An ion with an electron configuration with an even number of electrons($f^2, f^4, \ldots.,$ etc.) is called a non-Kramers ion. If the highest-symmetry axis is a C_2 axis, the crystal field will split an integer J term into $2J + 1$ singlets, and EPR will not be observed. If the highest-symmetry axis is C_3 or higher, a doubly or triply degenerate crystal field state could be lowest, and EPR might be observed. However, EPR has been reported only for the non-Kramers ions U^{4+} and PuO_2^{2+}, both $5f^2$, in the actinide series. Non-Kramers ions are discussed in detail by Abragam and Bleaney (1970).

For an f^n configuration, where n is the number of equivalent electrons, the electrostatic interaction between two f electrons results in a series of terms that can be classified by the total orbital and spin angular momenta, L and S, defined as:

$$L = \sum_i^n l_i \qquad S = \sum_i^n s_i \qquad (20.5)$$

where l_i and s_i are the orbital and spin angular momenta of the ith electron. The eigenstates are then labeled by the quantum numbers (or symbols) ^{2S+1}L. This classification is called Russell–Saunders coupling. Inclusion of the spin–orbit interaction will cause mixing of the spin and orbital angular momenta and requires the use of J, the total angular momentum, defined as:

$$\boldsymbol{J} = \boldsymbol{L} + \boldsymbol{S} \qquad (20.6)$$

The ^{2S+1}L multiplet is split into levels labeled by their J eigenvalues, $J = L + S, L + S - 1, \ldots., L - S + 1, L - S$, where each J level has a $2J + 1$ degeneracy. It is this J degeneracy which is split by the crystal field (Judd, 1963; Wybourne, 1965). Usually, the lowest J level is relatively isolated, the ligand-field splittings are approximately $100–1000$ cm^{-1}, and only the lowest few crystal field states as indicated above provide the main contribution to the measured magnetic susceptibility. The effects of the various interactions are shown in Fig. 20.1 for the f^2 configuration.

A large number of magnetic susceptibility and EPR measurements have been made on actinide ions in crystal fields of O_h or T_d symmetry. In these symmetries, the ordering of the energy levels of a J-term depends only on the ratio of two crystal field parameters, the fourth-order term and the sixth-order term. From magnetic data, the ground crystal field state may be determined, which in
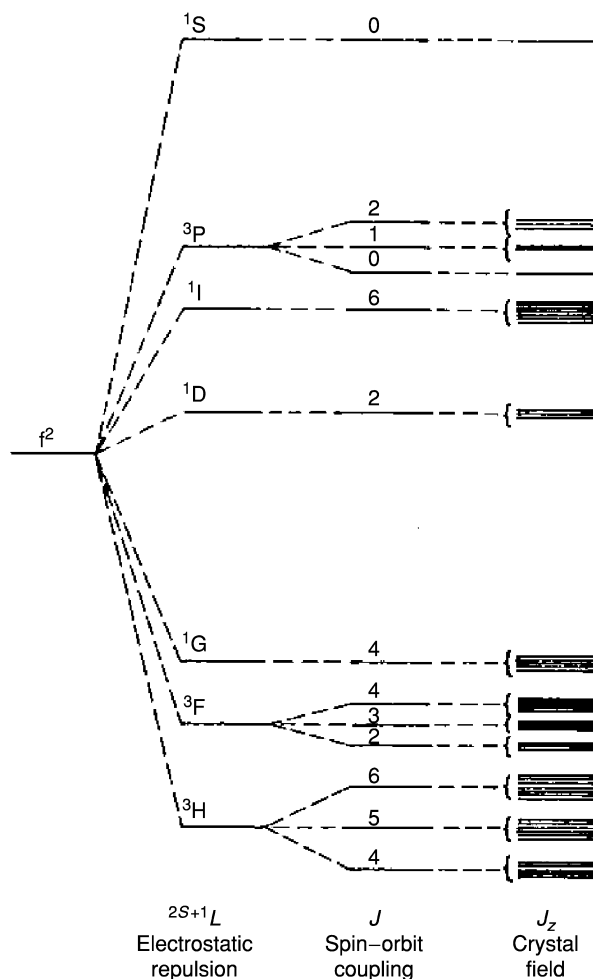
Fig. 20.1 *Schematic of the effects of the electrostatic, spin–orbit, and crystal field inter-actions on the f^2 configuration.*

turn can set a limit on the ratio of the fourth- to the sixth-order term. Lea *et al.* (1962) tabulated the results in reduced coordinates for all J levels of interest and their nomenclature is widely used. An illustration of the application of the Lea, Leask, and Wolf method (plus the effects of mixing other J states by the crystal field) is given in the study of Hendricks *et al.* (1974) on the temperature dependence of the magnetic susceptibility of the isostructural series, Cs_2NaMCl_6, $M = U^{3+}$, Np^{3+}, Pu^{3+}, Am^{3+}, Cm^{3+}, and Bk^{3+}. The data are shown in Table 20.2. From a consideration of these data, limits were placed on the possible values of the fourth- and sixth-order crystal field parameters B_0^4

Table 20.2 *Magnetic data for octahedral actinide(III) chlorides. Taken from Hendricks et al. (1974) unless otherwise noted.*

Compound	T range (K)	μ_{eff} (μ_B)	θ (K)	χ_{TIP} (10^{-6} emu mol^{-1})
Cs_2NaUCl_6	4–20	2.49 (6)	–0.53	
Cs_2NaUCl_6	25–50	2.92 (6)	–9.6	
$Cs_2NaNpCl_6$	3–50	1.92 (5)	–0.47	
$Cs_2NaPuCl_6$	3–21	0.97 (5)	–1.3	
$Cs_2NaPuCl_6$	25–50	1.16 (8)	–12.4	
$Cs_2NaAmCl_6$	15–70			5400 (400)
$Cs_2NaAmCl_6$[a]	40–300			660 (40)
$Cs_2NaCmCl_6$[b]	7.5–25	7.90 (10)	–3.87	
$Cs_2NaCmCl_6$[b]	25–45	7.48 (50)	–1.15	
$Cs_2NaBkCl_6$[b]	10–40			192 000 (30 000)
$Cs_2NaCfCl_6$[c,d]	2.2–14	7.36 (2)	–2.8	
$Cs_2NaCfCl_6$[c,d]	20–100	10.0 (1)	13.5 (4)	

[a] Soderholm *et al.* (1986).
[b] Diluted into $Cs_2NaLuCl_6$.
[c] Karraker and Dunlap (1976).
[d] Diluted into Cs_2NaYCl_6.

and B_0^6 (defined as described by Wybourne (1965)). However, recent optical results on U^{3+} ion diluted into the elpasolite host Cs_2NaYCl_6 yielded much different crystal field parameters than those obtained by Hendricks *et al.* (Karbowiak *et al.*, 1998).

Magnetic susceptibility data are usually represented by a plot of $1/\chi_M$ vs T. This plot is linear over a particular range of temperatures, and the data are fitted to the Curie–Weiss law:

$$\chi_M = C/(T - \theta) \tag{20.7}$$

where χ_M is the molar magnetic susceptibility (expressed in cgs units in cm^3 mol^{-1} or emu mol^{-1}), T and θ (the Weiss constant) are expressed in K (kelvin), and C is the Curie constant. Note that equation (20.7) uses $(T–\theta)$ in the denominator. Some authors use $(T+\theta)$ and this is a point of great confusion. All data quoted in this chapter using the Curie–Weiss law will use the form in equation (20.7).

Sometimes, in order to analyze magnetic susceptibility data that shows temperature-dependent behavior, a modified Curie law of the form

$$\chi = \chi_0 + C/T \tag{20.8}$$

has been utilized where χ_0 is the temperature-independent susceptibility and μ_{eff} may be obtained from the value of C, the Curie constant.

Another common way of representing data is to use the effective moment, μ_{eff} (in units of the Bohr magneton μ_B):

$$\mu_{\text{eff}} = 2.828 \ C^{1/2} = 2.828 \left[\chi_{\text{M}}(T - \theta)\right]^{1/2} \tag{20.9}$$

or

$$\mu_{\text{eff}}^2 = 8.0 \, \chi_{\text{M}}(T - \theta) \tag{20.10}$$

If the data do not follow the Curie–Weiss law, μ_{eff} is commonly defined as:

$$\mu_{\text{eff}} = 2.828 \left(\chi_{\text{M}} T\right)^{1/2} \tag{20.11}$$

Considering the temperature range where only the ground crystal field state is populated and there is no second-order Zeeman effect, the molar susceptibility in the z-direction may be written as:

$$\chi_z = N\mu_{\text{B}}^2 g_z^2 / 4kT \tag{20.12}$$

with similar equations for the x- and y-directions. In eq. 20.12 N is Avogadro's number and k is the Boltzmann factor. Because $\chi_{\text{ave}} = 1/3(\chi_x + \chi_y + \chi_z)$, therefore:

$$\chi_{\text{ave}} = \frac{N\mu_{\text{B}}^2 (g_x^2 + g_y^2 + g_z^2)}{12kT} \tag{20.13}$$

The g_x, g_y, and g_z in equation (20.13) are the same g-values obtained from EPR measurements on the ground crystal field state. Magnetic susceptibility measurements and units are discussed in detail by Myers (1973) and Boudreaux and Mulay (1976). All data quoted in this chapter will be in cgs units (see equation (20.7)).

For the lanthanide series, it is common to assume the ground term crystal-field splitting is much less than kT where k is the Boltzmann constant and T $\sim$300 K (at 300 K, $kT = 208.34$ cm$^{-1} = 25.85$ meV). In this case

$$\mu_{\text{eff}} = g_J[J(J + 1)]^{1/2} \tag{20.14}$$

where g_J is the free-ion g-value of the particular ground J multiplet. This equation is usually *not* valid for actinide compounds at room temperature as in most cases (see above) the crystal-field splittings of the ground term are larger than kT. Exceptions are found in the case of the 5f^7 ions, Am^{2+}, Cm^{3+}, and Bk^{4+}. For the Am^{2+} and Cm^{3+} ions, the total crystal-field splitting of the ground terms are much less than 100 cm^{-1}. Thus for Cm^{3+} compounds, $\mu_{\text{eff}} = 7.62\mu_{\text{B}}$ with $g_J = 1.925$ (Edelstein and Easley, 1968).

20.1.2 Introduction to neutron and synchrotron X-ray scattering

The techniques discussed so far, magnetic susceptibility and EPR, are useful in the sense that they can determine many details about the magnetic state of an actinide ion. On the other hand, what they cannot determine is the interaction *between* actinide ions. For example, at low temperature the actinide ions,

especially those with a Kramers ground state, frequently order magnetically. The *exchange interaction* between the actinide ions energetically prefers a certain configuration of neighboring dipoles. Naturally, it is important to know the exact form of this magnetic structure. In certain cases EPR and Mössbauer spectroscopies (which are both single-site sensitive) are able to determine the magnetic structure. For example, if all the moments are aligned along the unique axis in a uniaxial crystal structure, then this symmetry will be reflected in the spectra. In general, however, one needs a technique that is sensitive to the long-range ordering of the moments and one naturally turns to methods involving the scattering of radiation.

The technique of choice for studies of this type is the scattering of thermal neutrons. Pioneered for magnetic structures in the period 1949–60 at Oak Ridge National Laboratory by Shull and his collaborators, this technique is in very wide use and there are a number of good books introducing the technique (Bacon, 1962; Squires, 1978; Kostorz, 1979; Skold and Price, 1987). In very early work (Shull and Wilkinson, 1955; Wilkinson *et al.*, 1955) the famous ferromagnet UH_3 was examined (although to reduce the incoherent scattering from H they made a sample of isostructural UD_3). The key to magnetic structure determination is that for most antiferromagnetic (AF) structures, the repeat distances of the magnetic structure is more complex than the chemical structure. The result is new neutron diffraction peaks when the magnetic moments order. From the position and intensity of these diffraction peaks, the periodicity and the arrangements of the ordered moments, as well as their magnitude, may be deduced. Neutrons can, of course, be used also for chemical structure determinations, and the fact that the scattering from an actinide atom and an oxygen atom are roughly comparable means that the contrast is completely different from that of studies using X-rays. Much work in this respect is done on oxides and nitrides, and a summary of some of this work has been given (Lander, 1993) with particular reference to actinides. A good example of a study of this sort will be described later in connection with UO_2 at low temperature.

The *magnetic* scattering of neutrons is by the magnetic dipole moments in the material. For the actinides this arises from the 5f electrons around the nucleus. If the magnetic structure is well known, then the intensities may be measured as a function of momentum transfer Q ($= 4\pi \sin \theta/\lambda$, where θ is the Bragg angle and λ is the wavelength of the incident radiation) to give a so-called magnetic form factor $f(Q)$. By analogy with the scattering factor in X-ray studies, $f(Q)$ is proportional to the Fourier transform of the distribution of the outer 5f electrons. Again this is discussed (Lander, 1993), and there have been many studies of this type in actinides, including some Pu compounds.

Finally, thermal neutrons at 300 K have an energy corresponding to kT ($= 25.85$ meV, $= 208.34$ cm^{-1}) so that it is possible for them to lose energy to (or gain from) the sample and this energy change may be measured by inelastic neutron scattering. As with EPR and optical spectroscopies, the crystal field levels may be determined. Most importantly, and unlike spectroscopic methods

based on photons, the neutrons (which are electrically neutral) can penetrate deep into the solid so this technique is good also for opaque materials. This means that complex experimental environments can readily be used, for example, at low temperatures down to 100 mK, high temperatures up to 2500°C, and high magnetic fields. Furthermore, if single crystals are available, then the neutrons can map out the dispersion curves of both the phonons and the magnons. UO_2 is a famous example of this, where both types of excitations were published more than 30 years ago (Cowley and Dolling, 1968).

Unfortunately, there are two major disadvantages for neutron studies. The first one is caused by the presence of resonant terms in the neutron-nuclear cross sections for actinides (Lander, 1993). This interaction is a complex one, not easy to calculate from first principles. However, generally speaking, the heavier nuclides are less stable than the lighter ones, and part of this trend toward instability results in resonant terms in the cross section. Thus, when a neutron impinges upon the nucleus there are probabilities for scattering and absorption. The latter results in the formation of a compound nucleus, which usually rapidly decays and gives rise to other types of radiation. If a neutron is captured then it is no longer available for scattering; the beam penetration is restricted. Materials like Cd and Gd have enormous absorption cross sections for thermal neutrons, and are frequently used to stop neutron beams. In the actinides there is an appreciable absorption cross section for ^{237}Np, but, of course, the most famous absorption cross sections are those due to the fission process in both ^{235}U and ^{239}Pu. In the case of ^{235}U, the fission cross section is actually for low-energy neutrons, which can penetrate the nuclear barrier, forming an unstable compound nucleus that then breaks up with the emission of fast neutrons and γ-rays. This, of course, was the famous discovery of Hahn and Strassman in 1938. Fortunately, ^{235}U is only a small fraction of normal uranium. However, the most common isotope of Pu is ^{239}Pu with a very large cross section, so for most neutron experiments using Pu, the heavier isotope ^{242}Pu should be used.

The second disadvantage for neutrons is the available intensities. Neutron sources are weak, much weaker (in terms of flux per $cm^2 s^{-1}$) than synchrotron or laser sources, mainly because they are impossible to focus. Large samples are therefore needed. For neutron powder diffraction, samples of up to several grams are frequently used, although studies of much smaller samples are possible. Examples are the work on CmO_2 (Morss *et al.*, 1989) and Cm_2CuO_4 (Soderholm *et al.*, 1999), discussed below, in which amounts of ~50 mg were studied. For single-crystal studies, the samples can be at the few milligram level, but this still contrasts with samples of ~50 μg that can be examined by conventional laboratory X-ray sources. For inelastic neutron scattering and the study of phonons, samples sizes of grams are again required. This is a serious handicap for neutron diffraction on *any* element in the periodic table. For many studies, this is not a problem, but the acquisition of large single crystals for phonon or magnon measurements can be a serious limitation. For example,

despite the huge effort on high T_c superconducting materials after their discovery in 1986, it took approximately 5 years until the first details of the phonon and magnetic excitation spectra were published. This did not represent a lack of interest on the part of neutron specialists, but rather an absence of suitable crystals. Moreover, this technique can, of course, only be done at a central user facility, either a spallation source or reactor. The difficulty for actinides as compared to most other elements is that their quantity in user facilities is frequently restricted. The large quantities required in neutron scattering studies are not a problem with uranium, but have severely limited the possible range of experiments on transuranium materials. The restrictions continue to become more severe in 'open' facilities, and experiments that were readily performed (for example at Argonne in the 1970s) are no longer possible at most facilities.

Synchrotron radiation (another activity performed at large user facilities) is making a sizeable impact in actinide science, especially in the field of environmental studies using methods based on absorption spectroscopy. Can such beams be of any use in magnetic studies, the subject of this chapter? Initially, when the synchrotrons were built, their impact on magnetism was predicted to be small. It was known, for example, that photons do indeed have a 'magnetic' cross section, but it was very small. For example, for iron the magnetic photon cross section is some six orders of magnitude smaller than the Thompson (charge) cross section (Blume, 1985; Blume and Gibbs, 1988; Lovesey and Collins, 1996). Indeed, this cross section has been of only limited use, although as the synchrotron fluxes continually increase in intensity, this may change. One example is the work on UAs (Langridge *et al.*, 1997) in which the spin and orbital contributions to the magnetism were separated. The weak intensities resulted in large uncertainties, but this technique may well become more popular as synchrotron fluxes increase.

Synchrotron radiation is, of course, tunable in the sense that any wavelength (energy) may be chosen, unlike laboratory-based sources. This naturally led to the idea that the energy should be tuned to a resonant absorption edge – something incidentally also useful in protein crystallography as the cross section for charge scattering also changes appreciably near an absorption edge (James, 1962). The result in magnetic studies was the discovery of large *enhancements* in the (weak) non-resonant magnetic scattering. Although there had been some attempts to see these previously, the first really large effects were observed in holmium metal by Gibbs and his collaborators (Gibbs *et al.*, 1988) and were immediately interpreted in terms of atomic resonance theory (Hannon *et al.*, 1988). This general technique is called resonant X-ray scattering (RXS).

Turning to the actinides, enhancements at the M_4 and M_5 edges are shown in Fig. 20.2 taken from McWhan *et al.* (1990) on the antiferromagnetic material UAs. M-edges correspond to the initial states having a principal quantum number n of 3. The M_4 and M_5 edges have the azimuthal quantum number $l = 2$ and correspond to transitions from $3d_{3/2}$ and $3d_{5/2}$ core states, respectively.
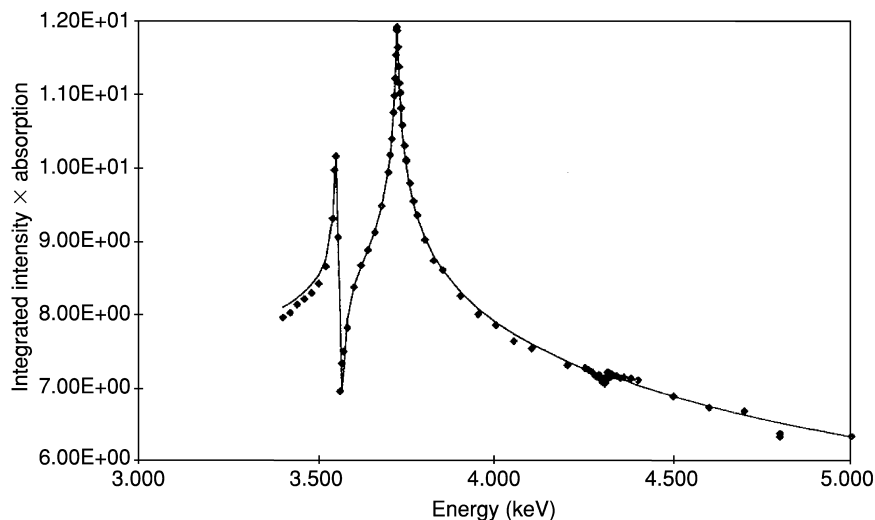
Fig. 20.2 *Intensity of the (003/2) reflection from a single crystal of UAs at T = 10 K as a function of photon energy. UAs (simple fcc NaCl crystal structure) has a magnetic structure that repeats in two unit cells. This results in magnetic reflections occurring at half integer Miller indexes. Notice that the intensity is plotted on a log scale so that the enhancement approaches 10^6 as compared to the intensity off resonance. The positions of the M resonances are M_5 = 3.550, M_4 = 3.726, and M_3 = 4.304 keV. The solid line is the result of a calculation involving three dipole oscillators, and fits the data very well. Reprinted from McWhan (1998), Copyright 1998 with permission from Elsevier.*

Electric dipole (E1) transitions change the azimuthal quantum number by ±1 so that the final states involve the $5f_{5/2}$ and $5f_{7/2}$ states, the valence band states. However, in the actinides, there may be already electrons in the 5f states. In UAs, for example, one would expect most of the three 5f electrons to be in the lower energy $5f_{5/2}$ orbitals. At low temperature, these states become polarized, leading to a magnetic moment on the atom. The promotion of an electron into the valence band 5f states causes a resonance between the states already there, resulting in a reemission of radiation when the excited state decays to annihilate the core hole. In the case of the valence states being polarized, as when UAs becomes antiferromagnetically ordered below T_N, the emitted radiation is also polarized, and it is this that leads to the large enhancement of magnetic scattering at the resonant energy. One can see immediately from this that for the light actinides the signal at the M_4 edge should be greater than that at the M_5, because the 5f polarized states are mostly in $5f_{5/2}$ levels corresponding to the M_4 transition. (Transitions at the M_5 edge involve mainly $5f_{7/2}$ states but also $5f_{5/2}$ with smaller matrix elements, hence the intensities are smaller. For a half-filled shell the intensities at the two edges should be similar.)

The process involving resonance effects also occurs in absorption spectroscopy. The development of the two techniques, so-called X-ray magnetic circular dichroism (XMCD) has been remarkably parallel (Thole *et al.*, 1985; Schütz *et al.*, 1987). The amplitude of the effects in either technique depends on a number of factors, in particular the overlap of the wavefunctions of the core and valence states and matrix elements summed over all possible excited states. The advantage of XMCD is that (provided a model of the magnetism is available) the signal may be related directly to the orbital moment of the valence states, and it is also possible with reasonable assumptions to deduce the spin moment. These so-called 'sum rules' (Carra and Altarelli, 1990) can be derived primarily because absorption involves only the imaginary part of the cross section. In the case of scattering one must deduce *both* the real and imaginary parts, and that has proved intractable so far for resonance scattering experiments. XMCD also has the advantage (see below) that any edge can be accessed without the necessity to fulfill Bragg's law as is necessary for scattering. However, XMCD has the major *disadvantage* that it cannot give any information about the spatial extent of the scattering centers as it is restricted to $Q = 0$, where Q is the momentum transfer. Moreover, it cannot examine antiferromagnets since (by definition) they have no net magnetization so no magnetic signal at $Q = 0$. (X-ray linear dichroism is a possible technique to overcome this, but the matrix elements are very small.) From this discussion, it is clear that RMS and XMCD are indeed complementary. There have been a number of experiments reported on U compounds (none yet on transuranium compounds), especially on UFe_2 (Finazzi *et al.*, 1997) and on the heavy-fermion intermetallic materials (Dalmas de Rotier *et al.*, 1999; Bombardi *et al.*, 2001).

Scattering experiments have played an important role in studies of one of the oxides, NpO_2. Before discussing particular experiments, a general overview (Fig. 20.3) of the energies of the resonances will be given. The boxes in Fig. 20.3 give the ranges of the electron binding energies across a series that are of interest for magnetism. For example in the 3d series the K-edges correspond to transitions from the 1s to the 4p states. Since the 4p states are not expected to be polarized strongly, the matrix elements are small. On the other hand, transitions at $L_{2,3}$ edges are to the strongly polarized 3d states, so it is these edges that need to be used to observe an appreciable signal. Similarly (as explained above) it is the $M_{4,5}$ edges that will be useful for f magnetism as found in the rare earths and actinides. No modification of these electron-binding energies is possible except perhaps at enormous pressures. For scattering processes Bragg's law, $2d \sin \theta / \lambda$, is utilized where d is the interplanar spacing, θ is Bragg's angle, and λ is the wavelength of the radiation. Using the relationship for photons that $E = 12.4/\lambda$, where E is in keV, and λ in Å, Bragg's law demands d spacings *larger* than 3.1 Å for radiation less than 2 keV in energy. Now 3.1 Å has been chosen as it represents a large d-spacing from a simple solid. Larger d-spacings require either more complex solids or the examinations of d-spacings in multilayers or domains. The latter can reach up to $\sim$1000 Å and represent science on the
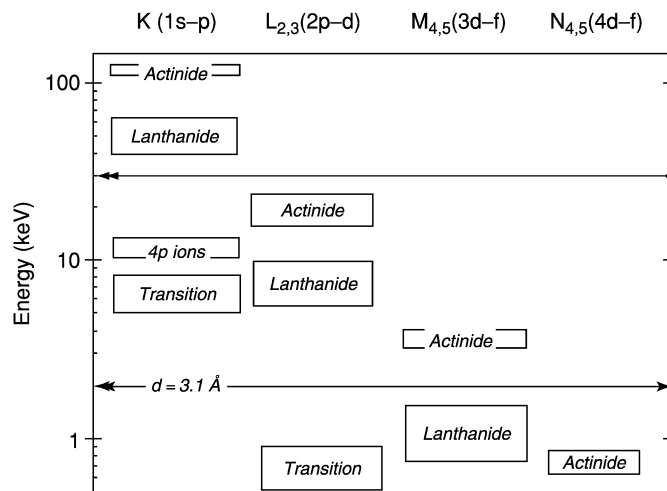
Fig. 20.3 *Each box shows the energy spread of the electron binding energies across the series for the transitions marked at the top of the figure. The upper horizontal line gives the approximate maximum energy (~30 keV) of most magnetic scattering beamlines. The lower horizontal line gives the d-space corresponding to the maximum that will fulfill Bragg's law for an incident photon energy of 2 keV. For lower energies, such as the transition metal $L_{2,3}$ edges, greater d-spaces are required. For a normal crystal structure with a small unit cell this implies these edges are beyond the Bragg cut-off and no scattering can be observed. For dichroism there are no such restrictions, and, in principle, all edges are accessible. Reprinted from Lander (2002). Copyright 2002 with permission from Elsevier.*

nanoscale. Now it can be understand why this technique has not been enormously useful for Å-level magnetism in the transition-element series, the important edge is simply too low in energy (Lander, 2002). Similarly, even in the rare earths most of the work is done at the L-edges, which represent transitions to the (sparsely polarized) 5d states. It is only recently with the building of dedicated magnetic scattering beamlines in vacuum that work on the rare-earth M-edges is being reported (Schüssler-Langeheine *et al.*, 2001). The M-edges of the actinides are then unique, magnetism on the atomic scale with the largest resonance effects can be examined. Accordingly a large amount of work, starting with the first study of UAs as shown in Fig. 20.2, has been done with U, Np, and even Pu compounds (Langridge *et al.*, 1994a,b; Lander, 2002; Normile *et al.*, 2002).

Compared to neutrons RXS can use minute amounts of material. Samples of about 1 mg are regularly used, and intensity corresponding to a doping of ~40 μg of Np was seen in one crystal. On the other hand, no method (yet) is available to relate the observed signal to the magnetic moment. In addition, it has not proved possible to observe signals from polycrystalline samples (except with

very poor q-space resolution (Collins *et al.*, 1995)). In principle, this could be remedied by building a special apparatus to collect more of the solid angle from the Debye–Scherrer cone, but the strong absorption means that the beam only would penetrate a few micrometers at most (and only $\sim$0.2 μm at the U M-edges) so the sampling through the powder would always be poor. Since neutrons are so good at sampling a large volume of material, very little effort has been made at synchrotron sources with RXS, but it might be justified for actinides because of the small sample quantities that could be used.

As is so often the case, the techniques are really complementary and scientists in this field should choose the technique for the problem, and not vice versa!

20.1.3 Scope, other reviews, and units

Although in this chapter the coverage has been primarily restricted to *ionic* actinide compounds, in actinide condensed matter physics a major interest is actually in studies of intermetallic and semiconductor compounds. Chapter 21 reviews the physical properties of actinide metals and alloys, including their magnetic properties. The two volumes edited by Freeman and Darby (1974) contain information about the magnetic properties of many actinide materials, including a review by Lam and coworkers (Lam and Chan, 1974; Lam and Aldred, 1974) on actinide salts, carbides, chalcogenides, pnictides (group V), and various intermetallic compounds, plus another review by Nellis and Brodsky (1974) on the pure metals and alloys. A later review article by Brodsky (1978) covered the magnetic properties of the actinide elements and their magnetic compounds. An earlier review covers the $5f^0$, $5f^1$, and some selected data for $5f^2$ and higher configurations (Sidall, 1976). Some magnetic data are given in the review by Keller (1972) on lanthanide and actinide mixed oxides and by Dell and Bridger (1972) in their review of actinide chalcogenides and pnictides. The review article by Boatner and Abraham (1978) summarizes all the EPR data on actinide ions published through 1976. Kanellakopulos (1979) reviewed the magnetic properties of cyclopentadienyl compounds of the trivalent and tetravalent actinides. Fournier (1985) reviewed the magnetic properties of actinide solid compounds and Huray and Nave (1987) have surveyed magnetic measurements on transplutonium actinides. A comprehensive survey of actinide metals and their compounds is given in Landolt-Börnstein (Troc *et al.*, 1991; Troc and Suski, 1993). Santini *et al.* (1999) reviewed the magnetism of actinide compounds that can be categorized as actinide intermetallics and strongly correlated systems.

The discovery of heavy-fermion materials in the early 1980s and the accompanying interplay between magnetism and superconductivity has been of great interest both in the neutron and synchrotron communities, as well as in the larger solid state physics community. Much of the corresponding neutron work has been reviewed (Lander and Aeppli, 1991; Lander, 1993; Holland-Moritz

and Lander, 1994). The general neutron trends were illustrated in the following papers (Bernhoeft *et al.*, 1998; Metoki *et al.*, 1998). For the high-intensity X-ray case, a good background and useful references are given in the reviews by McWhan (1998) and Lander (2002). Further excitement in the condensed matter physics community has been caused by the discovery of the *ferromagnetic* superconductor UGe_2 with $T_c \sim 0.5$ K (Saxena *et al.*, 2000), and the recent discovery of a Pu-based compound ($PuCoGa_5$) that becomes a superconductor at the astonishingly high temperature of 18 K (Sarrao *et al.*, 2002).

The remainder of this chapter is divided into two major sections. In the first section, the actinide ions are classified according to their electron configuration, and magnetic measurements are reviewed for each electron configuration. The actinide dioxides (AnO_2) are not included in this section but are reviewed separately in the second major section. The actinide dioxides are isostructural with a face-centered cubic (fcc) fluorite structure. Thus the crystal field parameters (which determine the ground state electronic and magnetic properties) for each of the dioxides should be correlated. Therefore, in principle, the results of the analyses for one of the dioxides should be relevant to the series. In fact the actinide dioxide story is complicated and considerable efforts, both experimental and theoretical, have been expended to try to understand their properties. For these reasons this subject is best treated separately.

Two different energy units are used in this review depending on the discussion. The units are meV and cm^{-1}. The conversions between these units are as follows: (1 eV $= 8065.479\ cm^{-1}$); (1 meV $= 0.001$ eV $= 8.065\ cm^{-1}$); (1 $cm^{-1} = 1.2399 \times 10^{-4}$ eV or 0.12399 meV). It is useful to note that kT (where k is the Boltzmann constant) at 300 K $= 25.85$ meV $= 208.34\ cm^{-1}$.

20.2 $5f^0\ {}^1S_0;\ Th^{4+},\ Pa^{5+},\ U^{6+},\ UO_2^{2+}$

For a closed-shell configuration, compounds formed with these ions should be diamagnetic. This is found to be true for Th^{4+} and Pa^{5+}, but uranyl compounds and UF_6 exhibit TIP. The weak paramagnetism for UF_6 was attributed by Eisenstein and Pryce (1960) to the coupling of higher-energy states into the ground configuration by the magnetic field. From an analysis of the observed susceptibility they concluded that the bonding in the actinide hexafluorides is at least partially covalent. A similar model was proposed earlier by Eisenstein and Pryce (1955) and later by McGlynn and Smith (1962) to explain the weak paramagnetism of uranyl salts. Studies by Denning and coworkers (Denning, 1992) on the high-resolution spectral characteristics, including Zeeman effect measurements of the uranyl ion in tetragonal and trigonal equatorial fields (perpendicular to O–U–O bond axis), has resulted in the determination of paramagnetic magnetic moments for some excited states and a consistent description of the bonding within the uranyl group. The magnetism of a number of ternary U(VI) oxides have been measured and their TIP were

Table 20.3 *Magnetic susceptibilities for some $5f^0$ uranates and neptu-nates. These data are from Bickel and Kanellakopulos (1993). The original references are given in this paper.*

Compound	χ_{TIP} (10^{-6} emu mol^{-1})
α-Na_2UO_4	152
β-Na_2UO_4	114
Li_2UO_4	240[a]
β-Na_4UO_5	142
$Li_2U_2O_7$	135
$Na_2U_2O_7$	133
Sr_3UO_6	158
Ca_3UO_6	156
$BaUO_4$	134
$SrUO_4$	143
Na_4UO_5	162
Li_5NpO_6	225
Li_5NpO_6	217[b]

[a] High value attributed to a ferromagnetic impurity.
[b] Second reported measurement.

attributed to a nonnegligible degree of covalency in the An–O bonds (Bickel and Kanellakopulos, 1993). These data are listed in Table 20.3.

20.3 $5f^1$ $^2F_{5/2}$; Th^{3+} ($6d^1$), Pa^{4+}, U^{5+}, Np^{6+}, NpO_2^{2+}, Pu^{7+}
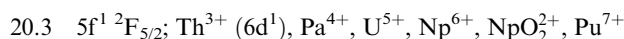
The $5f^1$ ions are good examples for the interpretation of magnetic data because electron repulsion is absent and at most six transitions are allowed in the optical spectrum.

An interesting change in the ground configuration occurs for the known Th^{3+} compounds. Initially a purple trivalent thorium complex, formulated as $Th(C_5H_5)_3$, was reported by Kanellakopulos *et al.* (1974), with a room-temperature magnetic moment of $0.331\mu_B$. A second compound, also formulated as $Th(C_5H_5)_3$ but green in color, was prepared by Kalina *et al.* (1977), who reported a magnetic moment of $0.404\mu_B$. Trisindenylthorium(III) has been prepared by Goffart and also has a very low magnetic moment (Kanellakopulos, 1979). Blake *et al.* (1986) prepared the first crystallographically characterized Th^{3+} compound, $[Th\{\eta^5\text{-}C_5H_3(SiMe_3)_2\}_3]$. Kot *et al.* (1988) showed that this compound has a room-temperature EPR spectrum that is consistent only with a $6d^1$ ground state. Subsequently two other Th^{3+} compounds (Parry *et al.*, 1999; Blake *et al.*, 2001) have been synthesized and shown to have EPR spectra consistent with the $6d^1$ ground configuration rather than a $5f^1$ configuration. Because the relative energies of these two configurations are so close in energy (for the Th^{3+} free ion, the ground configuration is $5f^1$ with the start of the $6d^1$

configuration at 9192.84 cm^{-1}, see Chapter 16, Table 16.1) it is possible that other new Th^{3+} compounds may indeed have a 5f^1 ground configuration.

The magnetic susceptibility of protactinium tetrachloride was measured between 3.2 and 296 K (Hendricks *et al.*, 1971), follows the Curie–Weiss law from 182 to 210 K with $\mu_{\mathrm{eff}} = 1.04(6)\mu_B$ and $\theta = +158$ K, and exhibits a ferromagnetic transition at 182 ± 2 K. A high degree of covalency has been suggested to explain this relatively high transition temperature. The magnetic susceptibility of protactinium tetraformate (Schenk *et al.*, 1975) was measured from 80 to 300 K and follows the Curie–Weiss law with $\mu_{\mathrm{eff}} = 1.23\mu_B$ and $\theta = -3$ K. The crystal structure of this compound and its Np analog were reported to have the M^{4+} ion at the center of a nearly undistorted cube of eight oxygen atoms. However, the U analog was stated to have lower symmetry, which appears inconsistent (Hauck, 1976). By assuming that the $J = 5/2$, Γ_7 state was lowest and is the only one that contributes to the measured susceptibility, a value of $\mu_{\mathrm{eff}} = 1.24\mu_B$ (with $g_J = 6/7$) was calculated from the wave functions given by Lea *et al.* (1962), in good agreement with the experimental value.

The susceptibility of tetrakis(cyclopentadienyl)protactinium was measured between 4.2 and 300 K (Kanellakopulos, 1979). Above 90 K, the magnetic susceptibility followed the Curie–Weiss law with $\theta = -8.6$ K, and the magnetic moment at room temperature is $0.725\mu_B$. A $J = 5/2$ state will split into at most three Kramers doublet levels, and in this compound it is reported that the first two levels are separated by approximately 15–30 cm^{-1} and that the third level is at about 600 cm^{-1}. J mixing cannot explain the low magnitude of the magnetic moment.

A large number of magnetic measurements have been reported for 5f^1 ions in compounds with octahedral or pseudo-octahedral nearest neighbor coordination. These studies include EPR measurements of the 5f^1 ion (Pa^{4+}, U^{5+}, Np^{6+}, and in one case Pu^{7+}) diluted in nonmagnetic hosts or magnetic susceptibility measurements of the 5f^1 compounds, either pure or again diluted in a host matrix. For a 5f^1 ion only the crystal (or ligand) field and the spin–orbit coupling are the important interactions. The necessary theory to interpret the magnetic and optical measurements may be easily formulated starting from the one-electron f-orbitals in a crystal field as the basis set (S, S_z representation) or from the spin–orbit coupled (J, J_z representation) basis set (Axe, 1960; Eisenstein and Pryce, 1960; Hutchison and Weinstock, 1960; Axe *et al.*, 1961; Judd, 1963; Reisfeld and Crosby, 1965; Hecht *et al.*, 1971). For O$_h$ symmetry, the energy levels and magnetic properties are dependent upon two crystal field parameters and the spin–orbit parameter as shown schematically in Fig. 20.4.

For one 5f^1 electron in a free ion (no crystal field), the ^{2}F Russell–Saunders state splits into two J states, $J = 5/2$ and $J = 7/2$, when the effect of spin–orbit interaction ζ is included with an energy splitting between the two states of $7\zeta/2$ (far right side of Fig. 20.4). Now assuming an octahedral array of ligands about the metal ion, the $J = 5/2$ state breaks up into a doubly degenerate
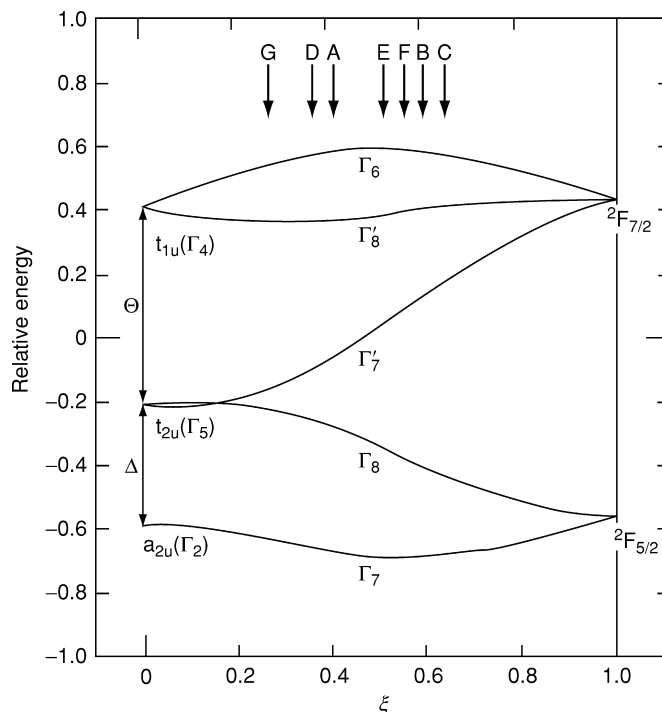
Fig. 20.4 *Relative energy splittings of an f^1 ion (O_h symmetry) as a function of the relative magnitudes of the crystal field and spin–orbit coupling interactions. The ordinate is defined as relative energy = $E/[(\Delta + \Theta)^2 + (7\zeta/2)^2]^{1/2}$ and the abscissa ξ can be determined from the equation $\xi = [(7\zeta/2)/(\Delta + \Theta)]/[1+(7\zeta/2)/(\Delta + \Theta)]$. The figure is drawn for the ratio $\Theta/\Delta = 13/8$. The arrows at the top represent the approximate parameter values for A, $(NEt_4)_2PaF_6$; B, $(NEt_4)_2PaCl_6$; C, $(NEt_4)_2PaBr_6$; D, $(NEt_4)UF_6$; E, $(NEt_4)UCl_6$; F, $(NEt_4)UBr_6$; G, NpF_6. The data are from Brown* et al. (1976).*

Γ_7 state and a four-fold degenerate Γ_8 state. The higher-lying $J = 7/2$ state breaks up into two doubly degenerate states, Γ_6 and Γ_7', and one four-fold degenerate Γ_8' state. The ground state in this symmetry is the $J = 5/2$, Γ_7 state. The parameters Θ and Δ represent the splittings of the f-orbitals for O_h symmetry when the spin–orbit interaction is zero. This is represented at the far left side of Fig. 20.4. As the relative strengths of the crystal field and spin–orbit interactions become comparable, the relative energy splittings change as shown in the center of Fig. 20.4. The ground Γ_7 state g-value depends only on the spin–orbit coupling constant and the difference in energy between the two lowest f-orbitals (Δ) in the limit of zero spin–orbit coupling.

If the ground Γ_7 state were a pure $J = 5/2$ state, the measured g-value could easily be calculated. However, the crystal field interaction is not small as compared to the spin–orbit coupling interaction so the excited $J = 7/2$,

Γ_7' state is mixed into the ground $J = 5/2$, Γ_7 state via this interaction. The resulting expression for the ground state g-value in $5f^1$ octahedrally coordinated complexes is given by Axe (1960):

$$g = -2\left(\frac{5}{7}\cos^2\phi - \frac{4\sqrt{3}}{21}\sin 2\phi - \frac{12}{7}\sin^2\phi\right)$$

where

$$\Gamma_7^{(1)} = |^2F_{5/2}\Gamma_7 > \cos\phi - |^2F_{7/2}\Gamma_7' > \sin\phi$$

and ϕ is determined by the relative magnitudes of the crystal field parameters. There are four electronic transitions (O_h symmetry) that should be observed in these systems. Three optical and/or near-infrared transitions between the $J = 5/2$ and $J = 7/2$ states have been reported for most of these octahedral complexes. In some cases the $\Gamma_7 \rightarrow \Gamma_8$ transition of the $J = 5/2$ state that occurs in the infrared or near-infrared region has also been observed. These electronic absorption data plus the EPR data on the ground state allow the parameters (including orbital reduction factors) of the Eisenstein–Pryce model (Eisenstein and Pryce, 1960; Hecht *et al.*, 1971; Edelstein, 1977; Eichberger and Lux, 1980) for an octahedral f^1 system to be evaluated as shown in Table 20.1. Note the much different ground state g-values for various compounds.

A careful study of the magnetic susceptibility of NpF_6 and NpF_6 diluted in UF_6 (very slightly distorted O_h symmetry) in the temperature range 4.2–336.9 K has been reported by Hutchison *et al.* (1962). The g-value extrapolated to infinite dilution was found to be 0.605 ± 0.004. The g-value was found to vary as a function of the mole fraction of NpF_6 (six different samples of varying mole fractions were measured), with a maximum value of 0.694 ± 0.011 at a mole fraction of 0.34. No explanation has been given for these observations. The magnetic measurements agree with EPR measurements of NpF_6 diluted in UF_6 (Hutchison and Weinstock, 1960) and with the calculations of Eisenstein and Pryce (1960). Analysis of the fluorine superhyperfine structure measured by electron-nuclear double resonance (ENDOR) in single crystals of NpF_6 diluted in UF_6 (Butler and Hutchison, 1981) indicates that 5f orbital covalency effects are approximately an order of magnitude larger in NpF_6 than in 4f complexes. This is consistent with the larger radial extension of 5f orbitals as compared to 4f orbitals. Similarly, a series of papers on the EPR of U^{5+} in complexes of the type MUF_6 (M = Li, Na, Cs, NO) measured at 77 K have been reported (Rigny and Plurien, 1967; Drifford *et al.*, 1968; Rigny *et al.*, 1971a). These octahedral complexes showed a small g-value anisotropy due to axial distortions. The data have been analyzed on this basis. Other, similar complexes with M = K, NH_4, Rb, Ag, and Tl showed no EPR spectra at 77 K, which has been attributed to larger distortions of the UF_6^- octahedra. Selbin and coworkers (Selbin *et al.*, 1972; Selbin and Sherrill, 1974) have measured and analyzed the room-temperature EPR spectra of a number of polycrystalline salts of the type

UX_6^- and UOX_5^{2-} (X = F^-, Cl^-, Br^-, no signal observed for UF_6^-). Their analysis was based on an extension of the standard octahedral theory to include a tetragonal distortion. Although observations of the room temperature signals for the UOX_5^{2-} species have been questioned (Lewis *et al.*, 1973), the magnitude of the *g*-value obtained is consistent with that of other $5f^1$ hexahalide or distorted hexahalide complexes. Some EPR and optical measurements have been reported or reanalyzed for NpF_6, UX_6^- (X = F, Cl, Br) (Eichberger and Lux, 1980), and PaX_6^{2-} (X = F, Cl, Br, I) (Brown *et al.*, 1976) (see Table 20.1).

Early studies on the optical and magnetic properties have been reported for $5f^1$ ions in uranates, neptunates, and one plutonate (Keller, 1972; Miyake *et al.*, 1977a, 1979, 1982, 1984; Kanellakopulos *et al.*, 1980a). For these compounds, the magnetic ions (U^{5+}, Np^{6+}, Pu^{7+}) are surrounded by an octahedral or distorted octahedral array of oxygen atoms. Hinatsu, in a series of recent papers, has reanalyzed earlier data and provided new measurements on some compounds plus other distorted actinide perovskites. He has given a consistent analysis of this body of data (Hinatsu and Edelstein, 1991; Hinatsu *et al.*, 1992a,b; Hinatsu, 1994a,b). Hinatsu's results are consistent with the *g*-values of about 0.7 reported by Lewis *et al.* (1973) from EPR measurements for U^{5+} diluted in $LiNbO_3$, $LiTaO_3$, and $BiNbO_4$. The latter study could not find any verifiable EPR spectra due to U^{5+} in a number of magnetically concentrated crystals including $NaUO_3$ and $LiUO_3$.

In an interesting paper, Bickel and Kanellakopulos (1993) compiled magnetic data on a number of $5f^1$ ternary actinide oxides that they analyzed in terms of a temperature-dependent term and a temperature-independent term (see equation 20.8). Table 20.4 lists the results of the magnetic measurements and some crystallographic data for a number of compounds. The compounds studied have the $5f^1$ ion at the center of a more or less distorted AnO_6 anionic array. For U^{5+} and Np^{6+} compounds in this symmetry, the first excited level is more than ~4000 cm^{-1} higher in energy. Therefore the room-temperature moment should reflect the value of $1.24\mu_B$ obtained from a Γ_7 ground state. Table 20.4 shows the experimental values, all of which are lower than the theoretical value. Bickel and Kanellakopulos (1993) argue that this can be interpreted, along with the observed TIP for these compounds, as due to the degree of covalency. They also point out that the observation of low-temperature magnetic transitions in these compounds, due to exchange interactions, depends on the shortest An–An distance. This behavior is reminiscent of that found in actinide metals and alloys. In that case, when the actinide ion–actinide ion distance is less than a certain critical distance (the Hill parameter), approximately 3.5 Å, the material exhibits itinerant behavior (TIP). At a distance greater than the critical distance, localized magnetism is found. For the ionic compounds discussed by Bickel and Kanellakopulos, the equivalent behavior is exchange interactions at shorter distances vs no magnetic ordering at larger distances. See Chapter 21 for further discussion.

Table 20.4 *Magnetic and crystallographic data for $5f^1$ ternary actinide oxides. All data are taken from Bickel and Kanellakopulos (1993).*

Compound	Crystal symmetry	Shortest An–An distance (pm)	$\chi_{TIP}\ (10^{-6}$ emu mol^{-1})	μ_{eff} ($\sim$300 K) (μ_B)	T_0 (K)*
$LiUO_3$	rhombohedral	400	364	1.117	16.9
$NaUO_3$	orthorhombic	413	395	1.125	31.1
KUO_3	cubic	429	440	1.216	16.0
$RbUO_3$	cubic	432		1.216	32.0
Li_3UO_4	tetragonal	449	280	0.922	6
Li_7UO_6	hexagonal	615	238	0.873	a
Na_2NpO_4	orthorhombic	444	372	1.053	7
K_2NpO_4	tetragonal	423			19.5
Li_4NpO_5	tetragonal	443	331	0.994	20
Na_4NpO_5	tetragonal	459	342	1.018	a
Li_6NpO_6	hexagonal	520	389	1.083	a
Na_6NpO_6	hexagonal	567	376	1.005	a
Ba_3NpO_6	orthorhombic	627	340	1.012	a
Sr_3NpO_6	orthorhombic	598	283	0.933	a
Ca_3NpO_6	orthorhombic	574	347	1.089	a
$BaNpO_4$	orthorhombic	404	335	1.089	18.3
Li_5PuO_6			300	0.955	

* Ordering temperature.
a No ordering observed above 4.2 K.

A recent report of a newly synthesized U^{5+} hexakisamido complex (Meyer *et al.*, 2000) reported $g = 1.12$ as measured by EPR at 20 K with a $\mu_{eff} = 1.16$ BM from 5 to 35 K. This complex has six N atoms arranged in octahedral coordination around the U^{5+} ion from each of six dbabh groups (dbabh = 2,3:5,6-dibenzo-7-azabicyclo[2.2.1]hepta-2,5-diene) and its g-value is in accord with those measured for hexahalogenated U^{5+} complexes.

The magnetic susceptibility of UCl_5 (a dimeric compound with a pseudo-octahedral array of chlorine atoms, two of which are bridging) as a function of temperature was first reported by Handler and Hutchison (1956) and later by Fuji *et al.* (1979). The latter authors have also reported the g-value as measured by EPR (Miyake *et al.*, 1977b). They have combined the magnetic data with optical measurements by Leung and Poon (1977) and fitted all the data with a crystal field model based on a weak C_{2v} distortion of the predominantly octa-hedral (O_h) crystal field. However, they calculated an isotropic g-value on the basis of octahedral symmetry when in fact their model predicts an anisotropic g-tensor. Soulie and Edelstein (1980) have adopted a different point of view by noting the large difference in distances between the two bridging chlorines (U–Cl $\sim$2.68 Å) and the four nonbridging chlorines (U–Cl $\sim$2.43 Å) in the crystal structure. They used the Newman superposition model (Newman, 1971) and fitted the optical and magnetic data. Their best fit gave $g_x = 0.226$ and $g_y \approx g_z \approx$ 1.186, as observed. This g_x-value could not be experimentally observed because

of the large magnetic field necessary to do so. However the derived spin–orbit coupling constant of 1196 cm^{-1} is much smaller than that observed in any U^{5+} compound and the calculated $\mu_{\text{eff}} \sim 0.85\mu_{\text{B}}$ is lower than the measured value of $1.08\mu_{\text{B}}$.

In the eight-fold cubic coordination of Na$_3$UF$_8$, Lewis *et al.* (1973) measured a *g*-value of 1.2 at 7 K. The magnetic susceptibilities of M$_3$UF$_8$ (M = Na, Cs, Rb, and NH$_4$) have been measured from 8 to 300 K (Rigny *et al.*, 1971b). The experimental data were fitted very satisfactorily with a model that assumed a trigonal (D$_{3d}$) distortion to the eight-fold cubic coordination of the fluorine atoms.

An interesting EPR study of six organouranium(v) complexes (five organouranium amides and one organouranium alkoxide) in dilute frozen solutions at 15 K has been published (Gourier *et al.*, 1997). From an interpretation of the anisotropic *g*-values obtained from the EPR spectra, a picture of the bonding was established for these compounds. The major assumption made was that all ligands, with the exception of the alkoxide ligands, were bound only weakly with the 5f orbitals of the U(v) ion so that only the ground $J = 5/2$ crystal field state has to be considered. With this assumption the experimental *g*-values of the organouranium(v) amide complexes could be quantitatively fit. This model did not work with the organouranium(v) alkoxide compound. This was attributed to a strong U(v) 5f-OR (where R is the alkyl group on the alkoxide) interaction so that the above weak field approximation is not valid.

The magnetic uranium bis-cycloheptatrienyl sandwich compound [K(C$_{12}$H$_{24}$O$_6$)][U(η^7-C$_7$H$_7$)$_2$] has been synthesized (Arliguie *et al.*, 1995). The ionic configuration of the U ion should be 5f^3 since the formal charge on each of the cycloheptatrienyl rings is -3. However, theoretical calculations by Li and Bursten (1997) have shown that the U ion has a localized 5f^1 configuration. Thus this molecule can be considered as the 5f^1 analog of uranocene because the molecular orbitals of the C$_7$H$_7$ rings have the same group theoretical symmetries as the cyclooctatetraenyl rings of uranocene. The EPR spectrum of a frozen solution of this compound in methyl-tetrahydrofuran (THF) was measured below 15 K and the ENDOR spectrum was measured at selected fields at 4 K (Gourier *et al.*, 1998). From an analysis of the measured *g*-tensor they concluded that the strong participation of the 5f$_\delta$ orbitals in bonding and spin–orbit effects were responsible for the f-orbital composition of the singly occupied molecular orbital. The proton ENDOR measurements allowed a lower limit of $\rho_\pi \geq 4 \times 10^{-2}$ to be set for the positive spin density on the 2pπ carbon orbitals of the cycloheptatrienyl ligands in this compound.

Two bimetallic, pentavalent uranium derivatives [(MeC$_5$H$_4$)$_3$U]$_2$[μ-1,4-N$_2$C$_6$H$_4$] and [(MeC$_5$H$_4$)$_3$U]$_2$[μ-1,3-N$_2$C$_6$H$_4$] have been synthesized and magnetic measurements have been performed from room temperature to 5 K (Rosen *et al.*, 1990). In each of these dimers, the two U atoms are coupled to the imido N atoms on the substituted benzene rings. The U-dimer coupled by the [μ-1,4-N$_2$C$_6$H$_4$] moiety can form a conjugated ring while the other U-compound

Table 20.5 *Magnetic data for some U(v) compounds. The values given below are for the range of temperatures where the Curie–Weiss formula approximately holds. The references should be checked for details.*

Compound	T range (K)	θ (K)	μ_{eff}[a] (μ_B)	References and notes
[(Me$_3$Si)$_2$N]$_3$UN(p-C$_6$H$_4$CH$_3$)	5–40	–1.3	1.49	Stewart and
	140–240	–98	2.26	Andersen (1998)
[(Me$_3$Si)$_2$N]$_3$UNSiMe$_3$	5–40	–3.6	1.61	Stewart and
	140–280	–54	2.04	Andersen (1998)
(C$_5$H$_5$)$_3$UNSiMe$_3$	5–40	–0.7	1.19	Rosen *et al.* (1990)
	140–280	–82	1.83	
(MeC$_5$H$_4$)$_3$UNPh	5–40	1.03	1.25	Rosen *et al.* (1990)
	140–280	–110	1.96	
[(MeC$_5$H$_4$)$_3$U]$_2$[μ-1,3-N$_2$C$_6$H$_4$]	5–40	–3.95	1.30	Rosen *et al.* (1990)
	140–280	–134	2.12	
[(MeC$_5$H$_4$)$_3$U]$_2$[μ-1,4-N$_2$C$_6$H$_4$]	5–40			Rosen *et al.* (1990). This compound becomes antiferromagnetic at ∼20 K. See discussion in text
	140–280	–147	2.08	

[a] All magnetic data are given per U atom. To obtain the value per formula unit for dimeric compounds multiply by the sqrt(2).

cannot. From room temperature down to ∼40 K the magnetic susceptibility measurements of these two compounds were similar. Below ∼40 K an antiferromagnetic coupling was observed for the [2μ-1,4-N$_2$C$_6$H$_4$] coupled dimer but no such coupling was observed from the [μ-1,3-N$_2$C$_6$H$_4$] coupled dimer. A value of the exchange constant *J*, of ∼–19 cm^{-1}, was obtained for the magnitude of the exchange interaction by a fit of the observed magnetism to that calculated for an isolated one-dimensional dimer as a model for the [μ-1,4-N$_2$C$_6$H$_4$] coupled dimer. Table 20.5 lists the magnetic properties of some U(v) imide compounds.

20.4 $5f^2\ {}^3H_4;\ U^{4+},\ Np^{5+},\ Pu^{6+}$

U(IV) compounds have been widely studied. The total crystal-field splitting for the $^3H_4$ ground term of the 5f^2 configuration is usually of the same order as or greater than 200 cm^{-1} (kT at room temperature). Thus only the ground crystal field state or perhaps the two or three lowest-lying states will provide first-order contributions to the observed magnetic susceptibility. Measurements over

as wide a temperature range as possible are clearly desirable. For most U^{4+} compounds, few optical data are available so magnetic data are usually interpreted by considering only the ground $^3H_4$ term, determining the crystal-field splittings for a particular point symmetry group (usually from crystallographic data), choosing a ground state either empirically or by calculation (e.g. point-charge or angular-overlap model), and then calculating the susceptibility. A $J = 4$ state in a point group symmetry lower than tetragonal will split into nine singlet states. In higher symmetries, there will be some singlet states and some doubly and/or triply degenerate states. If a singlet state lies lowest there will be a range of temperatures for which the compound will exhibit only TIP. Some examples from the voluminous literature follow.

One of the few cases for which anisotropic magnetic susceptibility measurements of a single crystal have been reported is UCl_4 (Gamp *et al.*, 1983). In this compound, the anisotropy of the susceptibility is very large ($\chi_\perp > \chi_\parallel$) which makes powder measurements difficult because the crystallites tend to reorient in a static homogeneous magnetic field with the axis of greatest susceptibility parallel to the field. This effect is stronger at low temperatures and depends on the magnitude of the applied field. Gamp *et al.* (1983) found it impossible to obtain reliable powder susceptibility data for UCl_4 at temperatures below 20 K, even with a field as small as 0.05 T. The powder reoriented slowly and the measured susceptibility data increased with time until it reached the value of $\chi_\perp$ measured in the single crystal. This is illustrated in Fig. 20.5. Using the available optical data, Gamp *et al.* (1983) obtained a reasonable fit between the calculated single crystal susceptibilities and the experimental values. The fit could easily have been improved with only minor changes in the crystal field parameter set or the introduction of orbital reduction factors.

The UCl_4 crystal field scheme was examined directly by neutron inelastic scattering by Delamoye *et al.* (1986). The first excited state ($\Gamma_4 \to \Gamma_5$) was found at 92(1) cm^{-1}, which is in disagreement with the 109 cm^{-1} deduced from susceptibility (Gamp *et al.*, 1983). The neutron study also observed the next higher level (Γ_5') at 1125(3) cm^{-1}. This last level is in good agreement with the predictions of the susceptibility. Here is an example where the susceptibility predicts a value of the crystal field energy splitting too large compared to that measured by neutrons. As in PuO_2 (see below), one could invoke the exchange interaction (Colarieti-Tosti *et al.*, 2002), but there appears a more direct explanation in terms of coupling between the magnetic and lattice modes (phonons). This is illustrated by the most unusual behavior of the temperature dependence of the $\Gamma_4 \to \Gamma_5$ excitation as shown in Fig. 20.6. From simple Boltzmann statistics, the peak should decrease by only 20% of its strength between 10 and 50 K. Instead it has lost 70% of its intensity, broadened considerably, and shifted to lower energy. At 160 K (where the peak should still be ~40% of its 10 K value), it has lost about 90% of its intensity and shifted to ~75 cm^{-1}, a decrease in frequency of almost 20%. The only explanation for these effects is that there is strong coupling to the lattice vibrations (phonons). It is not
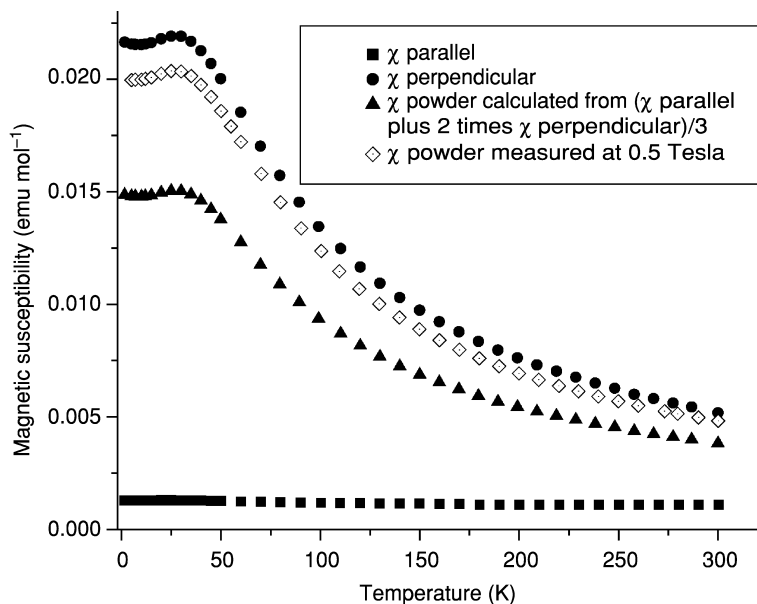
Fig. 20.5 *The values of $\chi_\parallel$ and $\chi_\perp$ obtained from measurements on a single crystal of UCl$_4$ and the calculated average magnetic susceptibility of polycrystalline UCl$_4$ derived from these measurements. The calculated average susceptibility is compared with susceptibility measurements on a polycrystalline sample of UCl$_4$ at 0.5 T. For the polycrystalline sample in a magnetic field, a strong force is applied along the strong magnetic axis of the crystallites and tends to reorient the crystallites. Thus the measured value of a powdered sample has a susceptibility greater than that calculated from the values of $\chi_\parallel$ and $\chi_\perp$ obtained from the single crystal measurements. See Gamp et al. (1983) for details.*

surprising, therefore, that simple predictions of the crystal-field splittings from the susceptibility should not agree with the neutron measurements, as interactions with the phonons are not considered. Efforts to include configuration interaction to explain the discrepancy between simple models and the experiments may also have to be taken into account (Zolnierek *et al.*, 1984), but before these large interactions with the lattice modes are understood, such an effort would appear premature.

Another interesting experiment was performed on UCl$_4$ to look for covalency effects between the U and Cl atoms (Lander *et al.*, 1985). In these experiments a single crystal is placed in a high magnetic field (4.6 T in this case) and then from the scattering of polarized neutrons the magnetization in the unit cell is deduced. If, for example, there would be strong mixing of the U 5f and Cl p-states then one might expect to observe a reduced spin density at the Cl site. Naively, it would be expected that covalency is small in compounds such as UCl$_4$, and such mixing of the 5f states unlikely. This indeed was the case, and no spin density was found at the Cl site. However, a small spin density midway between the
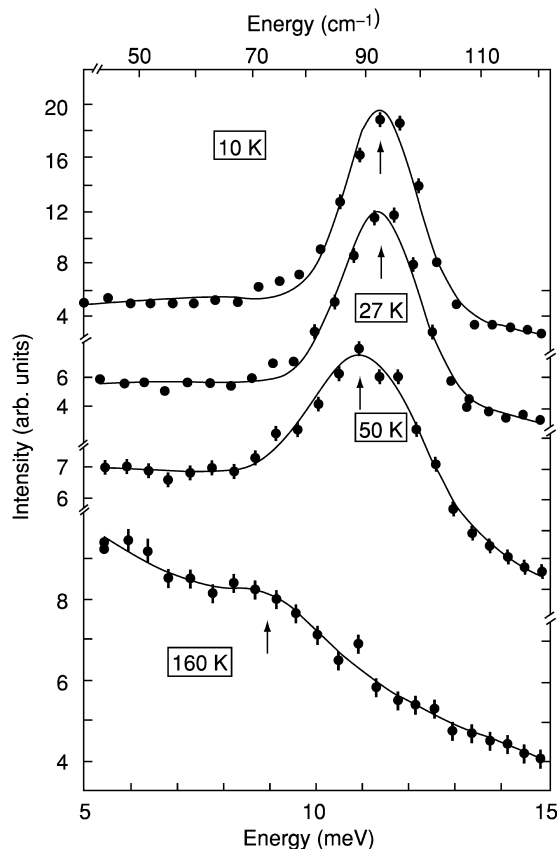
Fig. 20.6 *The temperature dependence of the intensities of the neutron inelastic scattering of the $\Gamma_4 \rightarrow \Gamma_5$ excitation in UCl_4. The shift in energy and the loss of intensity provide evidence for strong electronic–phonon coupling. Reprinted from Delamoye et al. (1986). Copyright* 1986 *with permission from Elsevier.*

U and Cl ions was modeled as an electron transfer from the 5f to the 6d antibonding orbital, and then a covalent bond formed between the U 6d and Cl p-states. Given the interesting possibilities for covalency in 5f compounds, it is perhaps surprising that experiments such as these have not been more common in the actinides. The difficulty is that single crystals are required (and they must be at least 10 mm^3) and their low-temperature properties must be well-known. For example, an experiment was reported on UCp$_3$Cl, where the covalency effects would be expected to be much larger than in the tetrachloride. Unfortunately, although good crystals were available, on cooling to low temperature many phase transitions occurred (Raison *et al.*, 1994a,b). Such complexities made it impossible to examine the spin densities and learn the details of the covalency. New efforts along these lines would seem worthwhile, especially

as neutron intensities have increased (which means that smaller crystals can be used), available magnetic fields have increased (now up to 10 T and in special cases to 15 T), and local-spin-density-approximation methods can be used to calculate the expected covalency effects.

Blaise *et al.* (1986) have measured the temperature-dependent magnetic susceptibility of a single crystal of tetrakis(1,1,1-trifluoro-4-phenylbutane-2,4-dionato) U(IV). The data were fit with a crystal field model based on distorted cubic symmetry. Optical and magnetic studies on $U(NCS)_8(NEt_4)_4$ (Et = C_2H_5) have been published by several groups (Folcher *et al.*, 1976; Soulie and Goodman, 1976, 1979; Carnall *et al.*, 1980; Kanellakopulos *et al.*, 1980c). In this compound the uranium ion is at a site of cubic symmetry (in cubic symmetry no magnetic anisotropy is possible) in the first coordination sphere surrounded by eight nitrogen atoms from the thiocyanate groups. By fitting the measured magnetic susceptibility in the temperature range 4.2–290 K, Soulie and Goodman (1976, 1979) evaluated the appropriate free-ion and crystal field parameters. They found good agreement above 30 K with the measured susceptibility but with significant deviations below this temperature. These deviations were attributed to a slight D_{4h} distortion of the cubic symmetry (confirmed by Raman spectra), which was not taken into account in their calculations. Subsequently Kanellakopulos and coworkers (Carnall *et al.*, 1980; Kanellakopulos *et al.*, 1980c) determined another set of empirical parameters using cubic crystal field parameters obtained from the assignment of the optical spectrum. They then took into account the lower symmetry by using perturbation theory to split the ground triplet state in cubic symmetry into a singlet state and a higher-lying doublet state. The use of this model and the introduction of an orbital reduction factor resulted in satisfactory agreement between the calculated and experimental susceptibility data.

The optical spectra of $U(BD_4)_4$ diluted in $Zr(BD_4)_4$ were measured by Bernstein and Keiderling (1973) and reinterpreted by Rajnak *et al.* (1984b). The U^{4+} ion in the $U(BD_4)_4$ molecule in this host crystal has tetrahedral symmetry (T_d) but the pure compound is polymeric with a lower site symmetry at the metal ion. Shinomoto *et al.* (1983) synthesized the $U(BH_3CH_3)_4$ compound which is monomeric and has the same (T_d) symmetry found for $U(BD_4)_4$ diluted in $Zr(BD_4)_4$. The magnetic susceptibility of $U(BH_3CH_3)_4$ has been measured from 2 to 330 K. Using the eigenvectors obtained from the reanalysis of the Keiderling data, the magnetic data could be fit. However in order to get the best fit, Rajnak *et al.* (1984b) empirically adjusted the energy splitting between the ground E-state and the first excited T_1 state (T_d) and included an orbital reduction factor of $k = 0.85$. In addition to the magnetic susceptibility, the temperature dependence of the solution shifts of the ^1H, ^{11}B, and ^{13}C NMR have been obtained for the $M(BH_3CH_3)_4$ (M = Pa, Th, U, Np) (Gamp *et al.*, 1987; Kot and Edelstein, 1995). Because of the high symmetry at the paramagnetic actinide metal ion, there is no contribution due to the metal ion dipolar term. Thus the measured NMR shifts should arise from the unpaired spin

density transferred from the metal ion to the ligand orbitals. The traditional equation used to determine the unpaired spin density is:

$$\frac{\Delta H}{H_0} = \frac{\beta}{3kT} \langle S_z \rangle \frac{A}{\gamma(h/2\pi)} \tag{20.15}$$

where $\Delta H/H_0$ is the NMR shift, β is the Bohr magneton, k is the Boltzmann constant, A is the hyperfine constant in energy units, γ is the nuclear gyromagnetic ratio, and h is Planck's constant. $\langle S_z \rangle$ is the thermal average of the spin operator and can be calculated from the eigenvectors obtained from the optical analyses. The usual assumptions made in these types of analyses is that the above equation is valid for all crystal field states using the same value of A, and that each of the f-orbitals is equally effective in transferring spin into ligand orbitals. Difficulties were encountered in analyzing the NMR shifts in the actinide methylborohydrides. McGarvey (1998) has shown that the data can be explained if it is assumed that each of the f-orbitals contributes a different amount of spin into the ligand orbitals.

The temperature dependence of the magnetic susceptibility of three U^{4+} sulfates, $U(SO_4)_2 \cdot 4H_2O$, $U_6O_4(OH)_4(SO_4)_6$, and $U(OH)_2SO_4$, in the temperature range 4.2–300 K has been reported by Mulak (1978). These three compounds have a similar antiprismatic coordination about the U^{4+} ion by oxygen anions with almost the same U–O distances. Using a simplified model of the U^{4+} ion with a $^3H_4$ ground term, $J = 4$ as a good quantum number in a D_{4d} crystal field, and only the energy splittings between the two lowest crystal field states as empirical parameters, the temperature dependence of the magnetic susceptibility was fitted. A further low-symmetry distortion has to be introduced (which split the energy levels that were doubly degenerate in D_{4d} symmetry) in order to obtain satisfactory agreement. Despite the very similar coordination environment about the U^{4+} ion in the three compounds, there are significant differences in the low-temperature magnetic behavior. In particular, the magnetic susceptibility for $U(OH)_2SO_4$ from 4.2 to 21 K is approximately constant while above 21 K the susceptibility decreases with a temperature dependence typical of a paramagnetic compound with a degenerate ground state. This low-temperature behavior was attributed to a crystallographic transition induced by the cooperative Jahn–Teller effect. Hinatsu *et al.* (1981) reported the temperature dependence from 1.8 to 300 K of a crystalline uranium(IV) sulfate that showed a broad maximum in the susceptibility at 21.5 K. They assumed a one-dimensional chain structure with U atoms linked by hydroxyl groups (or possibly oxygen atoms) and fitted their data to an exchange interaction between uranium atoms along this one-dimensional chain.

The synthesis of the organometallic 'sandwich' compound uranocene, $U(C_8H_8)_2$, by Müller-Westerhoff and Streitwieser (1968) led to a renaissance in the organometallic chemistry of the actinide series (Seyferth, 2004). Magnetic susceptibility measurements have played an important role in the discussions

of the electronic structure of these types of compounds. Karraker *et al.* (1970) initially reported the temperature-dependent susceptibility of $U(C_8H_8)_2$ and interpreted the data on the basis of a crystal field of C_{8h} symmetry acting on the ${}^3H_4$ ground term. The data were fitted with a $J_z = \pm 4$ ground state and the inclusion of an orbital reduction factor to account for covalency. This model also fitted the experimental results for $Np(C_8H_8)_2$ and $Pu(C_8H_8)_2$. Hayes and Edelstein (1972) then proceeded to calculate the necessary crystal field parameters using molecular orbital theory and the Wolfsberg–Helmholz approximation. From the calculated crystal field parameters and published free-ion parameters they found the ground crystal field state to be the $J_z = \pm 3$ level. More careful measurements by Karraker (1973) have shown that the susceptibility of $U(C_8H_8)_2$ at low temperature became temperature independent and was attributed by Hayes and Edelstein as being due to a possible low-temperature crystal structure phase transition causing the U^{4+} ion to be at a symmetry site lower than C_{8h}. This model was disputed by Amberger *et al.* (1975). They recalculated the crystal field parameters for uranocene in three ways: using the purely electrostatic approach, the angular overlap model, and a molecular orbital model. Assuming rigorous D_{8h} symmetry, they found that a crystal-field splitting with a singlet ground state ($J_z = 0$) and an excited doublet state at $17\ \mathrm{cm}^{-1}$ ($J_z = \pm 1$) gave the best agreement with their molecular orbital calculation and the experimental data. Subsequently, Edelstein *et al.* (1976) showed that some uranocene-type molecules with alkyl or phenyl groups attached to the cyclooctatetraene rings showed the temperature-dependent behavior expected for a degenerate ground state down to 4.2 K. This behavior is inconsistent with the Amberger *et al.* model. Warren (1977) has discussed the magnetic properties of uranocene-type compounds in his extensive review on ligand field theory of f-orbital sandwich complexes. Later experimental and theoretical papers have utilized the magnetic data as tests of the validity of their data and/or calculations (Dallinger *et al.*, 1978; Boerrigter *et al.*, 1988; Chang and Pitzer, 1989).

Another class of organometallic U(IV) compounds that have been thoroughly studied is tetrakis(cyclopentadienyl)uranium(IV), UCp_4, and its tris(cyclopentadienyl) derivatives, Cp_3UR, where R = BH_4, BF_4, OR, F, Cl, Br, I, etc (Kanellakopulos, 1979). These compounds have been divided into two categories: those showing a small dipole moment and a small range of temperature-independent susceptibilities; and a second category exhibiting larger dipole moments and a more extended range of temperature-independent susceptibilities. These differences have been attributed to an increasing trigonal distortion in the second category of compounds. Amberger *et al.* (1976) have used three different semiempirical calculations to estimate the two crystal field parameters needed for the assumed T_d symmetry of UCp_4. The temperature-dependent magnetic susceptibility of UCp_4 was then fitted assuming a weak crystal field of lower symmetry that split the tetrahedral energy levels. The tetrahedral wave functions were used for the calculations and the energy differences of four levels

plus one scaling parameter were varied. Satisfactory agreement with the experimental data was obtained. Amberger (1976a,b) also analyzed optical spectra of UCp_4 and Cp_3UCl assuming T_d symmetry. He further analyzed the fine structure of the spectrum and determined the crystal-field splitting of the ground $^3H_4$ term. Using tetrahedral wave functions and the crystal-field splitting of the ground term he was able to satisfactorily fit the observed susceptibility using only one scaling parameter. Magnetic data for a number of Cp_3UR compounds have been given by Aderhold *et al.* (1978).

A number of other structurally characterized U(IV) compounds were synthesized and magnetic measurements are reported. Some results are listed in Table 20.6. Most of these compounds are monomeric, but a number of dimers and even some higher oligomers have been found. Compounds with amido, amidoamine, alkoxide, and other ligands were characterized and are given in Table 20.6.

In general for U(IV) compounds Curie–Weiss behavior is found at higher temperatures with the susceptibility tending toward temperature-independent behavior at the lowest temperatures. The U^{4+} ion is a non-Kramers' ion with two 5f electrons and will usually have an orbital singlet ground state at low temperatures (this depends on the point symmetry at the U^{4+} ion and will generally be true for lower-symmetry groups) which is the reason for the temperature-independent behavior. For dimeric U^{4+} compounds and higher oligomers, if the U–U distances are short (less than 3.6 Å) or if the bridging ligand(s) facilitate electron exchange, deviations from this type of behavior suggest magnetic interactions between the two U centers.

Le Borgne *et al.* (2002) reported the syntheses, crystal structures, and magnetic properties of heteronuclear trimetallic compounds of the type [{ML (py)}$_2$U] (M = Co, Ni, Zn) and [{CuL(py)}M'{CuL}] (M' = U, Th, Zr) where L = N,N'-bis(3-hydroxysalicylidene)-2,2-dimethyl-1,3-propanediamine and py is pyridine. The crystal structures show that the two ML fragments are orthogonal and linked to the central U ion by two pairs of oxygen atoms from each of the Schiff base ligands. In each of the compounds the three metal ions are linear and the eight oxygen atoms exhibit similar dodecahedral geometry around the U ion. The magnetic susceptibilities of the Co_2U, Ni_2U, and Cu_2U compounds were measured and compared with that of the appropriate Zn_2U derivative, where the paramagnetic 3d ion was replaced by the diamagnetic Zn^{2+} ion. By subtracting the magnetic data of the U–3d diamagnetic ion complexes from similar data for the U–paramagnetic 3d ion complexes (in the temperature range from 300 to 2 K), a weak antiferromagnetic coupling was observed between the Ni^{2+} and the U^{4+} ions, and a ferromagnetic interaction was found between the Cu^{2+} and U^{4+} ions. In a later paper (Salmon *et al.*, 2003), this same group synthesized and magnetically and structurally characterized [ML^2(py)U(acac)$_2$] and [(ML^2)$_2$U], where M = Cu and Zn and L^2 = N, N'-bis(3-hydroxysalicylidene)-2-dimethyl-1,3-propanediamine, and acac is acetylacetonate ($C_5H_7O_2$). Again the Cu, U compounds and the Cu, Zn analogs

Table 20.6 *Magnetic data for some U(IV) and neptunyl(V) compounds. The values given below are for the range of temperatures where the Curie–Weiss formula approximately holds. At lower temperatures more complex magnetic behavior is observed. The references should be checked for details.*

Compound	T range (K)	θ (K)	μ_{eff}* (μ_B)	References and notes
Cp_3UOH	110–300	–125	2.45 ± 0.01	a
$[Cp_3U]_2O$	140–300	–108	2.17 ± 0.01	a
Cp_3USH	110–300	–83	2.65 ± 0.01	a
$[Cp_3U]_2S$	120–300	–62.5	2.64 ± 0.01	a
$Cp^+_2UCl_2$	100–300	–7.6	3.32	b
$Cp^+_2UF_2$	100–300	–137	3.11	b
$FU[N(Me_3Si)_2]_3$	5–280	–7	2.91	c
$MeU[(Me_3Si)_2N]_3$	25–100	–14	2.99	c
	120–280	–32	3.18	
$Te\{U[N(Me_3Si)_2]_3\}_2$	5–140	–19	3.10	c
	140–280	–40	3.28	
$\{U[N(Me_3Si)_2]_2\}_2[\mu-N(p\text{-tolyl})]_2$	5–40		4.37	c
	160–280		3.34	
$MeU[OC(CMe_3)_3]_3$	80–280	–54	3.15	c
$U[OC(CMe_3)_2H]_4$	5–120	–17	2.59	c
	140–280	–33	2.71	
$U[OSi(CMe_3)_3]_4$	5–90	–11	2.69	c
	100–200	–22	2.82	
$[(MeC_5H_4)_3U]_2[\mu\text{-}CS_2]$	120–300	–12.5	3.01	d
$[(MeC_5H_4)_3U]_2[\mu\text{-}S]$	100–300	–84.5	2.93	d
$[(MeC_5H_4)_3U]_2[\mu\text{-}Se]$	110–300	–72.2	2.85	d
$[(MeC_5H_4)_3U]_2[\mu\text{-}Te]$	120–300	–11.8	3.02	d
$[(MeC_5H_4)_3U]_2[\mu\text{-}PhNCO]$	110–300	–89.5	2.87	d
$U[N(CH_2CH_3)_2]_4$	20–100	–4.8	2.74	e
$U[N(CH_2CH_2CH_3)_2]_4$	30–102	7.2	2.69	e
$U[N(CH_2CH_2CH_2CH_3)_2]_4$	27–84	2.2	2.44	e
$U[N(C_6H_5)_2]_4$	40–90	24.8	2.84	e
$[U(CH_3NCH_2CH_2NCH_3)_2]_3$	4.6–100	–30.5	2.5	f
$(H_3N(CH_2)_3NH_3)U_2F_{10} \cdot 2H_2O$	20–300	–24.7 ± 1.3	4.00	g
$(H_3N(CH_2)_4NH_3)U_2F_{10} \cdot 3H_2O$	20–300	–30.9 ± 0.4	3.47	g
$(H_3N(CH_2)_6NH_3)U_2F_{10} \cdot 2H_2O$	20–300	–41.7 ± 1.1	3.94	g
$(C_5H_{14}N_2)_2U_2F_{12} \cdot 2H_2O$	150–300	–1.3	3.09	h
$(C_2H_{10}N_2)U_2F_{10}$	150–300	+21	3.24	h
$[(C_5N_2H_{14})_2(U_2F_{12}) \cdot 2H_2O]$	40–350	14.7	3.59	i
$[(C_5N_2H_{14})_2(H_3O)(U_2F_{11})]$	40–350	78.8	3.72	i
$[(C_4N_2H_{12})_2(U_2F_{12}) \cdot H_2O]$	40–350	15.7	3.35	i
$[(C_6N_2H_{14})_2(U_3O_4F_{12})]$	40–350	153.6	4.01	j
$(NpO_2)_2C_2O_4 \cdot 4H_2O$	15–40	12.5	2.71	k
$[NpO_2(O_2CH)(H_2O]$	50–300	12.7	2.81	l
$(NpO_2)_2(O_2C)_2C_6H_4 \cdot 6H_2O$	10–70	7.75	2.54	m
	150–300	29.8	2.29	

* All magnetic data are given per U atom. To obtain the value per formula unit for dimeric compounds multiply by the sqrt(2).
[a] Spirlet *et al.* (1996). Cp = C_5H_5.

were shown to be very similar structurally so that the magnetism of the appropriate Zn, U compound could be subtracted from the magnetism of the Cu, U compound to obtain the influence of the Cu^{2+} ion on the exchange interactions between the Cu and U ions. For the dimeric compound the difference in χT vs T was approximately constant from 300 to 100 K with a value of 040 ± 0.05 cm^3 mol^{-1} K, similar to that of an isolated Cu^{2+} ion. Below 100 K the difference in magnetic behavior is indicative of antiferromagnetic exchange between the $U^{4+} - Cu^{2+}$ ions. Similar experiments were performed with the trimetallic [(ML^2)$_2$U] complexes and it was found that the low-temperature magnetic behavior of the [(CuL^2)$_2$U] compound was also antiferromagnetic. The low-temperature magnetism in the latter compound is different from ferromagnetic interaction found in the somewhat structurally similar [{CuL(py)}U{CuL}] described earlier.

A similar type of experiment has been reported for an oxalate-bridged U(IV)– Mn(II) compound, K$_2$MnU(C$_2$O$_4$)$_4\cdot$9H$_2$O (Mortl *et al.*, 2000). In this compound the U(IV) ion is linked to four Mn(II) ions by each of the oxalate ligands and each of the Mn(II) ions are also linked by the oxalate ligands to four U(IV) ions. The magnetic susceptibility of this compound has been measured from 2 to 300 K. For this compound, the experimental magnetic measurements have been interpreted as the sum of the individual U(IV) and Mn(II) contributions. No indication of magnetic coupling has been found between the U(IV) ion and the Mn(II) ion down to 2 K.

A number of complex U^{4+} fluoride compounds have been synthesized and structurally characterized. As part of the determination of their physical properties, the temperature-dependent magnetic susceptibilities have been measured and analyzed (over the appropriate temperature range using the Curie–Weiss equation). Table 20.6 lists magnetic data for some structurally diverse U(IV) complex fluoride compounds.

---

[b] Lukens *et al.* (1999). Cp‡ = 1,3-(Me$_3$C)$_2$C$_5$H$_3$.
[c] Stewart (1988). If no θ values are given, the data are not very linear ($1/\chi$ vs T) in the given range and the μ_{eff} values are approximate.
[d] Brennan *et al.* (1986).
[e] Reynolds and Edelstein (1977).
[f] Reynolds *et al.* (1977). Three uranium atoms form a linear chain with the central U atom linked to the two terminal U atoms by a triple nitrogen bridge.
[g] Francis *et al.* (1998).
[h] Almond *et al.* (2000).
[i] Allen *et al.* (2000). The data ($1/\chi$ vs T) are not very linear in the 40–350 K range, the μ_{eff} values are approximate.
[j] Allen *et al.* (2000). This compound is formulated as a (U$_2^{VI}$U^{IV}O$_4$F$_{12}$) complex, the μ_{eff} given is for the formula unit or per the U(IV) atom, and is an approximate value due to the nonlinearity of the $1/\chi$ vs T data.
[k] Jones and Stone (1972).
[l] Nakamoto *et al.* (1999).
[m] Nakamoto *et al.* (2001).

There have been a few measurements performed on NpO_2^+ compounds. The compounds that are formulated as having dimeric neptunyl $(NpO_2^+)_2$ units exhibit complex magnetic behavior at low temperatures. Metamagnetism, that is the field-induced transformation of a compound from an antiferromagnetic state to a ferromagnetic state, was originally reported by Jones and Stone (1972) for the neptunyl(v) oxalate complex, $(NpO_2)_2C_2O_4 \cdot 4H_2O$. This compound exhibited Curie–Weiss behavior above 15 K (see Table 20.6). The susceptibility displayed a peak characteristic of an antiferromagnetic transition with $T_N = 11.6 \pm 0.1$ K. However the susceptibility maximum shifted to lower temperatures as the external magnetic field was increased, and above 0.075 T the susceptibility peak disappeared and ferromagnetic saturation was observed. From these observations, it was concluded that this compound was metamagnetic. Recent magnetic studies have been reported for neptunyl(v) formate and phthalate compounds $[NpO_2(O_2CH)(H_2O)]$ and $(NpO_2)_2(O_2C)_2C_6H_4 \cdot 6H_2O$ (Nakamoto $et\ al.$, 1999, 2001). The formate complex, which forms infinite two-dimensional sheets linked by NpO_2^+ bonding, follows the Curie–Weiss law from 50 K to room temperature (see Table 20.6). Below 50 K, this neptunyl compound exhibits complex magnetic behavior that is attributed to ferromagnetic ordering with $T_c = 12$ K. The authors note the situation in the neptunyl(v) formate complex is similar to that found earlier in the neptunyl(v) oxalate complex and attributed in the earlier work to metamagnetism. The neptunyl phthalate magnetic data can be fit in two regions with the Curie–Weiss law as shown in Table 20.6. Below 4.5 K, complex magnetic ordering is found that is attributed to the existence of two kinds of Np sublattices, one is ferromagnetic and the other is antiferromagnetic.

20.5 $5f^3\ ^4I_{9/2};\ U^{3+},\ Np^{4+},\ Pu^{5+}$

UH_3 has a ferromagnetic transition at approximately 172 K and a saturation magnetic moment in the temperature range 63–196 K of approximately $1\mu_B$ (Gruen, 1955). The magnetic susceptibilities of the uranium(III) halides are listed in Table 20.7 (Berger and Sienko, 1967; Jones $et\ al.$, 1974). UF_3 followed the Curie–Weiss law down to about 125 K, below which temperature the susceptibility increased more rapidly than expected from the higher-temperature data (Berger and Sienko, 1967). Jones $et\ al.$ (1974) reported the magnetic susceptibilities of U trihalides (Cl, Br, and I). For the most part, the properties could be understood on the basis of crystal field calculations. Of special interest was the report of antiferromagnetic magnetic ordering (as judged by a maximum in the susceptibility) at 22.0, 15.0, and 3.4 K in the U-trihalides Cl, Br, and I. Extensive neutron studies have also been performed on these compounds (Murasik and Furrer, 1980; Murasik $et\ al.$, 1981, 1985, 1986; Schmid $et\ al.$, 1990). Neutron diffraction confirmed the hexagonal crystal structure for UCl_3 and UBr_3, but then surprisingly found that the assumed T_N values of Jones $et\ al.$ were not

Table 20.7 *Magnetic data for some M(III) actinide halides, M = U^{3+}, Np^{3+}, and Pu^{3+}.*

Compound	T range (K)	θ (K)	μ_{eff} (μ_B)	T$_N$ (K)	χ_{TIP} (10^{-6} emu mol^{-1})	References
UF$_3$	125–293	–110 ± 5	3.67 ± 0.06			a
UCl$_3$	25–117	–89	3.70 ± 0.08	22.0 ± 1.0		b,c
UBr$_3$	25–76	–54	3.57 ± 0.08	15.0 ± 0.5		b,c
UI$_3$	5–14	–9.1	2.67 ± 0.10	3.4 ± 0.2		b,c
UI$_3$	25–200	–34	3.65 ± 0.05			b
NpCl$_3$	3.5–50				6400 ± 100	b
NpCl$_3$	75–240	–83.5	2.81 ± 0.09			b
α-NpBr$_3$	10–30				10 850 ± 320	b,d
α-NpBr$_3$	50–125	–86	3.26 ± 0.40			b
NpI$_3$	3–15				17 000 ± 7 000	b
NpI$_3$	25–60	–42	3.17 ± 0.40			b
PuCl$_3$	5–100	–7.9	1.11 ± 0.04	4.5 ± 0.5		b
PuBr$_3$	2.2–20	–0.55	0.81 ± 0.08			b
PuBr$_3$	25–60	–10.5	1.01 ± 0.10			b
PuI$_3$	5–50	+4.15	0.88 ± 0.08	4.75 ± 0.10		b,e

[a] Berger and Sienko (1967).
[b] Jones *et al.* (1974).
[c] Further magnetic ordering in these compounds have been observed from neutron scattering experiments (Murasik *et al.*, 1986; Schmid *et al.*, 1990).
[d] Sample is estimated to contain 5% NpOI$_2$ impurity.
[e] Low-temperature phase is ferromagnetic.

correct. The actual ordering temperatures in UCl$_3$ and UBr$_3$ are 6.5 and 5.4 K, respectively. The ordered moments are $\sim 2\mu_B$ for both systems. However, at lower temperatures there is a second transition (3.8 K for UCl$_3$ and 3.0 K for UBr$_3$) to a more complex magnetic structure. On cooling, the moments are initially parallel to the crystallographic *c*-axis, but then rotate to perpendicular to *c*-axis at low temperature, and with a magnetic moment of only about $0.8\mu_B$. These lower-temperature transitions were not apparently observed by Jones *et al.* (1974). The neutron work also determined the crystal field transitions that range from about 20 to 400 cm^{-1}. From the crystal field level scheme they showed that many of the properties could be understood on the basis of the extreme magnetic anisotropy. There is antiferromagnetic exchange *only* along the chains of U atoms along the *c*-axis. The peak in the susceptibility in this case is actually *not* an indication of the antiferromagnetic order, but rather the competition between the exchange and anisotropic contributions to the susceptibility. All these measurements, both the original magnetic and more recent neutron studies, were performed on polycrystalline samples, which makes the amount of information extracted in the neutron study quite remarkable.

Furthermore, a relatively sharp mode was observed at 32 cm^{-1} in both UCl_3 and UBr_3 at low temperature and was assigned to one-dimensional spin–wave excitations along the c-axis.

These studies would be most interesting to continue with single crystals. The whole question of one-dimensional magnetism is now much in fashion; the exchange interactions in actinides are usually stronger than in the lanthanides, thus making the examples more interesting. It is furthermore a salutary lesson in making a simple interpretation of the susceptibility curves.

EPR measurements have been reported for surprisingly few U^{3+} compounds and the data up to 1977 were discussed by Boatner and Abraham (1978). Crosswhite et al. (1980), from their analysis of the optical spectrum of U^{3+} diluted in LaCl$_3$, have calculated $g_{\parallel} = -4.17$, which agrees well with the magnetic resonance value of $|g_{\parallel}| = 4.153$ (Hutchison et al., 1956). Magnetic susceptibility data for Cs$_2$NaUCl$_6$ (Hendricks et al., 1974) (Table 20.2) as a function of temperature have been given. A recent optical study of U^{3+} diluted in Cs$_2$NaYCl$_6$ has given the energy levels for this system and shown that a Γ_8 (O$_h$) state is lowest in energy (Karbowiak et al., 1998) consistent with the magnetic data.

The temperature-dependent magnetic susceptibility of a number of substituted tris-cyclopentadienyl U and Nd compounds and their Lewis base adducts has been measured and are listed in Table 20.8. The EPR spectra of these compounds also have been measured as powders or frozen glasses and compared with the corresponding Nd^{3+} compounds (4f^3 configuration) (Lukens, 1995).

Table 20.8 *Magnetic data for some* Cp$_3''$ M *and* Cp$_3''$ M L *complexes* (M = Nd, U).[a,b]

	μ_{eff}[c] (5 K) (μ_B)	μ_{eff}[d] (200–300 K) (μ_B)	g_1[e]	g_2[e]	g_3[e]	μ_{eff}[f] (5 K) (μ_B)
Cp$_3''$Nd	1.65	3.70	2.48 (48)	2.08 (1.29)	0.18 (0.69)	1.62
Cp$_3''$Nd · (C$_6$H$_{11}$NC)	1.75	3.60	2.51 (21)	1.76 (29)	0.88 (7)	1.60
Cp$_3''$Nd · (^tBuNC)	1.69	3.91	2.25 (19)	2.08 (11)	0.86 (9)	1.59
Cp$_3''$U	2.03	3.32	3.41 (50)	1.65 (2.08)	0.85 (75)	1.94
Cp$_3''$U · (C$_6$H$_{11}$NC)	1.76	3.25	2.51 (96)	1.59 (1.17)	0.72 (1.76)	1.53
Cp$_3''$U · (^tBuNC)	1.78	3.14	2.41 (12)	1.75 (9)	0.29 (65)	1.49
Cp$_3^{\ddagger}$U	2.13	3.37	3.60 (16)	2.36 (34)	0.70 (0.98)	2.21

[a] From Lukens (1995).
[b] Cp$''$ = 1,3-(Me$_3$Si)$_2$C$_5$H$_3$, Cp‡ = 1,3-(Me$_3$C)$_2$C$_5$H$_3$.
[c] Calculated directly from measured magnetic susceptibility value at 5 K, $\chi = C/T$, $\mu_{eff} = (8C)^{1/2}$.
[d] $\chi = C/(T-\theta)$, $\mu_{eff} = (8C)^{1/2}$, θ values are not given.
[e] Values obtained by fitting EPR spectra obtained from powders at ~5 K. The g_3 component has been obtained for some complexes solely from the least squares fit. In cases where the error is greater than the value, g_3 is considered unreliable.
[f] Calculated from the EPR g-values.

Table 20.9 *Magnetic data for some U(III) compounds. The values given below are for the range of temperatures where the Curie–Weiss formula approximately holds. At lower temperatures more complex magnetic behavior is observed. The references should be checked for details.*

Compound	T range (K)	θ (K)	μ_{eff}[a] (μ_B)	References and notes
SrUCl$_5$	90–300	–127	3.65	Karbowiak and Drozdzynski (1998a)
Ba$_2$UCl$_7$	105–300	–95	3.25	Karbowiak and Drozdzynski (1998a)
CsUCl$_4$	60–300	–36	3.16	Karbowiak and Drozdzynski (1998b)
Cs$_2$LiUCl$_6$	85–300	–103	3.56	Karbowiak and Drozdzynski (1998b)
RbU$_2$Cl$_7$	210–300	–80	3.74	Karbowiak *et al.* (1996)
[(Me$_3$Si)$_2$N]$_3$U	35–280	–12 ± 1	3.37 ± 0.02	Stewart and Andersen (1998)
{U[N(Me$_3$Si)$_2$]$_2$}$_2$ [μ−N(H) (2,4,6-Me$_3$C$_6$H$_2$)]$_2$	80–280 9–60	–71 –22.5	3.53 2.87	Stewart (1988)

[a] All magnetic data are given per U atom. To obtain the value per formula unit for dimeric compounds multiply by the sqrt(2).

Magnetic susceptibility results for some other U(III) compounds are given in Table 20.9.

Two interesting dimeric molecules were reported by Korobkov *et al.* (2001). One of these two dimeric molecules, [Li(THF)$_4$]$_2${U$_2$[(–CH$_2$–)$_5$]$_4$-calix[4]tetrapyrrole}[μ-I]$_4$ had two U(III) ions held together by the [(–CH$_2$–)$_5$]$_4$-calix[4]tetrapyrrole ligand with a short U–U distance of 3.4560(8) Å. The second compound [Li(THF)$_2$]$_2$(μ-Cl)$_2${U$_2$[(-CH$_2$-)$_5$]$_4$-calix[4]tetrapyrrole}Cl$_2$ · THF, formally a mixed valence U(III)–U(IV) dimer with a similar geometry as the first dimer, also had a short U–U distance of 3.365(6) Å. The magnetic moment of the U(III)–U(III) dimer was 1.99μ_B (per U) at 300 K falling to 0.55μ_B (per U) at 2 K. For the U(III)–U(IV) dimer the magnetic moment at 300 K was 3.04μ_B (per mole) and 1.03μ_B (per mole) at 2 K. The authors suggest that the low moment for the U(III)–U(III) dimer could be due to antiferromagnetic behavior at low temperatures while the U(III)–U(IV) dimer could be explained by the sum of the magnetic moments of two isolated U(III) and U(IV) compounds (no magnetic exchange). Clearly much further work has to be done to determine whether magnetic exchange takes place in these dimers.

NpCl$_4$ (Table 20.7) was reported to have a ferromagnetic transition at 6.7 K (Stone and Jones, 1971). Kanellakopulos *et al.* (1980c) reported the temperature dependence of the magnetic susceptibility data for NpCl$_4$ and ((C$_2$H$_5$)$_2$N)$_4$Np (NCS)$_8$ and presented an analysis of these data. This group (Stollenwerk *et al.*, 1979; Dornberger *et al.*, 1980; Stollenwerk, 1980) also measured and discussed

the optical spectra and magnetic susceptibilities of Cp_4Np ($Cp = C_5H_5$) and Cp_3NpX where $X = Cl$, Br, and I. Low-temperature magnetic susceptibility data for $NpBr_4$ are given in Table 20.7.

From magnetic susceptibility measurements (Karraker and Stone, 1980) and EPR measurements (Bernstein and Dennis, 1979; Edelstein *et al.*, 1980) of hexachloro complexes of Np^{4+}, the ground state of the ${}^4I_{9/2}$ term was shown to be Γ_8 (O_h). Limits on the ratios of the fourth- to the sixth-order crystal field parameters have been determined, and these limits are consistent in the isostructural series MCl_6^{2-}, $M = Pa^{4+}$, U^{4+}, Np^{4+}. Depending on the cation involved, the Γ_8 state may be split by 5–10 cm^{-1} due to small deviations from O_h symmetry. The free-ion g-value (~ 0.6) for Np^{4+} deduced from the data are much reduced from the value of 0.77 obtained from optical data. Warren (1983) has suggested that the rather large value of the orbital reduction factor needed to fit the EPR data could be due to the occurrence of the Ham effect (which would change the value of the ratios of the crystal field parameters needed to fit the data). However EPR data obtained at liquid-helium temperatures for $Np(BH_4)_4$ and $Np(BD_4)_4$ diluted in the corresponding $Zr(BH_4)_4$ and $Zr(BD_4)_4$ hosts show that the doublet Γ_6 state (T_d) of the ${}^4I_{9/2}$ term is lowest (Rajnak *et al.*, 1984a). Again the free-ion g-value (0.515) is much lower than expected. Richardson and Gruber (1972) claimed that they observed the EPR spectrum of Np^{4+} diluted in ThO_2. EPR and optical spectra of Np^{4+} diluted in $ZrSiO_4$ at 4.2 K were obtained by Poirot *et al.* (1988) with measured ground Γ_6 state (D_{2d} symmetry) g-values of $|g_\parallel| = 0.8$ (6) and $|g_\perp| = 2.59$ (2), consistent with the optical analysis.

$SrNpO_3$ and $BaNpO_3$ show magnetic transitions at 31 and 48 K, respectively (Kanellakopulos *et al.*, 1980b; Bickel and Kanellakopulos, 1993). A sharp increase in magnetization was observed below the transition temperature, which suggests a complicated magnetic structure.

20.6 $5f^4 \, {}^5I_4$; Np^{3+}, Pu^{4+}

The magnetic susceptibility and magnetization of NpH_x ($x = 2.04$, 2.67, and 3) have been measured in the temperature range 4–700 K (Aldred *et al.*, 1979). The dihydride data could be fitted with a crystal field model based on cubic symmetry (O_h) for the Np^{3+}, $5f^4$ configuration, with a nominal ${}^5I_4$ ground state split into a ground Γ_3 doublet and a Γ_4 and a Γ_5 triplet at 512 and 549 cm^{-1}, respectively. The Γ_1 singlet is calculated to be at 1851 cm^{-1} above the Γ_5 state. Magnetic data for $Cs_2NaNpCl_6$ (Hendricks *et al.*, 1974) are shown in Table 20.2 and were assigned as due to the magnetic properties of the Γ_5 (O_h) ground state. The magnetic properties of NpX_3 ($X = Cl$, Br, and I) are given in Table 20.7 (Jones *et al.*, 1974).

Magnetic susceptibilities from 2.5 to 50 K for Pu^{4+} in three hexachloro complexes were reported by Karraker (1971). Surprisingly, one of the compounds,

Cs_2PuCl_6, had a temperature-dependent paramagnetism at low temperatures, which means a non-Kramers doublet is the lowest state. The other two $PuCl_6^{2-}$ complexes had temperature-independent susceptibilities at the lowest temperatures, which arises from a singlet state being the ground state. These data have been interpreted on the basis of a model based on the distorted O_h symmetry of the $PuCl_6^{2-}$ octahedron.

Magnetic susceptibility measurements have been reported for $Pu(C_8H_8)_2$ and $Pu(C_8H_7R)_2$, where R is an alkyl group (Karraker *et al.*, 1970; Karraker, 1973). These compounds were reported to be diamagnetic. However, the susceptibility is expected to exhibit TIP for the $^5I_4$ state in C_{8h} symmetry if the $J_z = 0$ state is lowest.

20.7 $5f^5\ ^6H_{5/2}$; Pu^{3+}, Am^{4+}

The magnetic properties of PuH_x ($2.0 \leq x \leq 3$) have been measured between 4 and 700 K (Aldred *et al.*, 1979). The cubic PuH_2 appears to order antiferromagnetically at 30 K. Cubic Pu compounds with higher hydrogen concentrations order ferromagnetically with higher transition temperatures as x increases. A maximum is reached at $T = 66$ K and $x = 2.7$. Hexagonal PuH_3 becomes ferromagnetic at 101 K. The temperature dependence of the magnetic susceptibility indicates that the ground state configuration is Pu^{3+}, $5f^5$. The magnetic properties of PuX_3 (X = Cl, Br, and I) (Jones *et al.*, 1974) are given in Table 20.7. $PuCl_3$ shows an antiferromagnetic transition at 4.5 K while PuI_3 has a ferromagnetic transition at 4.75 K. For $PuCl_3$, magnetic susceptibility calculations using wave functions obtained from optical data on Pu^{3+} diluted in $LaCl_3$ reproduce the observed susceptibility. Magnetic data for the octahedral complex $Cs_2NaPuCl_6$ (Hendricks *et al.*, 1974) are given in Table 20.2.

EPR measurements of $|g_{\parallel}| = 0.585$ (2) and $|g_{\perp}| = 0.875$ (1) were reported for $^{239}Pu^{3+}$ diluted in $LaCl_3$ at 4.2 K by Lämmermann and Stapleton (1961). These values agreed well with the results obtained from a subsequent optical analysis of this system (Lämmermann and Conway, 1963). Kot *et al.* (1993b) measured the EPR spectra of Pu^{3+} in $LuPO_4$ at 4.2 K and found $|g_{\parallel}| = 0.772(2)$ and $|g_{\perp}| = 0.658(2)$. Pu_2O_3 becomes antiferromagnetic at $T_N = 19$ K, as judged by the specific heat (Flotow and Tetenbaum, 1981). Magnetic susceptibility and neutron diffraction measurements ($T = 4$–300 K) also indicate that hexagonal β-Pu_2O_3 becomes antiferromagnetic at $T \sim 19$ K (McCart *et al.*, 1981) with a second transition at 4 K. Neutron diffraction was not initially able to determine the magnetic configurations, but in subsequent neutron work by Wulff and Lander (1988) the configuration with a moment of $0.60\mu_B$/Pu and the moments aligned parallel to the unique c-axis of the hexagonal structure were determined. The ground state moment is consistent with that from the Kramers doublet $|J = 5/2, J_z = \pm 3/2\rangle$ and the valence state is (as expected) trivalent Pu.

Table 20.10 *Measured g-values for $5f^5$ ions at cubic sites in crystals with the fluorite structure. For each type of host or ion, the matrices are listed in order of increasing lattice constant, or decreasing CF. Data taken at $\sim$5 K (Kolbe et al., 1974).*

Matrix	Ion	$|g|$
CeO_2	Pu^{3+}	1.333 (1)
ThO_2	Pu^{3+}	1.3124 (5)
CaF_2	Pu^{3+}	1.297 (2)
SrF_2	Pu^{3+}	1.250 (2)
BaF_2	Pu^{3+}	1.187 (4)
$SrCl_2$	Pu^{3+}	1.1208 (5)
CeO_2	Am^{4+}	1.3120 (5)
ThO_2	Am^{4+}	1.2862 (5)

EPR measurements on Pu^{3+} and Am^{4+} at liquid-helium temperatures in various cubic hosts have been summarized by Boatner and Abraham (1978). For both Pu^{3+} and Am^{4+} with a nominally $^6H_{5/2}$ ground state, strong intermediate-coupling effects cause the Γ_7 state (O_h) to be the ground crystal field state, rather than the Γ_7 (O_h) state as expected for pure Russell–Saunders coupling (Edelstein *et al.*, 1969). Crystal field mixing between the ground state and the excited *J*-states makes the measured *g*-value a very sensitive indicator of the magnitude of the crystal field (Lam and Chan, 1974). Table 20.10 illustrates the effect of the decreasing crystal field strength on the measured ground state *g*-values. For each type of crystal or ion, the crystal field decreases (the lattice constant of the host matrix increases) as one scans down Table 20.10, and the magnitude of *g* decreases also. In the limit of zero crystal field mixing of excited multiplets, the ground state *g*-value should be $|g| = 0.700$. ENDOR measurements on Pu^{3+} in CaF_2 have shown the interaction with the nearest neighbor fluorine ions is much stronger than found for the 4f series (Kolbe and Edelstein, 1971). The magnetic data for Am^{4+} given above have been utilized in conjunction with optical data for Am^{3+} in ThO_2 to estimate the crystal field parameters for AnO_2 series (Hubert *et al.*, 1993).

The magnetic susceptibility of the high-T_c superconductor-related compound $Pb_2Sr_2AmCu_3O_8$ has been measured from $\sim$4 to 300 K. The data can be fit with an effective moment for the Am^{4+} ion of $0.94\mu_B$ after subtracting off the contribution from the Cu sublattice. This compound shows no superconductivity (Soderholm *et al.*, 1996).

20.8 $5f^6\ ^7F_0;\ Am^{3+},\ Cm^{4+}$

A $^7F_0$ ground term has a singlet ground state that is expected to show TIP. The magnitude of the TIP depends on the energy differences to the excited states. Measurements on some Am^{3+} and Cm^{4+} compounds sometimes show a

Table 20.11 *Magnetic susceptibility of Am metal, and some Am^{3+} and Cm^{4+} compounds. If more than one set of data are given, the results are from different samples.*

Compound	Temp. range (K)	TIP (10^{-6} emu mole^{-1})	μ_{eff} (μ_B)	References and comments
^{241}Am metal	102–848	881 (62)		Cunningham (1962)
^{241}Am metal	~50–300	675		Nellis and Brodsky (1974)
^{241}Am metal	100–300	780 (10), 880 (40)		Kanellakopulos *et al.* (1975)
^{241}Am^{3+} in solution	room temperature	720		Howland and Calvin (1950)
^{243}Am(C$_5$H$_5$)$_3$	30–300	715 (14)		Kanellakopulos *et al.* (1978)
Cs$_2$Na^{243}AmCl$_6$	15–70	5400 (400)		Hendricks *et al.* (1974)
Cs$_2$Na^{243}AmCl$_6$	40–300	660 (40)		Soderholm *et al.* (1986)
^{243}Am$_2$O$_3$	5–300	640 (20)		Soderholm *et al.* (1986)
^{243}AmF$_3$	~4.2–280	714	0.63	Nave *et al.* (1983)
^{248}CmF$_4$	~4.2–280	328 (144), 1700 (527), 2800 (224)	3.24 (4), 3.49 (7), 3.04 (3)	Nave *et al.* (1983)
Ba^{248}CmO$_3$	~4.2–300	2130 (213), 988 (20)	1.63 (6), 1.71 (1)	Nave *et al.* (1983)
^{248}CmO$_2$	~4.2–300	1900 (171), 4100 (164), 2464 (1232)	1.63 (4), 1.96 (3), 2.27 (20)	Nave *et al.* (1983)
^{248}CmO$_2$	5–125		3.36 (6)	Morss *et al.* (1989)

temperature dependence that is not understood. In order to analyze these data, a modified Curie law has been utilized and is given in equation (20.8).

The few available data for these ions are given in Table 20.11. Karraker *et al.* measured the magnetic susceptibility of Cs$_2$NaAmCl$_6$ (Hendricks *et al.*, 1974) and found the susceptibility was temperature independent, as expected for a $J = 0$ ground state, but the magnitude found was much larger than that calculated considering only the second-order Zeeman effect to the optically determined $J = 1$ state at 2720 cm^{-1}. Subsequent measurements on Cs$_2$NaAmCl$_6$ and Am$_2$O$_3$ agreed much better with the calculated value (Soderholm *et al.*, 1986). Am metal was found to exhibit TIP, suggesting a localized 5f^6 configuration plus conduction electrons (Cunningham, 1962; Nellis and Brodsky, 1974; Kanellakopulos *et al.*, 1975). The susceptibility of ^{248}CmO$_2$ should also be temperature-independent but exhibits Curie–Weiss behavior (Nave *et al.*, 1983; Morss *et al.*, 1989). Nave *et al.* (1983) also have measured two other ^{248}Cm^{4+} compounds and have found complex magnetic behavior that they have analyzed using equation (20.8). Their measurements were performed on samples of mass ~50–1000 μg and it should be noted that measurements of different samples of nominally the same material were not very reproducible. A recent

calculation of the Cm magnetic moment in CmO_2 gave $3.39\mu_B$/atom. The authors suggested that an itinerant magnetism model based on delocalized electrons might be more appropriate for this system rather than the usual crystal field theory (Milman *et al.*, 2003). See Section 20.14.5 for a more detailed discussion of CmO_2.

20.9   5f⁷ ⁸S₇/₂; Am²⁺, Cm³⁺, Bk⁴⁺

In the limit of pure Russell–Saunders coupling an f^7-configuration has an $^8S_{7/2}$ ground term. A crystal field interaction will not split the orbitally non-degenerate S state. For the $4f^7$ ion, Gd^{3+}, it is indeed found that crystal-field splittings of the ground $J = 7/2$ term are of the order of about 0.2 cm^{-1}. However, the ground term for Cm^{3+} is only 87% $^8S_{7/2}$ because spin–orbit coupling mixes in substantial amounts of the $^6P_{7/2}$, $^6D_{7/2}$, and higher terms that result in crystal-field splittings of about 5–100 cm^{-1}. Early EPR studies have been reviewed by Boatner and Abraham (1978). The first authentic identification of the EPR spectra of the Cm^{3+} ion was by Abraham *et al.* (1963) in single crystals of lanthanum ethylsulfate and lanthanum trichloride. The strongest observed EPR resonance for Cm^{3+} in $LaCl_3$ was assigned as the ground state with $J_z = \pm1/2$. Later calculations based on optical data conflicted with this assignment (Carnall, 1992). High-resolution laser spectroscopy measurements (Liu *et al.*, 1993) have shown the total ground term $J = 7/2$ splitting is ~2 cm^{-1} and that the $J_z = \pm1/2$ level is not the ground state but the first excited state, in agreement with the Carnall's assignments. Am^{2+} ions have approximately the same magnetic properties as Cm^{3+}, and it was this fact that was used for the first identification of Am^{2+} as a chemically stable oxidation state (Edelstein *et al.*, 1966). A considerable amount of EPR studies have been performed on the Cm^{3+} and Am^{2+} ions at cubic symmetry sites in single crystals with the fluorite structure MX_2 (M = Ca, Sr, Ba; X = F), $SrCl_2$, ThO_2, and CeO_2. For a $5f^7$ ion in this symmetry, the ground state is an isotropic Γ_6 state and the first excited state is a Γ_8 state. If the splitting between these two states is of the order of magnitude of the magnetic splittings, these states can be mixed by the magnetic field in the EPR experiment and will result in the ground Γ_6 state showing anisotropy as the crystal orientation is changed with respect to the magnetic field. From the magnitude of the anisotropy, the Γ_6–Γ_8 splitting can be deduced. Later optical measurements on Cm^{3+} in ThO_2 confirmed the Γ_6–Γ_8 splitting of 15.5 (3) cm^{-1} found for this system (Thouvenot *et al.*, 1994). The measured ground state g-values and splittings are shown in Table 20.12. Detailed EPR measurements have been reported for Cm^{3+} in YPO_4 and $LuPO_4$ (Abraham *et al.*, 1987; Kot *et al.*, 1993a). Interestingly, for the Cm^{3+} diluted into $LuPO_4$ system, EPR measurements at ~300 K were observed for the Cm^{3+} ion. Subsequent high-resolution optical measurements showed the zero-field splittings deduced from the EPR spectra were not accurately determined

Table 20.12 *EPR g-values and zero-field splittings for Cm^{3+} and Am^{2+} ions in cubic sites in fluorite-type crystals. Under O_h symmetry, a $J = 7/2$ state will split into a ground Γ_6 state, a Γ_8 state, and the highest energy Γ_7 state.*

Crystal	Ion	ΔE (Γ_6–Γ_8)	g_J[a]	$g(\Gamma_6)$[b]	References
$SrCl_2$	Cm^{3+}	5.13 (5)[c]	1.928 (2)	$g_{100} = 4.501$ (2) $g_{111} = 4.473$ (2) $g_{110} = 4.482$ (2)	Kolbe *et al.* (1972)
SrF_2	Cm^{3+}	11.2 (4)	1.9257 (10)	4.493	Kolbe *et al.* (1972)
CaF_2	Cm^{3+}	13.4 (5)	1.926 (1)	4.492 (2)	Edelstein and Easley (1968)
ThO_2	Cm^{3+}	15.5 (3)	1.9235 (20)	4.484 (2)	Kolbe *et al.*, (1972); Abraham *et al.* (1968)
CeO_2	Cm^{3+}	17.8 (3)	1.918	4.475 (2)	Abraham *et al.* (1968); Kolbe *et al.* (1973)
$SrCl_2$	Am^{2+}	5.77 (5)	1.9283 (8)	$g_{100} = 4.504$ (3) $g_{111} = 4.481$ (3) $g_{110} = 4.489$ (3)	Abraham *et al.* (1970)
SrF_2	Am^{2+}	15.2 (4)	1.9254 (10)	4.493	Kolbe *et al.* (1972)
CaF_2	Am^{2+}	18.6 (5)	1.926 (1)	4.490 (2)	Edelstein and Easley (1968)
ThO_2	Bk^{4+}	>50	1.923	4.488	Boatner *et al.* (1972)

[a] Derived free-ion g-value.
[b] Measurements at ~9.2 GHz and 4.2 K.
[c] For Cm^{3+} in $SrCl_2$ $\Delta E(\Gamma_8$–$\Gamma_7) = 15.3$ (4) cm^{-1}.

(Murdoch *et al.*, 1996). In the Cm^{3+}:$LuPO_4$ system, the energy levels occur in pairs with two lowest levels separated by 3.49 cm^{-1} and the two highest levels separated by 1.39 cm^{-1}. The splitting between these pairs of levels is 4.64 cm^{-1}. This splitting was not determined accurately in the EPR measurements because the data were not sensitive to small perturbations of the first-order Zeeman splitting of each of the Kramers' doublets that occurs between Kramers' doublets separated by such a large energy gap.

There has been one early study of the magnetic properties of AmI_2, a divalent Am compound. The results are given in Table 20.13 along with values for Cm metal and some trivalent Cm compounds.

As discussed earlier, Cm^{3+} compounds are expected to have ground term crystal-field splittings of less than 50 cm^{-1}. Thus at temperatures where all the ground term levels are populated, μ_{eff} should equal the free-ion value of 7.64μ_B. Early work on the preparation of Cm compounds and the metal were performed with ^{244}Cm, $\tau_{1/2} = 18.1$ years. Later studies have been conducted with ^{248}Cm, $\tau_{1/2} = 340\,000$ years. Studies with ^{248}Cm should, in principle, be more reliable as problems from radiation damage and the growth of daughter isotopes are minimized. Magnetic susceptibility measurements of Cm^{3+} diluted in Cs_2Na-$LuCl_6$ (Table 20.2) suggested a crystal-field splitting of 5–10 cm^{-1}. Recent optical studies on the related system, Cm^{3+} diluted in Cs_2NaYCl_6, have

Table 20.13 *Summary of magnetic susceptibility data for $5f^7$ compounds and Cm metal.*

Compound	T range (K)	μ_{eff} (BM)	Θ (K)	T_o (K)	References and comments
$^{243}AmI_2$	37–180	6.7 (7)			a
^{244}Cm metal	145–550	7.99 (15)			b
^{244}Cm metal	100–300	8.07, 8.8	–386, –560	52 (1)	c
^{248}Cm metal	270–307	5.5	176	$T_N = 65$ K, $T_o = \sim 200$ K	d
^{248}Cm metal	200–300	6.2	202		e
^{248}Cm metal	300–340	7.7	138		e
^{244}Cm metal	140–300	6.0	72.2		f
$^{244}CmF_3 \cdot 1/2H_2O$	77–298	7.7	–5		g
$^{244}CmF_3$ in LaF_3	77–298	7.7	–6		g
$^{248}CmF_3$	$\sim$30–280	7.67	3.6		h
$^{244}CmOCl$	77–298	7.6	–22		g
$^{244}Cm^{3+}$:$Cs_2NaLuCl_6$	7.5–25	7.90 (10)	–4		i
$^{244}Cm^{3+}$:$Cs_2NaLuCl_6$	25–45	7.48 (50)	–1		i
$^{248}Cm_2O_3$	20–80	8.20	–149		j
$^{248}Cm_2O_3$	100–300	7.89	–130		j
$^{248}Cm_2O_3$	50–300	7.74	–130	$T_N \sim 15$ K	h
$^{248}Cm_2O_3$	4.2–300	7.51	–110		h
$^{248}CmBa_2Cu_3O_7$	$\sim$50–300	8.9 (3)		$T_N = 22$	k
$^{248}CmCuO_4$	50–300	7.89 (5)		$T_N = 25$	l
$Pb_2Sr_2{}^{248}CmCu_3O_8$	120–320	8.7 (2)	–96.8		m
$Pb_2Sr_2{}^{248}CmCu_3O_8$	30–90	7.8 (2)		$T_N = 18$	m

a Baybarz *et al.* (1972).
b Marei and Cunningham (1972). The Cm metal sample measurement was repeated four times with widely varying Θ values.
c Kanellakopulos *et al.* (1975) and Fournier *et al.* (1977). The first value of Θ is associated with the first value of μ_{eff}, etc.
d Huray *et al.* (1980) dhcp phase.
e Huray *et al.* (1980). fcc phase, another more complex analysis is also given.
f Fujita *et al.* (1976).
g Marei and Cunningham (1972).
h Nave *et al.* (1983).
i Hendricks *et al.* (1974).
j Morss *et al.* (1983).
k Soderholm *et al.* (1989) and Soderholm (1992). Includes a contribution from the Cu^{2+} ions to μ_{eff}.
l Soderholm *et al.* (1999). No value of Θ is given, low-temperature neutron diffraction indicates the spins order ferromagnetically within the *a–b* plane and are antiferromagnetically ordered along the *c*-axis.
m Skanthakumar *et al.* (2001). The large value of μ_{eff} above 100 K is attributed to a local paramagnetic moment on Cu^{2+} plus that of the Cm^{3+} ion. It is suggested that Cu^{2+} moment ordering occurs below 100 K resulting in the expected Cm^{3+} free-ion moment.

reported a 4.8 cm^{-1} splitting between the ground state and the first excited state. Because the ionic radius of the Lu^{3+} ion is less than that of the Y^{3+} ion, the crystal-field splitting in the Lu system should be larger, in accord with the susceptibility measurement. Above 7.5 K, there is reasonably good agreement

with the calculated free-ion moment. The temperature-dependent magnetic susceptibility of BkO_2 diluted in ThO_2 showed the ground state to be a Γ_6 (O_h) and the excited Γ_8 (O_h) state to be at about $80\ cm^{-1}$ (Karraker, 1975b). The *g*-value of the ground state was 5.04, about 10% higher than the more accurate value of 4.488 ± 0.004 measured by EPR (Boatner *et al.*, 1972). The total overall splitting of the ground $J = 7/2$ state was estimated to be about $300\ cm^{-1}$. A possible antiferromagnetic transition at 3 K has been suggested to account for the anomalous magnetic behavior of these samples below 10 K. This transition would require segregation of the BkO_2 in the host ThO_2 matrix. Nave *et al.* (1983) measured the magnetic susceptibility of a 56.6 µg sample of BkO_2 (containing a 3% Cf impurity at the time of the measurement) and find Curie–Weiss behavior from 4.2 to 300 K with $\mu_{eff} = 7.92\mu_B$ and $\theta = -250$ K. Their value agrees with the calculated value for an $^8S_{7/2}$ state. However, it does conflict with the EPR results and Karraker's results which indicate a considerable splitting of the ground $J = 7/2$ term.

Interactions involving Cm^{3+} may be judged from a very complete work on Cm_2CuO_4 by Soderholm *et al.* (1999), where $\mu_{eff} = 7.89\ (5)\mu_B$, $T_N = 25$ K, and the ordered moment is $4.8\ (2)\mu_B$ at 15 K. This is a lower moment than expected, which might be due to measurements being made at an elevated temperature compared to T_N, but also may be caused also by covalency effects. The sample used for the neutron experiments was 42 mg (^{248}Cm), and the magnetic structure is the same as found for Gd_2CuO_4, which orders at 6.4 K. As far as known this is the only observation of magnetism in a Cm compound with neutrons. Cm_2CuO_4 is isostructural with the famous high-T_c-related La_2CuO_4 and it would be interesting to know what is the value of the moment on the Cu atom in the Cm compound. Unfortunately, this was below their experimental cut-off.

Another similar study (but without neutrons) was done by Skanthakumar *et al.* (2001) on the compound $Pb_2Sr_2Cm_{1-x}Ca_xCu_3O_8$ with $x = 0$ and 0.5. Again, these materials are related to high-T_c analogs with rare earths, although none of the Cm-doped compounds becomes superconducting.

A number of magnetic susceptibility measurements have been reported for Cm metal (Table 20.13), but reports by various investigators disagree (Marei and Cunningham, 1972; Kanellakopulos *et al.*, 1975; Fournier *et al.*, 1977; Huray *et al.*, 1980). The Soderholm group has been using the Cm^{3+} ion as a probe to study the influence of magnetic electrons on the superconductivity of some high-T_c-related oxides (Soderholm, 1992). In the course of this work, some new Cm compounds have been synthesized and their susceptibilities determined as shown in Table 20.13.

20.10 $5f^8\ ^7F_6$; Bk^{3+}, Cf^{4+}

The magnetic data for $^{249}Bk^{3+}$ diluted in $Cs_2NaLuCl_6$ are given in Table 20.2 (Hendricks *et al.*, 1974). The magnetic susceptibility is temperature independent, which shows that a singlet state is the ground state. From the systematics

of the crystal field parameters for the host crystal, the ground state is assigned as a Γ_1 (O_h) state, and from the magnitude of the susceptibility, the first excited state is calculated to be a triplet Γ_4 (O_h) state at about 85 cm^{-1}. Magnetic measurements for other ^{249}Bk compounds and the metal are listed in Table 20.14. The theoretical value for the $5f^8$ ground term free-ion g-value in intermediate coupling is 1.446 (1.50 for the pure $^7F_6$ ground term). From the magnetic susceptibility of Bk^{3+} adsorbed on ion-exchange beads, Fujita (1969) measured from 9.3 to 298 K (Table 20.14) a $\mu_{\mathrm{eff}} = 9.40(6)\mu_B$, which corresponds to a free ion $g = 1.452$ (8) in excellent agreement with the expected value. The magnetic susceptibility of ^{249}BkF$_3$ has also been reported and is in agreement with the free-ion value. The results of measurements of the magnetic susceptibility of Bk metal (Fujita, 1969; Nave *et al.*, 1980) are also given in Table 20.14. These measurements were performed on very small amounts (µg) of ^{249}Bk metal. Since $\tau_{1/2}$ of ^{249}Bk is only 320 days, there were varying amounts of ^{249}Cf metal (although corrections were applied for the amount of Cf) in the samples. Thus it is not surprising that different ^{249}Bk samples showed different magnetic behavior, especially at lower temperatures. Clearly these very difficult measurements need to be repeated. Measurements have been reported for ^{249}CfO$_2$ and for ^{249}Cf$_7$O$_{12}$. The latter compound can be thought of as comprising 40% Cf^{3+} and 60% Cf^{4+} and, assuming that susceptibilities can be simply added, the free-ion moment should be $9.7\mu_B$. As can be seen from Table 20.14, the measured higher temperature values are slightly lower than the expected free-ion values.

20.11 $5f^9\ ^6H_{15/2};\ Cf^{3+}$

The EPR spectrum of ^{249}Cf^{3+} in Cs$_2$NaLuCl$_6$ powder has been observed at 4.2 K (Edelstein and Karraker, 1975). From the measured isotropic g-value of 6.273 (10), the ground crystal field was identified as the Γ_6 (O_h) state and a free-ion g-value of 1.255 was deduced as compared with a calculated intermediate-coupling g-value of 1.279 for the nominally $^6H_{15/2}$ term. For the $4f^9$ analog, Dy^{3+}, the free-ion g-value is 1.333. The magnetic susceptibility of ^{249}Cf^{3+} ($\sim$2.4 mg) diluted into octahedral Cs$_2$NaYCl$_6$ (Table 20.2) was reported in the temperature range from 2.2 to 100 K (Karraker and Dunlap, 1976). From an analysis of the data, the Γ_6 state was determined to be the ground state, in agreement with EPR measurements, with a Γ_8^1 level as the first excited level at about 50 cm^{-1}. The total crystal-field splitting was calculated to be about 860 cm^{-1}. Limits were set for the ratio of B_0^4/B_0^6, which were consistent with those determined previously for the trivalent actinide compounds Cs$_2$NaMCl$_6$ $\left(M = U^{3+}, \ldots, Bk^{3+}\right)$. EPR measurements of $|g_{\parallel}| = 3.56(2)$ and $|g_{\perp}| = 7.79(3)$ were reported for Cf^{3+} diluted in LuPO$_4$ at 4.2 K by Kot *et al.* (1993b).

Table 20.14 also lists magnetic susceptibility data for ^{249}Cf^{3+} compounds and for ^{249}Cf metal. From the magnetic susceptibility of Cf^{3+} adsorbed on ion-exchange beads (Fujita, 1969) measured from 77 to 297 K (Table 20.14),

Table 20.14 *Magnetic data for $5f^8$ and $5f^9$ metals, ions, and compounds.*

Compound	T range (K)	θ (K)	μ_{eff} (μ_B)	T_N (K)	References and notes
^{249}Bk metal	170–350	64.4	8.23	$T_o = 140$ (15)	a
^{249}Bk metal	50–298	–72.7	8.52	35 (3)	b
^{249}Bk metal	100–298	–33.0	8.83		c
^{249}Bk metal	70–300	–101.6	9.69	∼34	d
^{249}Bk metal	70–300	–84.4	8.82	∼34	e
^{249}Bk^{3+}	∼10–300	–11.0 (1.9)	9.40 (6)		f
^{249}BkF$_3$	4.2–300	–77.9	9.38		g
^{249}CfO$_2$	∼80–320	–70 (10)	9.1 (2)	7 (2)	h
^{249}Cf$_7$O$_{12}$	∼80–320	95 (15)	9.5 (2)	8 (2)	i
^{249}CfF$_4$	150–340	–51 (3)	9.4 (1)		j
^{249}CfF$_4$	150–340	–33 (3)	9.1 (1)	9–12	k
^{249}Cf metal	28–298	3.24	9.84		l
^{249}Cf metal	22–298	–3.00	9.67		l
^{249}Cf metal	100–340	40 (3)	9.7 (2)	$T_o = 51$ (2)	m
^{249}Cf^{3+}	77–298	–5.6 (3.2)	9.14 (6)		n
Ba^{249}CfO$_3$	∼80–320	–210 (20)	9.2 (2)	7 (2)	o
^{249}Cf$_2$O$_3$	∼80–320	–80 (15)	10.1 (2)	8 (2)	p
^{249}Cf$_2$O$_3$	∼80–320	–115 (15)	9.8 (2)	19 (2)	q
^{249}Cf$_2$O$_3$	90–300	–80 (10)	9.7 (2)		r
^{249}CfF$_3$	150–340	–20 (3)	10.2 (1)	6–7	s
^{249}CfCl$_3$	100–340	37 (10)	10.3 (2)	13	t
^{249}CfCl$_3$	60–340	13 (5)	10.1 (2)	7	u
Cs$_2$Na^{249}CfCl$_6$	2.2–14	–2.8 (1)	7.36 (20)		v
Cs$_2$Na^{249}CfCl$_6$	20–100	–13.5 (4)	10.0 (1)		v

[a] Fujita (1969) predominantly fcc, mass 1.669 μg, ∼20% ^{249}Cf, possible ferromagnetic impurities.

[b] Fujita (1969) predominantly dhcp, mass 5.629 μg, ∼16% ^{249}Cf.

[c] Fujita (1969) approximately equal amounts of the dhcp and fcc phases, mass 1.725 μg, ∼1.7% ^{249}Cf.

[d] Nave *et al.* (1980) dhcp, ∼12% ^{249}Cf, 21.0 (3) μg.

[e] Nave *et al.* (1980) mainly dhcp, some fcc, ∼16% ^{249}Cf, 19.0 (3) μg, indication of a second transition (small amplitude) at ∼42 K.

[f] Bk^{3+} absorbed on ion-exchange beads, two samples of 0.546 and 1.012 μg, less than 0.8 and 0.4 at % ^{249}Cf respectively in the two samples. Average value is given.

[g] Nave *et al.* (1981) 143 μg sample.

[h] Moore *et al.* (1986) fcc, two samples of 6 and 53 μg.

[i] Moore *et al.* (1986) rhombohedral, three samples of 25, 42, and 100 μg.

[j] Chang *et al.* (1990) monoclinic, results for two of three freshly prepared samples of mass ranging from 30 to 90 μg.

[k] Chang *et al.* (1990) monoclinic, results for two aged and one of three freshly prepared samples of mass ranging from 30 to 90 μg. The aged samples showed antiferromagnetic behavior.

[l] Fujita *et al.* (1976) fcc, two samples of 8.85 (top) and 5.64 μg (next).

[m] Nave *et al.* (1985) dhcp, two samples of 73.0 and 98.0 μg, average value is given.

[n] Fujita (1969) Cf^{3+} absorbed on ion-exchange beads, three samples of 0.342, 0.806, and 1.190 μg, average value is given.

[o] Moore *et al.* (1986) perovskite type, 24 μg sample.

[p] Moore *et al.* (1986) monoclinic, two samples of 11 and 22 μg.

[q] Moore *et al.* (1986) bcc, 31 μg sample.

[r] Morss *et al.* (1987) bcc, two samples of 3.097 and 1.23 μg, the numbers given in the table are the recommended average of measurements on the two samples, no indication of magnetic ordering was observed down to ∼2 K.

[s] Chang *et al.* (1990) one hexagonal and three orthorhombic samples, masses ranging from 30 to 90 μg, high temperature results did not depend on the age of the samples.

a $\mu_{\text{eff}} = 9.14(6)\mu_B$ was obtained. This value is significantly lower than the expected free-ion value of $10.21\mu_B$ for the ${}^6H_{15/2}$ ground term. The magnetic susceptibilities of a number of compounds of Cf^{3+} have been measured. For the most part, the high-temperature data that could be fit by the Curie–Weiss law gave effective moments that were close to the free-ion value. However, as found before for small samples of highly radioactive isotopes, the low-temperature data were quite complex and sample dependent. Magnetic susceptibility measurements of ${}^{249}Cf$ metal samples were reported by two groups and are listed in Table 20.14. The high-temperature results are in fair agreement although one group reported complex low-temperature data for the metal.

20.12 $5f^{10}; {}^5I_8; Es^{3+}$

Very few measurements have been reported for trivalent Es compounds because of the difficulties associated with measurements on materials with short-lived isotopes. The most abundant isotope of Es is ${}^{253}Es$ with $\tau_{1/2} = 20.4$ days. A magnetic susceptibility measurement was reported for Es_2O_3 in the temperature range 4.2–180 K on an amorphous sample. The data fit the Curie–Weiss law with $\mu_{\text{eff}} = -10.5\mu_B$ and $\Theta = -53$ K. Correcting for the growth of ${}^{249}Bk$ (the sample was 4 days old and contained 13% Bk) gave a value of $10.5\mu_B$, consistent with the free-ion value. Measurements were reported for a 3.25 µg sample of EsF_3 in the temperature range 4.2–200 K 10 days after separation and preparation, which meant there was 31% ${}^{249}Bk$ in the sample. The data were fit with the Curie–Weiss law with $\mu_{\text{eff}} = -10.9\mu_B$ and $\Theta = -37$ K. After correction for the Bk content, the effective moment was $11.4\mu_B$. These measurements on Es samples should be treated conservatively as the true sample temperatures, the container corrections, and ${}^{249}Bk$ corrections lead to large uncertainties (Huray and Nave, 1987).

Elements beyond Es have half-lives that are too short to permit magnetic measurements of metals or compounds by conventional methods discussed here.

20.13 $5f^{11}; {}^4I_{15/2}; Es^{2+}$

The only reported Es metal (a divalent metal) magnetic measurement was made on a 0.25 µg sample. The purity of this sample is questionable since the preparative method may have resulted in an Au–Es alloy. Data were taken for

---

[t] Nave et al. (1987) and Moore et al. (1988) orthorhombic form obtained after melting the hexagonal samples, two polycrystalline samples of mass of 12.3 and 19.3 µg, exhibits metamagnetic behavior at low temperatures.
[u] Nave et al. (1987) and Moore et al. (1988) hexagonal, two microcrystalline samples of mass of 12.3 and 19.3 µg, exhibits metamagnetic behavior at low temperatures.
[v] Karraker and Dunlap (1976) 2.37 mg of ${}^{249}Cf^{3+}$ diluted in $\sim$0.2 g of polycrystalline Cs_2NaYCl_6.

this sample with apparent temperature readings from 4.2 to 90 K. In this interval, a local moment of $11.3\mu_B$ was obtained, higher than the $10.2\mu_B$ free-ion value. The authors note the small sample size, large corrections for the sample holder, and uncertainty in the sample temperature due to self-heating as well as corrections for ^{249}Bk growth lead to a large uncertainty in the measured value (Huray and Nave, 1987).

The EPR spectrum at 4.2 K of $^{253}Es^{2+}$ diluted in CaF_2 was reported by Edelstein and coworkers (Edelstein *et al.*, 1970; Edelstein, 1971) and used to identify the stabilization of this oxidation state by the CaF_2 host. The measured g-value of 5.809 ± 0.005 identified the ground state as a Γ_6 (O_h) state. Subsequently, Boatner *et al.* (1976) found that the ground state of $^{253}Es^{2+}$ diluted in $SrCl_2$ had a g-value of 6.658 ± 0.003, which was assigned to the Γ_7 (O_h) state. Boatner *et al.* (1976) also reported the EPR spectrum of $^{253}Es^{2+}$ diluted in BaF_2, which was similar to that of Es^{2+} in CaF_2. Thus, the ratio of the crystal field parameters changed on going from CaF_2 or BaF_2 to $SrCl_2$, causing the ground state to switch. Analogous behavior had been found for the $4f^{11}$ ion, Ho^{2+}, in the same host crystals. The magnitude of the measured g-values is smaller than expected, and has been attributed primarily to covalency effects (Edelstein, 1971; Boatner *et al.*, 1976).

20.14 THE ACTINIDE DIOXIDES

Starting with the actinide oxides, AnO_2, one would intuitively expect that the situation might be relatively simple. If one takes oxygen as divalent, then an ionic compound can be made with An^{4+} and $2O^{2-}$. Indeed, from many considerations this appears a good approximation. All compounds have the well-known fcc CaF_2 fluorite structure. (See Chapter 15, Table 15.9, for a list of lattice constants.) This apparently simple cubic structure belies the complications that occur for the different oxides. As in so many cases, the devil is in the details. Despite half a century of effort, there remain many puzzles in the actinide dioxides, and they will be discussed at some length in this article. The magnetic properties should reflect this ionic nature, i.e. for UO_2 a $5f^2$ configuration is anticipated with a crystal-field splitting that gives a well-defined ground state.

20.14.1 Uranium dioxide

Early work on the magnetic susceptibilities of solid solutions of UO_2 in ThO_2 (cubic symmetry) was interpreted as showing 'spin only' behavior for the d^2 configuration on extrapolation to infinite dilution. Subsequently Hutchison and Candela (1957) showed that a model based on the $5f^2$ configuration with a strong spin–orbit interaction and the ratio of the crystal field parameters such that the Γ_5 (O_h) triplet state is lowest would also fit the observed magnetism. Ordered magnetism of UO_2 was first suggested by Jones *et al.* (1952) from their
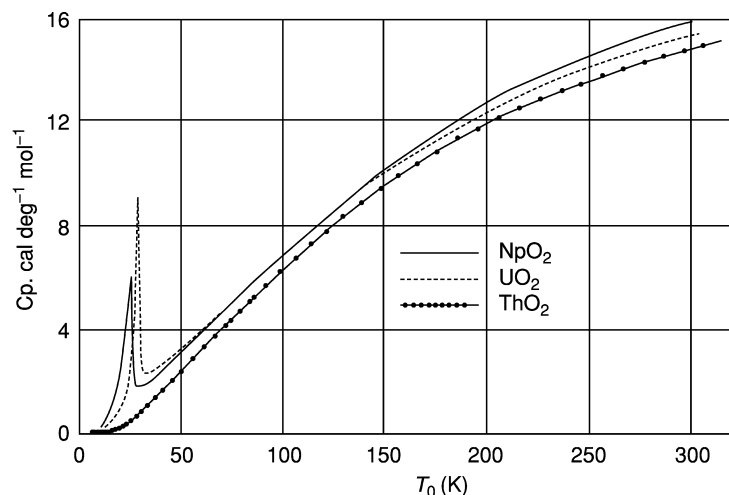
Fig. 20.7 *Heat capacities of* ThO_2, *UO_2, and NpO_2. Figure reprinted with permission from Osborne and Westrum* (1953). *Copyright* 1953 *by the American Institute of Physics.*

heat capacity measurements. Within a year, the heat capacities of ThO_2, UO_2, and NpO_2 were measured (Osborne and Westrum, 1953) and are reproduced in Fig. 20.7. These showed important anomalies for UO_2 and NpO_2, at 30 and 25 K, respectively. The assumption, of course, was that both materials exhibited a phase transition to a magnetically ordered state. Although magnetic susceptibility measurements were made on UO_2 in 1950, the best data were presented by Arrott and Goldman (1957). They showed that the magnetic phase transition disappeared when additional oxygen entered the lattice to the level of $UO_{2.07}$. Almost a decade then passed before the microscopic proof of antiferromagnetism was given by neutron diffraction. Two papers were published essentially simultaneously, Willis and Taylor (1965) and Frazer *et al.* (1965). Both reported work on single crystals and showed that UO_2 has a first-order transition to an antiferromagnetic state at 30.8 K. The uranium moments (of $1.75\mu_B$ at 5 K) are aligned in alternating ferromagnetic (100) sheets in a sequence $+ - + -$. The magnetic repeat may be characterized by a wave vector of $\mathbf{k} = 1$, i.e. the magnetic and chemical unit cells are the same. The magnetic moments are perpendicular to the propagation direction, i.e. $\boldsymbol{\mu} \perp \mathbf{k}$, in what may be described as a transverse structure (Fig. 20.8). These experiments, the availability of single crystals, and the increasing interest in f-electron magnetism ushered in the 'golden era' of experiments on UO_2, essentially the period from 1965 to 1980. Blume (1966), assuming a model where the electronic structure of U^{4+} consisted of a nonmagnetic singlet ground state with a low-lying magnetic triplet state and including bilinear isotropic exchange interactions, was able to account semiquantitatively for the first-order magnetic phase transition (see also
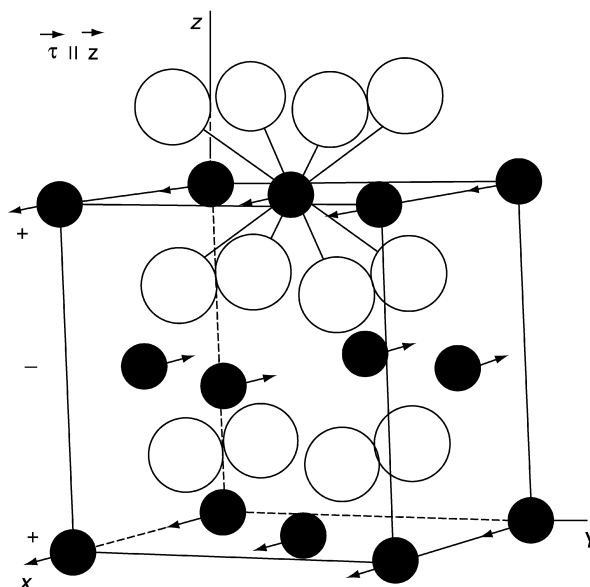
Fig. 20.8 *Magnetic structure of UO$_2$. The open circles are oxygen and the closed circles are uranium. In the arrangement shown the propagation direction* **k** *= [001],* (**k** *and* **τ** *are equivalent) and the moments are transverse to this direction. There are two domains, one with μ ∥ [100], and the other with μ ∥ [010]. Figure reprinted with permission from Faber and Lander (1976). Copyright 1976 by the American Physical Society.*

Alessandrini *et al.*, 1976). Rahman and Runciman (1966) showed that this was unlikely, their full manifold calculation showed that the crystal field ground state was most probably the triplet Γ_5. This could also explain the moment (which should be 2.0μ_B for a pure $^3H_4$ ground state) as the mixing of higher L and S components would tend to reduce the ordered moment. They obtained crystal field parameters $V_4 = -409$ meV and $V_6/V_4 \sim -0.06$. They could not easily explain the first-order phase transition, but did predict a splitting of $\sim$171 meV between the ground state and the doublet Γ_4 and $\sim$630 meV to the next excited crystal field state. Neutron inelastic scattering was incapable of verifying these energy splittings in the 1960s and the opaque character of UO$_2$ make the optical technique of limited value. However, on a lower energy scale, neutrons had already been used to measure the complete phonon dispersion spectra at room temperature (Dolling *et al.*, 1965). At lower temperature, the neutron inelastic experiments by Cowley and Dolling (1968) showed a possible strong interaction between the magnons and the lattice, and this was reinforced by the elastic constant measurements as measured by Brandt and Walker (1967, 1968). Interestingly, they showed that the c_{44} elastic mode actually started to soften just below room temperature, and showed a strong minimum at the phase

transition. Within a year, in two remarkable papers, Allen (1968a,b) proposed a theory for the spin–lattice interaction in UO_2 that was based on a Jahn–Teller (JT) interaction and first introduced the idea of *quadrupole* interactions in the actinides. Allen proposed that the quadrupoles ordered and would thus give rise to an internal strain that would lead to a change in the position of the oxygen atoms without giving rise to an external change in the symmetry of UO_2. No measurements had found evidence for a large *external* (i.e. a lowering of the overall cubic symmetry) crystallographic distortion at the phase transition. Pirie and Smith (1970), using X-rays, searched for possible shifts of the U-atoms, but in such a measurement any oxygen shift would have been impossible to observe.

Following the work of Allen, an important paper was published by Sasaki and Obata (1970) giving new insights into the Jahn–Teller effects that might occur in the oxides. Their essential contribution was to realize that there could also be a *dynamic* JT effect that could occur at temperatures above the phase transition, and by coupling to the lattice this would explain the anomalies found in both the elastic constant work of Brandt and Walker (1967, 1968), and the susceptibility measurements of Arrott and Goldman (1957).

There is no evidence that the neutron experts understood the theory of Allen, which was advanced for its time, or Sasaki and Obata's work. It was not until 1975 that the internal distortion of the oxygen cage was discovered with neutron diffraction in the course of precise measurement of the intensities from a single crystal (Faber *et al.*, 1975; Faber and Lander, 1976). The experiment was designed to study something completely different, the magnetic form factor of U^{4+} at high values of Q, and the observation of the oxygen internal distortion was accidental! The full theory of this distortion was published by Siemann and Cooper (1979). The exact internal modes proposed by Allen are incorrect, but other modes are found. This does not distract from the originality of Allen's ideas. The coupling of magnetism and internal modes is illustrated in Fig. 20.9. The oxygen displacement from the equilibrium position is 0.014 Å. That such a small movement of the oxygen atoms could be measured is an example of how the neutrons are sensitive to light atoms in the presence of heavy ones.

The next step in the UO_2 saga came with the experiments on many actinide compounds at the Commissariat à l'Energie Atomique (CEA) in Grenoble, France during the period 1977–87 under the leadership of J. Rossat-Mignod. This group determined that many of the NaCl-type actinide compounds had a more complicated form of magnetic structure than originally proposed (Rossat-Mignod *et al.*, 1984). Instead of having a single **k** propagation vector in a certain volume of the crystal, a number of symmetry equivalent **k** vectors coexist in the same volume of the crystal. UO_2 was determined to have a triple **k** magnetic structure both by cooling the material in a magnetic field, as well as by applying uniaxial stress to the sample. This does not change the understanding of the magnetic structure or internal distortion, as long as one realizes that only one component of the moment and distortion are shown in Figs. 20.8 and 20.9. It did, however, lead to a reinterpretation of the magnon dispersion curves of
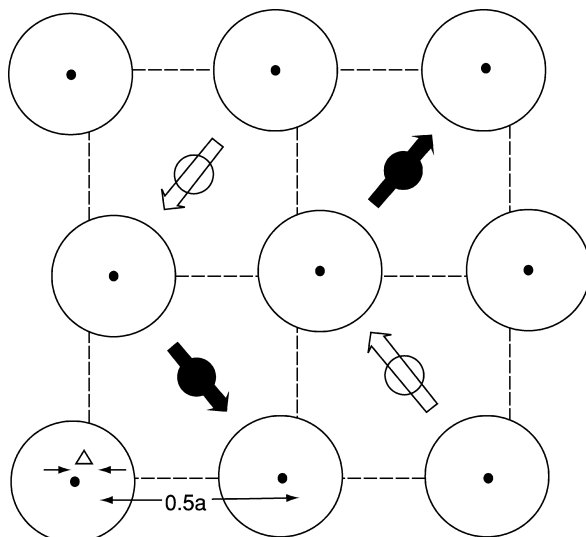
Fig. 20.9 *The* (001) *projection of the fluorite structure. The large circles represent oxygen atoms at z = 1/4 and 3/4 displaced from the ideal fluorite structure (indicated by the dashed lines). The shift of the oxygen atoms is not drawn to scale, Δ = 0.014 Å. The smaller closed and open circles represent the uranium atoms at z = 0 and 1/2, respectively. The arrows indicate the directions of moments for the four sublattice antiferromagnetic structure. Figure reprinted with permission from Faber and Lander (1976). Copyright 1976 by the American Physical Society.*

Cowley and Dolling (1968) and Giannozzi and Erdos (1987). However, efforts to reproduce the dispersion of the magnons (discussed later), despite the **3k**-structures were not successful. Apparently some element was still missing in the understanding of these curves.

During this period many other experiments were, of course, conducted on UO_2. It is a semiconductor with a band gap of ~2 eV, and much of the electronic structure aspects were reviewed by Schoenes (1980) and by Brooks *et al.* (1984). There is little doubt from photoemission that the 5f states are considerably removed from the Fermi level E_F in UO_2. They are measured at 1.4 eV below E_F, a strong indication of the localization of the $5f^2$ state. Kelly and Brooks (1987) have shown that the local density approximation can account for the lattice parameter and estimate the width of the valence band. However, these electronic structure calculations show also that the simple concept of an ionic solid is not a good approximation in any of the light actinide oxides. There is appreciable mixing of the actinide 6p states with the 2p states of oxygen resulting in a measure of covalency for all actinide oxides.

In examining the optical properties (Schoenes, 1980) the localized nature of the 5f electrons in UO_2 also became apparent, and many features of the

electronic structure were observed as interband transitions. One extraordinary effect, shown in Fig. 20.10a was the presence below T_N of intense and sharp peaks at 151 and 154 meV. Schoenes identified these as two-phonon excitations as they are at exactly double the highest energy longitudinal optic (LO) modes involving principally oxygen atoms as measured by Dolling *et al.* (1965). The question is why they should be so strong and temperature dependent
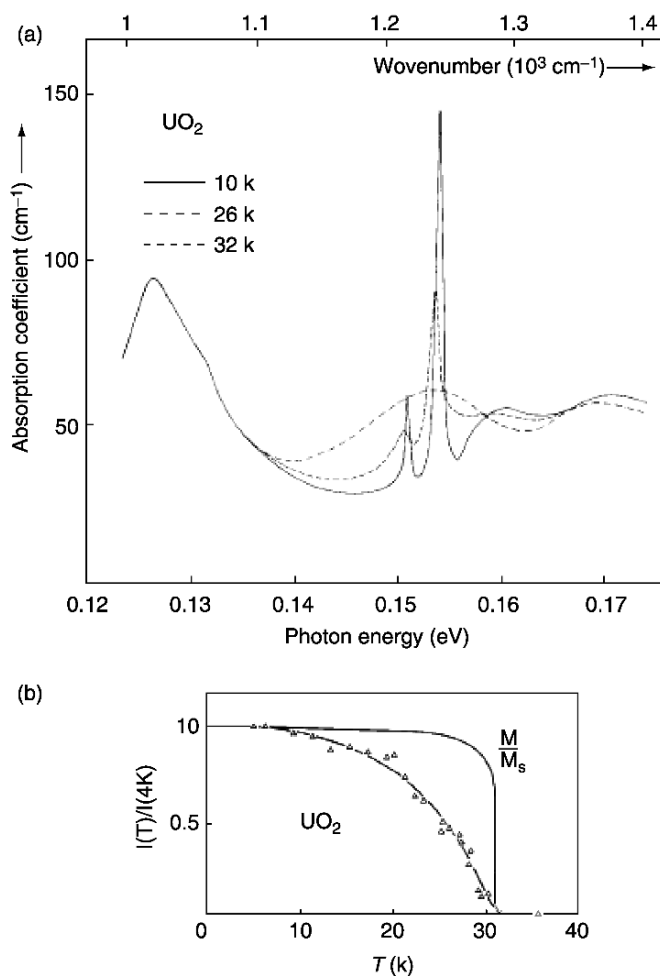
Fig. 20.10 (*a*) *The absorption coefficient of UO$_2$ measured in optical spectroscopy for various temperatures above and below $T_N = 30.8$ K. The sharp peaks at 151 and 154 meV are thought to be multiphonon excitations. (b) The temperature dependence of the area of the 154 meV peak compared to the normalized sublattice magnetization as measured by neutrons. Reprinted from Schoenes (1980), Copyright 1980 with permission from Elsevier.*

(see Fig. 20.10b)? As found from the experiments that will be described for NpO$_2$ (see below), it now appears that these excitations are a consequence of the LO phonon coupling to the quadrupolar distortion induced by the 5f quadrupole moment around the uranium nucleus. The fact that the *T*-dependence is continuous rather than discontinuous, as seen in the sublattice magnetization, suggests that the quadrupole coupling is a higher-order effect, and the dipole ordering is the primary-order parameter. It would seem worthwhile to measure this LO phonon as a function of temperature with neutron inelastic scattering.

Rahman and Runciman (1966) utilized the crystal field model to predict that there was a large splitting of the $^3H_4$ ground state manifold, with the first excited state being at least 150 meV above the ground state. With the advent of spallation neutron sources in the early 1980s, these types of crystal field energies became accessible, and the first indication for crystal field excitations in UO$_2$ was published in 1985 (Kern *et al.*, 1985). *Two* excitations were observed at 155 and 172 meV, whereas only *one* was expected according to the Rahman and Runciman calculation. These authors suggested that the R&R calculations might still be correct but that the V_6/V_4 ratio might be rather different from the –0.06 suggested by Rahman and Runciman. Three years later, using the more powerful spallation source ISIS near Oxford in UK, Osborn *et al.* (1988) showed that the crystal field spectra of UO$_2$ consisted of *four* excitations spread over the range 152–183 meV; these are shown for various temperatures in Fig. 20.11. They also searched up to energy transfers of 800 meV, but found no evidence of further transitions. The first point to note is that in the crystal field model for the $^3H_4$ multiplet there should be only two transitions in the ground state multiplet. (Transitions from Γ_5 to Γ_3 and Γ_4 are allowed, but not to Γ_1.) Since the overall multiplet is now within 180 meV, rather than the ∼700 meV proposed by Rahman and Runciman, the crystal field interaction is much weaker than in the Rahman and Runciman model. In a detailed paper, Amoretti *et al.* (1989) showed that $V_4 \sim$ –123 meV, less than 1/3 that was proposed by Rahman and Runciman, and V_6/V_4 = –0.21. The extra lines (above the two expected) arise from the lowering of the symmetry due to the internal distortion of the oxygen cage (Fig. 20.9). Amoretti *et al.* (1989) were able to show that the spectra are better explained with a 3**k** magnetic structure (physical displacements along ⟨111⟩) rather than a 2**k** model (physical displacements along ⟨110⟩). Interestingly, one can see that the four lines are still present *above* T_N, whereas there is no longer a static distortion of the oxygen cage. However, dynamic effects are still present, as pointed out by Sasaki and Obata (1970), and these will give rise to a splitting of the crystal field levels, although it is noticeable that the transitions are starting to broaden in width by 35 K.

Following this direct measurement of the crystal-field splitting, the theorists returned to the fray and showed that the smaller value of V_4 (as compared to the original calculations of Rahman and Runciman) could be understood (Gajek *et al.*, 1988; Rahman, 1998). The latter paper shows that the ground state is ∼90% $^3H_4$, justifying the approximations made in interpreting the neutron
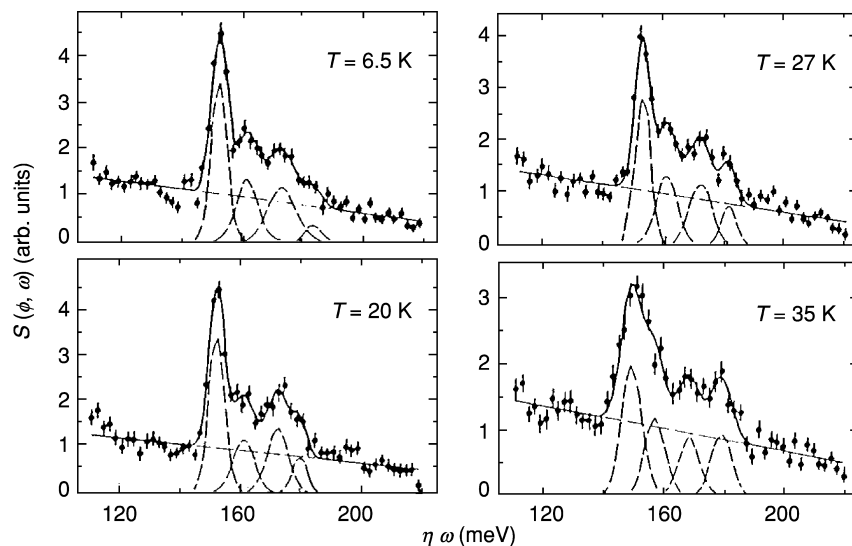
Fig. 20.11 *Neutron spectra measured with an incident energy of* 290 meV *for different temperatures between* 6.5 *and* 35 K, *where* $T_N = 30.8$ K. *The smooth line is the fit to four Gaussian line shapes and a sloping background. These five components are shown by the dashed lines. Figure reprinted with permission from Amoretti* et al. (1989). *Copyright* 1989 *by the American Physical Society.*

spectra. The moment calculated is $1.94\mu_B$, only a small reduction from the $2.00\mu_B$ in the simple Russell–Saunders coupling for the Γ_5 ground state. The reduction from 1.94 to $1.75\mu_B$ is thus due to the JT effect, as discussed above. All of this established beyond doubt that the ground state was the triplet Γ_5.

For the ground states of the heavier actinides, more mixing of excited states into the ground state is expected, but this work on UO_2 shows that although taking into account intermediate coupling (mixing of excited L and S values) is necessary, J-mixing is probably not so important for *any* ground state properties of the actinides. This result suggests many of the earlier calculations, e.g. Chan and Lam (1974) were not relevant. Furthermore, this has important implications for studies of intermetallics compounds, which are not covered in this review (but see Chapter 21 and Vol. 17, 19, and 32 of *Handbook of Physics and Chemistry of the Rare-Earths*). Because the conduction-electron states in intermetallic compounds are known to shield the crystal field interactions, the crystal field parameters are expected to be *lower* than in the actinide oxides. Thus it is expected that crystal-field splittings in intermetallics should be in the range 20–50 meV, as compared to 150 meV in UO_2. The range for intermetallics is thus excellently matched to neutron spectroscopy, and in practice this has been found (Holland-Moritz and Lander, 1994). However, when the crystal field transitions in intermetallics are *not* observed with neutron spectroscopy, it

cannot be argued that the crystal field transitions are outside the range of neutron spectroscopy. More subtle interactions, due to the hybridization of the 5f electrons with the conduction-electron states, are involved.

An elegant NMR study has been performed at low temperature on both the ^{235}U and ^{17}O NMR nuclei in UO_2 (Ikushima *et al.*, 2001). The results lend support to the idea of a 3**k** magnetic structure in UO_2 below T_N. Furthermore, Ikushima *et al.* (2001) give strong evidence for a local distortion driven by the U quadrupoles, and an excitation spectrum that shows the presence of magnon–phonon coupling.

The understanding of UO_2 is almost complete, but there are still the magnon dispersion curves, first measured in 1968, that still defy a complete theoretical interpretation, despite the realization of the 3**k** state. Again, new neutron technology has come into play, in this case in the ability to have enough neutron intensity to analyze the polarization of the scattered neutrons. Briefly, when a neutron is scattered from a magnetic moment the spin state of the neutron is *changed*; on the other hand, when the neutron is scattered from a nucleus, the spin state is *unchanged*. With a sufficiently large single crystal of UO_2, it proved possible to examine the magnon dispersion curves with polarization analysis, and the results are shown in Fig. 20.12 (Caciuffo *et al.*, 1999). The hope in these
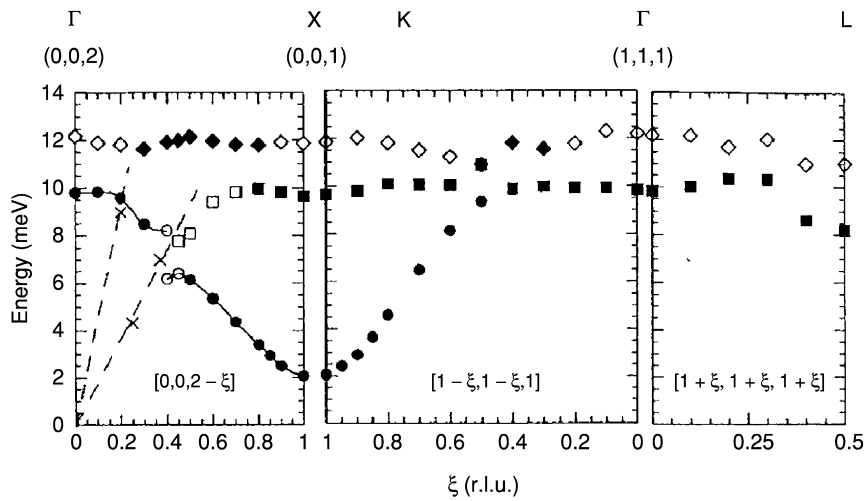
Fig. 20.12 *Magnon dispersion curves of UO_2 measured at* 16.5 K *along the principal crystallographic directions. The broken lines and crosses correspond to acoustic phonon branches measured at* 270 K. *Open symbols indicate a qualitatively smaller magnon intensity than the filled points. In all measurements the neutron spin state was spin flip, i.e. changed, and the nonspin-flip cross section was found negligible. Figure reprinted with permission from Caciuffo* et al. (1999). *Copyright* 1999 *by the American Physical Society.*

experiments was that a 'mixed' mode would be found to identify the famous magnon–phonon coupling first proposed by Cowley and Dolling (1968). No sign of this interaction was found. However, if it occurs in the region $\xi \sim 0.5$ in the $\left[00\bar{2}\xi\right]$ zone, then it is difficult to observe as the intensity drops to almost zero, for reasons that are not immediately clear. Theory is still unable to reproduce the magnon dispersion curves. This is certainly the most important question to resolve before a complete understanding of the magnetism of UO_2 is achieved.

In this long story of the magnetism of UO_2 not a word has been said about the new technique of RXS. In a sense this technique came too late! One discovery still needing confirmation in UO_2 is the presence of the quadrupole moments. Rather than treat this here, it is more appropriate to raise it after the discussion of NpO_2 (below). However, one interesting story using synchrotrons is worth recounting. The signal from uranium in resonant magnetic scattering is so strong (see Fig. 20.2 and discussion) that it opens the possibility for doing different kinds of experiments. One of these is the possibility of observing the scattering from *surface magnetism* in UO_2. Experiments of this sort to study the surface *charge* arrangements are common with synchrotrons, but are extremely rare for *magnetism* because they require scattering from a very small magnetic volume near the surface of the material. After many efforts involving surface preparation and different experiments, *surface magnetic scattering* was observed from UO_2 (Watson *et al.*, 1996). Strictly speaking, the parameters investigated have little specific to UO_2; they concern what happens near the surface of an antiferromagnet that undergoes a discontinuous phase transition in which the magnetism melts. One of the more interesting aspects is that as emphasis is put more and more on the surface layers it is found that the phase transition is in fact continuous. The crucial data are shown in Fig. 20.13. Although it is not strictly correct to interpret the different values of the L index in Fig. 20.13 as representing different depths into the antiferromagnet, as a first approximation it is acceptable. The bulk magnetism signal (similar to that observed with neutrons) is shown at (001). The model of magnetism near the surface in UO_2 is that near the phase transition, the top few surface layers lose their magnetism, and below them is an interfacial layer of reduced moments that grows in spatial extent as the temperature approaches T_N. These results are in agreement with some of the theories, based on symmetry arguments, but in disagreement with a simple melting transition, which is observed for ferromagnets. That there is a difference is perhaps not surprising as a ferromagnet has a net magnetization, which couples to the lattice, whereas such an interaction is absent in an antiferromagnet. More recent experiments have gone on to study the roughening of the magnetic order just before the phase transition. Interestingly, such studies are relevant to a current problem in magnetic multilayers, viz. the interplay of charge and magnetic roughness in defining the interfacial structure of the multilayers.
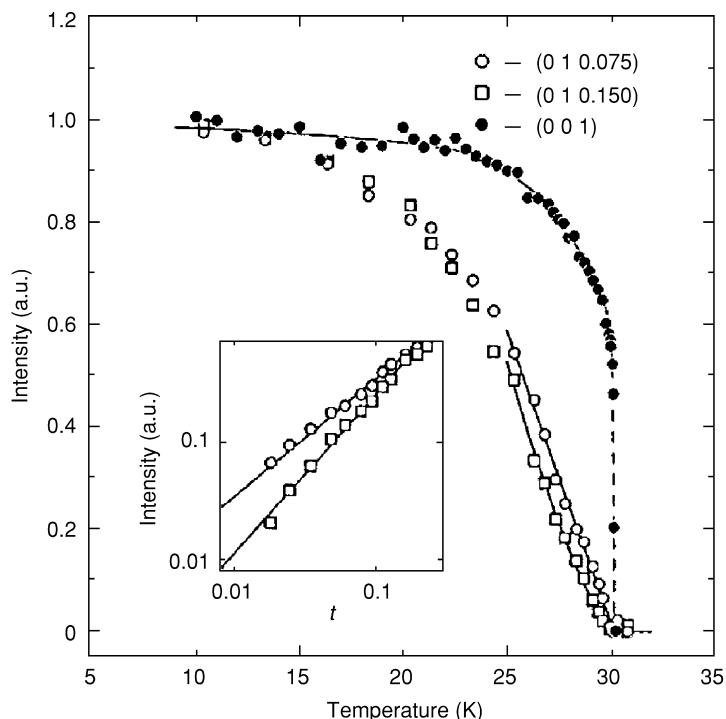
Fig. 20.13 *Temperature dependence of the magnetic scattering at the* (001) *bulk Bragg reflection* (*solid circles, which agrees with neutrons*) *and at various positions along the* (01L) *magnetic truncation rod* (*open symbols*). *Essentially one can think of these data having a greater component of the surface as L increases. Data are normalized to unity at low temperature. Inset: log–log plot of the scattering intensity at two different positions along the* (01L) *rod as a function of reduced temperature. Figure reprinted with permission from Watson* et al. (2000). *Copyright* 2000 *by the American Physical Society.*

20.14.2 Neptunium dioxide

Progress in understanding was slow and steady over the last 50 years in the study of UO_2. Not so with NpO_2. The problem turned out to be considerably more complicated. The story starts with the same paper on the heat capacity from Osborne and Westrum (1953) (Fig. 20.7). Since NpO_2 has a $5f^3$:Np^{4+} configuration, the ground state is $^4I_{9/2}$, a Kramers' ion in which the lowest ground state must be a magnetic doublet. This means given even the smallest amount of magnetic exchange the compound should order magnetically as no crystal field interaction can induce a singlet (nonmagnetic) state. The transition at $T_o = 25$ K in the heat capacity was thus assumed to be due to magnetic ordering. Note that the entropy at the transition (area under the curve) is very similar for both UO_2 and NpO_2, reinforcing the supposition of

ordered magnetism in both. Magnetic susceptibility measurements by Ross and Lam (1967) showed a strong peak at T_o, again suggesting antiferromagnetic order, as in UO_2. The first surprise came when neutron diffraction (on polycrystalline samples) by Cox and Frazer (1967) and Heaton *et al.* (1967) failed to find any change in the diffraction pattern on cooling below 25 K. They put an upper limit of $\sim 0.4\mu_B$ on any possible moment, much less than expected from the $5f^3$ ground state quartet. This limit was drastically reduced by the Mössbauer experiments of Dunlap *et al.* (1968) that showed that there was a very small amount of line broadening developing below T_o. When interpreted in terms of magnetic dipole ordering, this line broadening suggested a moment of $\sim 0.01\mu_B$. At that time, in the 1960s, a moment so small was unheard of, so the problem remained unsolved. The discovery of the internal distortions in UO_2 in the mid-1970s led those involved, especially theorists, to return to the unsolved mystery of NpO_2. Erdos and coworkers published a number of papers trying to explain the low-temperature magnetic properties of NpO_2 (Erdos *et al.*, 1980; Solt and Erdos, 1980). The essential point was to introduce a *quadrupole* interaction and allow this to cause an internal distortion. The magnetism was then 'removed' by postulating an unusual ground state or other assumptions about the presence of Np^{3+} ions. Since the UO_2 studies had shown that small extra diffraction peaks were present at low temperature as a consequence of the rearrangement of the oxygen atoms, an effort was made to see whether similar peaks could be found from NpO_2. Boeuf *et al.* (1983) reported a null effect, but the crystals of NpO_2 were small (no crystals larger than ~ 2 mm^3 have ever been produced), so these experiments could not be as sensitive as in the case of UO_2. Given the sensitivity of the Mössbauer signal from the ^{237}Np ion, it was not surprising that Friedt *et al.* (1985) returned to this technique and made a series of precise measurements down to 1.5 K, including applying a magnetic field. They suggested that there was *no* dipole magnetism at all, and that all the effects could be explained by a JT distortion of the oxygen cage. However, since this had not been observed in the experiments of Boeuf *et al.* (1983), they suggested that the distortion should be dynamic in nature. If it were, then this should give rise to a change in the phonon spectra, which might be reflected in the thermal parameters at low temperatures. Caciuffo *et al.* (1987) searched for any such changes, but without success.

By this time experimentalists were unenthusiastic about working on NpO_2, but it seemed at least important to establish the crystal field parameters, as there had been the suggestion that NpO_2 was not even Np^{4+} (Zolnierek *et al.*, 1981). The first attempts by Kern *et al.* (1988) showed that any crystal field peaks were broad, much broader than the experimental resolution. The problem needed the higher intensity of the ISIS (UK) source and this experiment was performed by Amoretti *et al.* (1992). The data and fits are shown in Fig. 20.14. Clearly these are less convincing than those found for UO_2 (Fig. 20.11). Any crystal field scheme with Np^{4+} predicts the highest Γ_6 state at well over 200 meV and the matrix element is small. The transition(s) observed, therefore, must be between
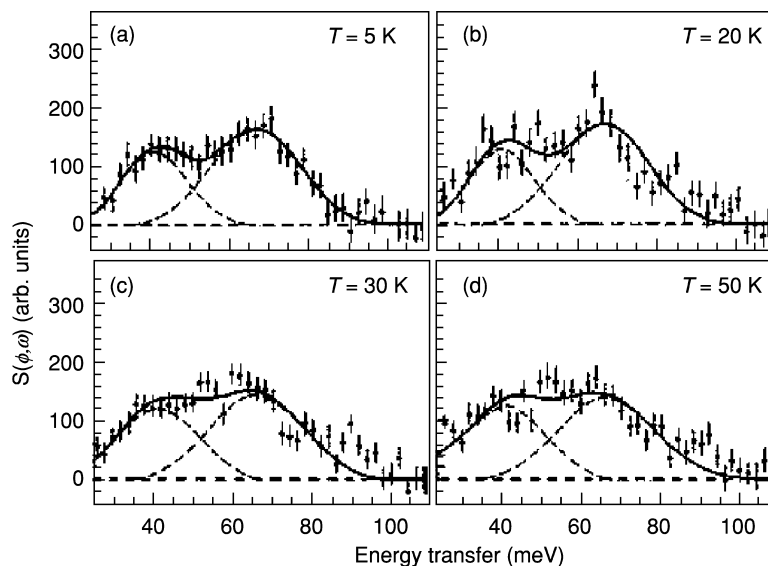
Fig. 20.14 *Neutron inelastic magnetic scattering cross section for NpO₂ as a function of temperature. The incident neutron energy was* 180 meV *and the average scattering angle* 5°. *The phonon contribution, which is small at these angles, has been subtracted. The full curve is a fit to the data of two Gaussians* (*shown as broken curves*) *plus a background. Reprinted from Amoretti* et al. (1992). *Copyright* 1992 *with permission from Elsevier.*

the two Γ_8 states. The extent of this splitting, around 55 meV, with evidence for a splitting of the peak as observed in UO_2, is completely consistent with the V_4 parameter deduced for UO_2, after taking into account the change in the cation. Amoretti *et al.* (1992) also made measurements at lower energy and saw an interesting effect as the temperature was lowered through T_o, which is shown in Fig. 20.15. The transition must correspond to the splitting of the ground state Γ_8 quartet below T_o. It thus appeared after these measurements that the crystal field parameters were as expected (based on UO_2) for NpO_2 and one really had a Np^{4+} ion (as the chemists and the Mössbauer spectroscopists insisted all the time!) and there was a need for a new idea.

Muon spectroscopy (Kalvius *et al.*, 2001) is also sensitive to the presence of dipole moments. The difficulty with this method is that there is always some uncertainty about at which point the muon annihilates, giving rise to the measured signal. However, Kopmann *et al.* (1998) showed that the signal from magnetic ordering was readily observed in UO_2 and went on to observe a small effect in NpO_2. Again, as with the neutron signal shown in Fig. 20.15, there is an 'effect' at T_o, but if it was dipole moment ordering, then the Mössbauer spectroscopy would have observed it.

Given the huge sensitivity to magnetism in 5f shells that was discussed in connection with RXS (see Fig. 20.2), one of the first samples to try with this
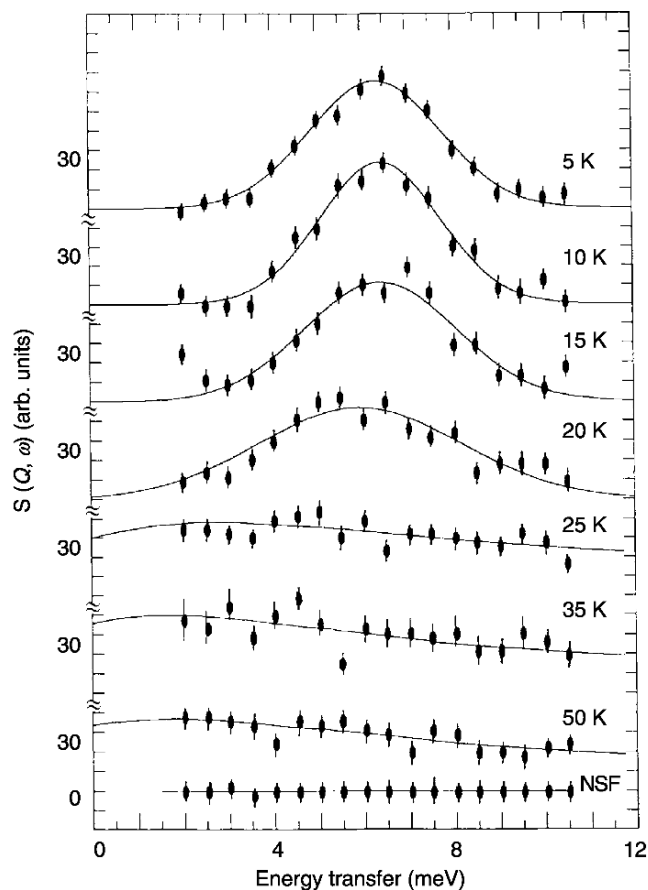
Fig. 20.15 *Evolution of the spin-flip scattering (i.e. the neutron spin state is changed on scattering indicating a magnetic cross section) as the temperature is lowered through the 25 K transition in NpO₂. The momentum transfer is Q = 1.3 Å⁻¹ and the sample is polycrystalline. The solid lines are fits to the data with a Gaussian function. The transition energy is 6.3 meV. Reprinted from Amoretti et al. (1992). Copyright 1992 with permission from Elsevier.*

technique was NpO_2, once the problem of looking at transuranium samples at the ESRF in Grenoble was solved. A large signal was indeed observed below T_o by Mannix *et al.* (1999). Because Mannix *et al.* (1999) did not have all the necessary tools to analyze the polarization of the scattered photons, they were cautious in ascribing this signal to dipole ordering, and, of course, the RXS technique cannot relate the intensity of the scattering to the magnitude of the dipole moment. They did, however, measure the dependence of the scattered intensity on the photon energy, and this is shown for UO_2 and NpO_2 in

NpO$_2$ and UO$_2$ M$_4$ and M$_5$ Resonances
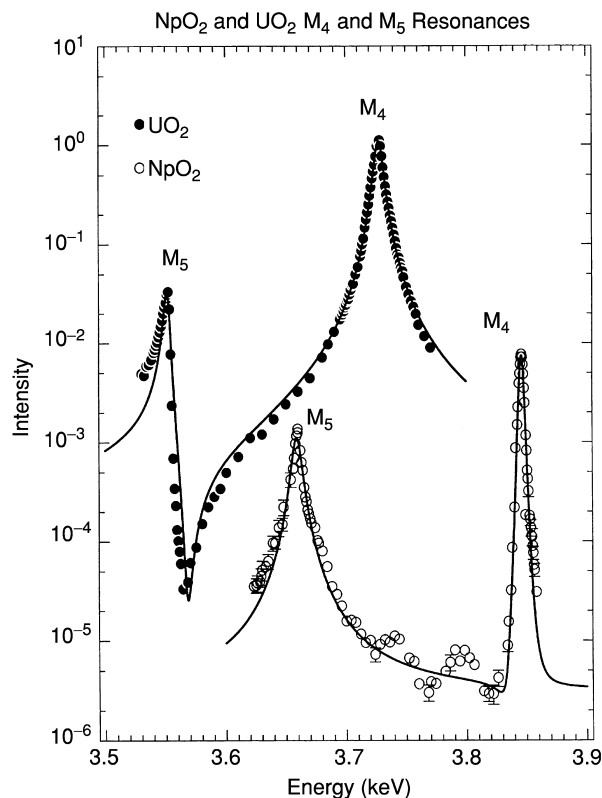
Fig. 20.16 *The energy dependence of the integrated intensity from UO$_2$ and NpO$_2$ as a function of incident photon energy. Note that the signal for UO$_2$ is fit to simple Lorentzian curves, as was the case for UAs, shown in Fig. 20.2. On the other hand, the NpO$_2$ spectra, especially that at the strong M$_4$ cannot be fit to a Lorentzian and requires a Lorentzian-squared function to fit the observed variation. Notice also the different energies for the M$_{4,5}$ edges for U and Np. This allows the RXS technique to be element selective, and one can look at mixed (U,Np)O$_2$ oxides and probe independently the magnetism on the two types of cations. For a study like this see Normile* et al. (2002). *Reprinted from Lander* (2002). *Copyright* 2002 *with permission from Elsevier.*

Fig. 20.16. The energy dependence, which was not published by Mannix *et al.* (1999), as it was not understood, suggested that perhaps the scattering was not simple dipole.

At the same time that these experiments were in progress, Santini and Amoretti (2000) proposed that the ordering in NpO$_2$ was not dipole $\langle M \rangle$ but rather of an octupole $\langle M^3 \rangle$ nature. These can be best understood in terms of the shapes of the resulting charge distributions. For dipole ordering the magnetic moment is a vector quantity but it does not require a distortion of the charge density, which can then remain spherical around the atom. For *quadrupole*

ordering $\langle M^2 \rangle$ there is *no* net magnetic moment as the (even) operator does not destroy time reversal symmetry, however, it does change the shape of the charge density of the electrons around the nucleus. Shapes such as prolate or oblate are typical symmetries of quadrupoles. For octupole moments $\langle M3 \rangle$ time reversal symmetry is broken as the operator is odd; in addition, the charge distributions become even more aspherical. Santini and Amoretti (2000, 2002) proposed this model for NpO_2 to explain the essentially 'zero' of Mössbauer spectroscopy, and yet to have a magnetic operator that would break time-reversal symmetry to explain the results of the muon experiments.

As the capabilities increased at the ESRF synchrotron, it became important to return to these experiments on NpO_2. The new capabilities allowed the polarization of the scattered photons to be analyzed and, at the same time, the crystal to be rotated about the scattering vector while the intensity was monitored. This proved crucial. The scattering at the (001) and (003) reflections, first reported by Mannix *et al.* (1999), were found to originate totally from *quadrupole* charge distributions. This can be understood by both the azimuthal and polarization dependence, see Paixão *et al.* (2002). Furthermore, the absence of either internal or external lattice distortions in NpO_2 implies that the configuration involves 3**k** quadrupole ordering. A schematic picture of this is shown in Fig. 20.17. It is important to realize that the scattering observed here is *not* magnetic in origin. It arises from the aspherical nature of the charge distribution
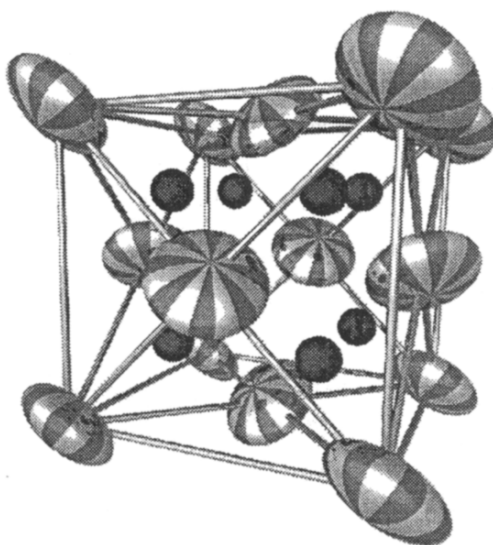
Fig. 20.17 *Crystal structure of NpO_2 in the antiferromagnetic-quadrupole state. The ellipsoids represent the orientation of the local symmetry axis at the Np position, not the actual charge distributions. The oxygen atoms are shown as spheres. Figure reprinted with permission from Paixão et al. (2002). Copyright 2002 by the American Physical Society.*

of the 5f states. The local symmetry around the Np atoms is broken by the quadrupole distribution of the 5f states, and this gives rise to new reflections that are not allowed by the original space group. RXS is a particularly powerful tool as it tells us the nature of the electrons that make up the quadrupole distribution. In this case the strong energy dependence (Fig. 20.16) is related to the particular matrix elements that give rise to the scattering. This particular feature of RXS is becoming more important, and has also been used in the 3d series, see for example, Zimmerman *et al.* (2001). In general this is called Templeton scattering, after the pioneering crystallography of Templeton and Templeton (1985) even before tunable synchrotron beams were available.

This section on NpO_2 will finish by returning to UO_2 and asking whether it would not also be possible to demonstrate directly the presence of the quadrupoles. Indeed, it would be, but in the case of UO_2 there is also strong *dipole* scattering. If both of these occur at the same place in the reciprocal lattice then distinguishing the much weaker quadrupole effects becomes difficult. As far as known, NpO_2 is the only material that exhibits quadrupolar ordering without an ordering of dipoles at the same or a lower temperature. On the other hand, the observation of a temperature-independent susceptibility (Erdos *et al.*, 1980) and the asymmetry in the muon experiments suggests that there exists an operator that lifts time reversal. (This cannot be done by the quadrupole operator as it is even in M.) The only possibility is that there is simultaneous ordering of an octupole moment, but a symmetry analysis has shown that it must be a different type from that proposed by Santini and Amoretti (2000). Observing this is almost impossible with the RXS technique and 5f electrons because the matrix elements will be small. Thus, the saga of NpO_2 is not over completely, but at least the field now is illuminated, as opposed to the darkness surrounding research on NpO_2 for almost 50 years!

20.14.3 Plutonium dioxide

The electronic state of Pu^{4+} is $5f^4$:$^5I_4$ and relatively simple considerations lead to the suggestion that the crystal field ground state might be a singlet Γ_1. (In a simple picture, the crystal field states for Pu^{4+} are simply the inverse of those for U^{4+}.) This idea was strongly reinforced by the first reported measurement of the susceptibility of stoichiometric PuO_2 by Raphael and Lallement (1968). Remarkably they showed that the susceptibility was completely independent of temperature up to 1000 K, with a value 0.54×10^{-3} emu mol^{-1} (after correcting for the small diamagnetism of the radon core). In order to calculate the above value of the TIP from the simple crystal field model, the necessary crystal-field splitting between the ground state (singlet) Γ_1 and first excited (triplet) Γ_4 was found to be ~280 meV. (If χ is temperature independent up to 1000 K, then the magnetically active triplet state must be at least ~2000–3000 K away in energy). The resulting V_4 is approximately –320 meV, and this is not far from the value first proposed for UO_2 (Rahman and Runciman, 1966) of $V_4 \sim$ –400 meV.

Yet, as discussed above, this value was found to be much smaller from experiments on UO_2.

Performing crystal field measurements on PuO_2 with neutrons proved *much* harder than on UO_2. For these measurements, samples of 30–80 g of materials are needed; moreover, it is quite impossible to use the ^{239}Pu isotope for inelastic scattering, so one has to use samples with the rare isotope ^{242}Pu. Still, these measurements were clearly of great importance, and finally a suitable sample (79 g, triply encapsulated) was transported to Intense Pulsed Neutron Source (IPNS) at Argonne and the experiment performed. At least *two* peaks were seen, spread over $\sim$85–125 meV. In the crystal field scheme only *one* transition is expected as the matrix elements for transitions from the Γ_1 singlet state are zero except for the one transition $\Gamma_1 \rightarrow \Gamma_4$. However, by examining the Q-dependence of the scattering it became clear that most of the observed peaks increased in intensity with Q, whereas electronic transitions should decrease with Q. In fact only the transition at $\sim$120 meV appeared electronic and the others were assigned to H-modes from an impurity, probably from water in the PuO_2 (Kern *et al.*, 1990). (Neutron scattering is extremely sensitive to hydrogen and, although these impurities were later detected by infrared spectroscopy, neutrons are still a wonderful analytical tool – if rather expensive – for free or bound H.) This was rather an unfortunate situation, and it took almost a decade to get the sample purified at Los Alamos, and then actually run on the Los Alamos spallation source. However, the result (Kern *et al.*, 1999) merited the wait. A single peak at 123 (4) meV was observed, but with a width significantly greater than the experimental resolution (Fig. 20.18). By calibrating the spectrometer with the known scattering from vanadium, Kern *et al.* (1999) were able to put the scattering on an absolute scale. They then took the crystal field parameters (V_4 and V_6) from UO_2 and extrapolated them to PuO_2 where they predicted a single transition at 115 meV. Moreover, the absolute calculated intensity of the transition also agreed perfectly with the experiment, so this gives considerable confidence to the crystal field parameters.

However, there is now a *major* discrepancy between χ as determined by Raphael and Lallement (1968) and χ calculated from the crystal field scheme. Using the observed V_4 and V_6 parameters, the calculated $\chi = 0.90 \times 10^{-3}$ emu mol^{-1}, a value almost twice as great as measured! Many thought that the 1968 measurement must be wrong, but any impurities in the Pu would normally lead to a *larger* value, and the amount of diamagnetic impurities (e.g. ThO_2) to make the difference exceeded 10% and appeared unreasonable. Recently, this value of the experimental χ has been remeasured (Kolberg *et al.*, 2002) and found to be correct.

Earlier attempts by Goodman (Kern *et al.*, 1990) to question the crystal field scheme and develop a so-called strong coupling approach are still a possibility to explain these results (and those for CmO_2 as discussed below), but they have not yet been fully developed. More recently, Colarieti-Tosti *et al.* (2002) have reported on a first principles calculation of the crystal field scheme, and they
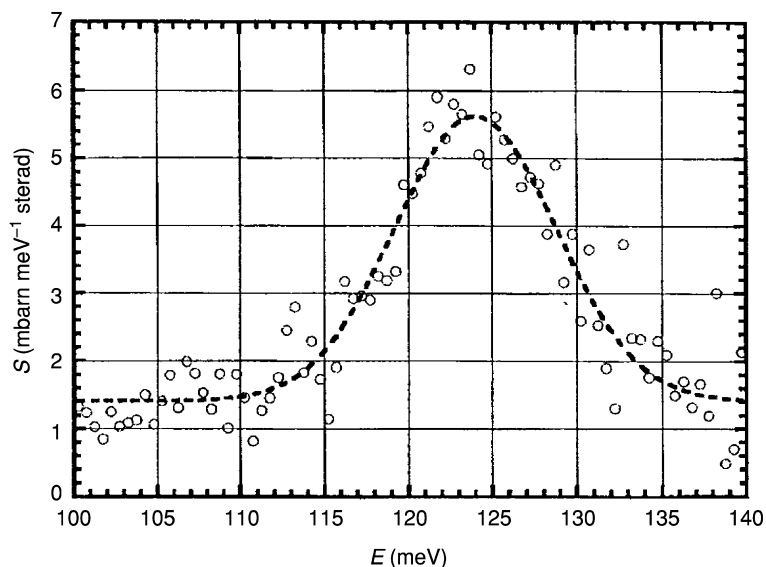
Fig. 20.18 *Neutron inelastic spectra from PHAROS of* 29 g *of* $^{242}PuO_2$ *at* $T = 30$ K. *The incident neutron energy was* 184 meV. *The resolution of the instrument is* ~4 meV *at these energy transfers, but the Gaussian fit gives a width of* 11 meV. *No other electronic signal was found between* 10 *and* 100 meV. *Figure reprinted with permission from Kern* et al. (1999). *Copyright* 1999 *by the American Physical Society.*

arrive at an energy separation $\Gamma_1 \rightarrow \Gamma_4$ ~99 meV, which is relatively close to the observed value of 123 meV. These authors went on to consider the discrepancy between the measured and calculated susceptibility, and they introduced the idea that there is an *antiferromagnetic* exchange interaction between the Pu^{4+} ions, mediated by the admixture of the actinide 6d states into valence band. Knowing that UO_2 orders antiferromagnetically, a rough value of the exchange parameter may be deduced, and then scaled to the case of Pu. The resulting calculations (demonstrated with other data in Fig. 20.19) are in good agreement with experiment, except that they show some curvature for $T > $ ~400 K. It is still difficult to understand what appeared to be the amazingly uninteresting susceptibility of PuO_2 first measured in 1968.

Recently Kolberg *et al.* (2002) have suggested that the dynamical JT effect may play a role also in $(U,Pu)O_2$ materials, as discussed earlier for pure UO_2. Indeed, with this additional interaction agreement between theory and experiment might be possible. All this work shows that the complications in PuO_2 have, like those in the other oxides, now stretched over almost half a century. The broadening of the crystal field transition remains so far unexplained. However, a slight broadening of the excited Γ_4 state could either come from antiferromagnetic exchange or the dynamic JT effect.
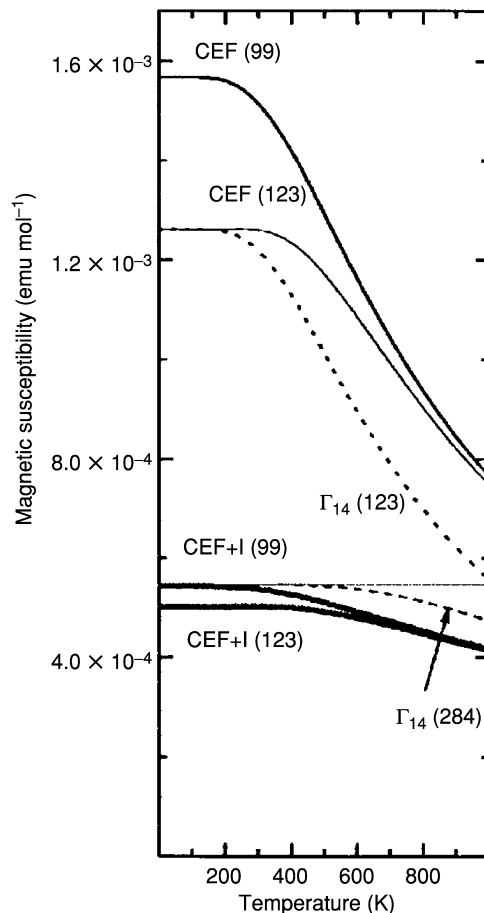
Fig. 20.19 *The magnetic susceptibility of PuO$_2$. The measurements are the T-independent straight dotted line. The calculated bare susceptibility with a single $\Gamma_1 \rightarrow \Gamma_4$ excitation energy of* 284 meV *fits the data at T = 0 and is shown as the dashed line labeled Γ_{14} (284). The corresponding bare susceptibility with $\Gamma_1 \rightarrow \Gamma_4 =$ 123 meV, which fits the neutron experiment, is the dotted line labeled Γ_{14} (123). Adding additional CF transitions to the 123 meV model produces the improvement shown by the solid line labeled CEF (123). Similarly the CEF (99) line uses all the CF transitions with $\Gamma_1 \rightarrow \Gamma_4 =$ 99 meV. The effect of using the antiferromagnetic molecular field deduced from that of UO$_2$ to enhance the bare susceptibility is given by the curves labeled CEF+I. Figure reprinted with permission from Colarieti-Tosti et al. (2002). Copyright 2002 by the American Physical Society.*

20.14.4 Americium dioxide

For the heavier elements starting with Am, experiments become really sparse. Am^{4+} in AmO_2 should have a ground $5f^5$:$^6H_{5/2}$ state, i.e. a Kramers' ion so that the degeneracy cannot be lifted by a crystal field interaction (the same as Np in

NpO$_2$). EPR studies of Am^{4+} doped into ThO$_2$ and CeO$_2$ establish the Γ_7 doublet as the ground state (Abraham *et al.*, 1971; Kolbe *et al.*, 1974) with a g_{eff} = 1.27. Karraker (1975a) has made susceptibility measurements (on a sample with 224 mg of ^{243}Am and a radiation field of $\sim$150 roentgen h^{-1} at the sample!) and found an effective moment of 1.31μ_{B} at low temperature. Since S = 5/2, this gives g = 0.44 which is in excellent accord with the value for a 5f^5 state when intermediate coupling is taken into account (Lander, 1993). With an effective spin of S_{eff} = 1/2, corresponding to the Γ_7 doublet, one obtains g_{eff} = 1.51, in reasonable agreement with the EPR work.

Karraker (1975a) also found clear evidence for a phase transition at T_{o} = 8.5 K. The susceptibility shows a peak and then decreases as the temperature decreases. This was puzzling at the time, as a Mössbauer experiment (Kalvius *et al.*, 1969) had found *no* evidence for any phase transition. Later, Boeuf *et al.* (1979) prepared another sample of ^{243}AmO$_2$ and performed neutron scattering experiments at the Institute Laue Langevin in Grenoble. They observed no magnetic diffraction peaks below T_{o} in agreement with the Mössbauer results. No further experiments have been reported on the low-temperature properties of AmO$_2$ since 1979.

Of course, given what happens in the case of NpO$_2$ (the ordering of the quadrupoles) in a Kramers ion with an odd number of 5f electrons (Paixão *et al.*, 2002), it is easy to suggest that the same thing happens in AmO$_2$. This would make a really beautiful experiment with RXS, but one would need a single crystal, even if only of $\sim$20 μg.

20.14.5 Curium dioxide

With Cm^{4+} the ground state should be a 5f^6 ^{7}F$_0$ state. Since $L = |S| = 3$, there should be *no* sign whatsoever of magnetism, particularly in the susceptibility. The splitting to the first excited state is at $\sim$400 meV, so the susceptibility should be temperature-independent and small. The difficulty is that Cm^{3+} is more stable thermodynamically than Cm^{4+} so it is not difficult to imagine small amounts of Cm^{3+} in the CmO$_2$ matrix. Cm^{3+} has the 5f^7 ^{8}S$_{7/2}$ configuration and so it could contribute $\sim$7μ_{B} of magnetism. Many early efforts on CmO$_2$ reported a sloping susceptibility, but in all cases it was expected that was a consequence of contamination with Cm^{3+}.

In 1986 Morss at Argonne set out to make stoichiometric CmO$_2$ from the rare isotope ^{248}Cm. This had the advantage that the radiation from ^{248}Cm is relatively small compared to the more abundant ^{244}Cm so that radiation damage and production of defects, which could convert Cm^{4+} into Cm^{3+}, were reduced. The sample ($\sim$55 mg) was then studied with neutron diffraction at the IPNS spallation source at Argonne. The small sample and the relatively modest flux at IPNS meant that the strongest powder diffraction peak in CmO$_2$ gave $\sim$1 ct min^{-1}, with a peak/background ratio of 0.6. (Part of the background came from the neutrons emitted from the ^{248}Cm sample itself.) Despite these difficulties,

Rietveld analysis was successful and gave a Cm:O stoichiometry of 1.97 (3), which is statistically insignificant from the stoichiometric composition (Morss *et al.*, 1989). The X-ray pattern from CmO_2 is, of course, totally dominated by the scattering from the Cm, so this is a good illustration of the power of neutrons, where the scattering from curium and oxygen have almost equal scattering lengths. In agreement with X-rays, no evidence of additional phases was found.

Susceptibility measurements were then made and showed, once again, a slope, which corresponded to $\mu_{eff} = 3.36$ (6)μ_B. More than 10 years have gone by since this work and no suggestion has been made to resolve the difficulty between simple crystal field theory (with a $^7F_0$ ground state) and the finite effective moment. However, taking the theory, developed for another *even* 5f electron material (Pu with four 5f electrons), can be utilized by assuming that the susceptibility is affected by the exchange and possibly also JT interactions as found in another even-f system, UO_2. Although $J = 0$, there is an S quantum number of 3 (6f electrons) and the spin state of Cm will give rise to antiferromagnetic exchange via coupling to the excited (magnetic) $J = 1$ state. Detailed calculations for this have not been made, but should be. Furthermore, this effect is not expected to give a constant μ_{eff} for all Cm^{4+} ions. The antiferromagnetic exchange passes through the actinide 6d states and their mixing with the oxygen p-states. This will change depending on the anions involved, for example it will be different for CmO_2 than CmF_4. More experiments on these materials would be interesting and should further increase our understanding of the interactions in the ionic actinide systems. As discussed in Section 20.8, Milman *et al.* (2003) performed density functional theory (DFT) calculations for Cm compounds and suggested that an itinerant magnetism model might be appropriate for CmO_2.

20.14.6 Summary of the magnetic properties of the actinide dioxides

Many physicists have been kept busy for the last half a century studying the properties of the actinide dioxides. Initially it was expected that the data would be relatively straightforward to analyze because of the very simple fcc structure. As happens frequently in actinide research, the trail has been tortuous, and in all cases there are still experiments to be done, although a general understanding of the ground state magnetic properties now appears reasonably sound. Neutron inelastic scattering has played an important role in establishing the crystal field interactions and showing that the earlier theoretical models were incorrect. The crystal field ground states are then perturbed by higher-order interactions, notably the quadrupolar ones, and this is a consequence of the aspherical nature of the 5f electron states. The effect is particularly apparent in NpO_2 ($5f^3$), in which the quadrupoles order at 25 K, presumably because of their interactions with the lattice, and there is *no* accompanying dipole ordering (at least down to 1.5 K). For the moment NpO_2 appears unique in this respect, but no doubt

other materials will be found; AmO_2 appears a good candidate. The interactions with the lattice are very strong for all the oxides, and give rise to a number of effects. Most notably, the Jahn–Teller interactions cause an internal *static* distortion in UO_2, but can be dynamic in nature as well (Sasaki and Obata, 1970). If the susceptibility of PuO_2 ($5f^4$) is reasonably well explained by the indirect exchange through the oxygen p-states (thus implying a measure of covalency in these materials), the situation in CmO_2 ($5f^6$) is more complicated. Perhaps some of the same arguments can be used, together with the JT effect, but it is still not possible to exclude the presence of Cm^{3+} ions in the compound, and these would give a large susceptibility term, as they are $5f^7$. The detailed exchange interactions (measured by neutron inelastic scattering on single crystals, Caciuffo *et al.*, 1999) in UO_2 still are not understood from first principles, illustrating the complexity of the interactions that occur in these oxides.

ABBREVIATIONS

AF	antiferromagnetic
bcc	body-centered cubic
BM (β)	Bohr magneton
^{t}Bu	^{t}butyl – tertiary butyl – $(CH_3)_3C$
CEA	Commissariat à l'Energie Atomique
CF	crystal field
cm^{-1}	wave numbers
Cp	cyclopentadienyl – C_5H_5
dhcp	double hexagonal close-packed
DFT	density functional theory
ENDOR	electron-nuclear double resonance
EPR or epr	electron paramagnetic resonance
Et	ethyl – C_2H_5 – CH_3CH_2
fcc	face-centered cubic
IPNS	Intense Pulsed Neutron Source
JT	Jahn–Teller
LO	longitudinal optic
Me	methyl – CH_3
meV	millielectron volts
mK	milli-Kelvin
NMR or nmr	nuclear magnetic resonance
RXS	resonant X-ray scattering
T_c	temperature below which superconductivity occurs
TIP	temperature-independent paramagnetism
T_N	Neel temperature

T_o	Temperature at and below which a magnetically ordered phase appears
XMCD	X-ray magnetic circular dichroism

UNITS

Two different energy units are used in this review depending on the discussion. The units are meV and cm^{-1}. The conversion between these units is as follows: (1 eV = 8065.479 cm^{-1}); (1 meV = 0.001 eV = 8.065 cm^{-1}); (1 cm^{-1} = 1.2399 × 10^{-4} eV or 0.12399 meV). It is useful to note that kT (where k is the Boltzmann constant) at 300 K = 25.85 meV = 208.34 cm^{-1}.

REFERENCES

Abragam, A. and Bleaney, B. (1970) *Electron Paramagnetic Resonance of Transition Ions,* Clarendon Press, Oxford.

Abraham, M. M., Judd, B. R., and Wickman, H. H. (1963) *Phys. Rev.*, **130**, 611–12.

Abraham, M. M., Finch, C. B., and Clark, G. W. (1968) *Phys. Rev.*, **168**, 933.

Abraham, M. M., Boatner, L. A., Finch, C. B., Reynolds, R. W., and Zeldes, H. (1970) *Phys. Rev. B*, **1**, 3555–60.

Abraham, M. M., Boatner, L. A., Finch, C. B., and Reynolds, R. W. (1971) *Phys. Rev. B*, **3**, 2864

Abraham, M. M., Boatner, L. A., Finch, C. B., Kot, W. K., Conway, J. G., Shalimoff, G. V., and Edelstein, N. M. (1987) *Phys. Rev. B*, **35**, 3057–61.

Aderhold, C., Baumgartner, F., Dornberger, E., and Kanellakopulos, B. (1978) *Z. Naturforsch.*, **33a**, 1268–80.

Aldred, A. T., Cinader, G., Lam, D. J., and Weber, L. W. (1979) *Phys. Rev. B*, **19**, 300–5.

Alessandrini, V. A., Cracknell, A. P., and Przystawa, J. A. (1976) *Commun. Phys.*, **1**, 51–5.

Allen, S. J. (1968a) *Phys. Rev.*, **167**, 492–6.

Allen, S. J. (1968b) *Phys. Rev.*, **166**, 530–9.

Allen, S., Barlow, S., Halasyamani, P. S., Mosselmans, J. F. W., O'Hare, D., Walker, S. M., and Walton, R. I. (2000) *Inorg. Chem.*, **39**, 3791–8.

Almond, P. M., Deakin, L., Porter, M. J., Mar, A., and Albrecht- Schmitt, T. E. (2000) *Chem. Mater.*, **12**, 3208–13.

Amberger, H. -D., Fischer, R. D., and Kanellakopulos, B. (1975) *Theor. Chim. Acta*, **37**, 105–27.

Amberger, H.-D. (1976a) *J. Organomet. Chem.*, **116**, 219–29.

Amberger, H.-D. (1976b) *J. Organomet. Chem.*, **110**, 59–66.

Amberger, H.-D., Fischer, R. D., and Kanellakopulos, B. (1976) *Z. Naturforsch.*, **B31**, 12–21.

Amoretti, G., Blaise, A., Caciuffo, R., Fournier, J. M., Hutchings, M. T., Osborn, R., and Taylor, A. D. (1989) *Phys. Rev. B*, **40**, 1856–70.

Amoretti, G., Blaise, A., Caciuffo, R. C., Di Cola, D., Fournier, J. M., Hutchings, M. T., Lander, G. H., Osborn, R., Severing, A., and Taylor, A. D. (1992) *J. Phys. Condensed Matter*, **4**, 3459–78.

Arliguie, T., Lance, M., Nierlich, M., Vigner, J., and Ephritikhine, M. (1995) *J. Chem. Soc. Chem. Commun.*, 183–4.

Arrott, A. and Goldman, J. E. (1957) *Phys. Rev.*, **108**, 948.

Axe, J. D. (1960) University of California, Radiation Laboratory Report, UCRL-9293.

Axe, J. D., Stapleton, H. J., and Jeffries, C. D. (1961) *Phys. Rev.*, **121**, 1630.

Bacon, G. E. (1962) *Neutron Diffraction,* Oxford University Press, Oxford.

Baybarz, R. D., Asprey, L. B., Strouse, C. E., and Fukushima, E. (1972) *J. Inorg. Nucl. Chem.*, **34**, 3427–31.

Berger, M. and Sienko, M. J. (1967) *Inorg. Chem.*, **6**, 324–6.

Bernhoeft, N., Sato, N., Roessli, B., Aso, N., Hiess, A., Lander, G. H., Endoh, Y., and Komatsubara, T. (1998) *Phys. Rev. Lett.*, **81**, 4244.

Bernstein, E. R. and Keiderling, T. A. (1973) *J. Chem. Phys.*, **59**, 2105–22.

Bernstein, E. R. and Dennis, L. W. (1979) *Phys. Rev. B*, **20**, 870.

Bickel, M. and Kanellakopulos, B. (1993) *J. Solid State Chem.*, **107**, 273–84.

Blaise, A., Genet, M., Chong- Li, S., and Soulie, E. (1986) *J. Less Common Metals*, **121**, 209–15.

Blake, P. C., Lappert, M. F., Atwood, J. L., and Zhang, H. (1986) *J. Chem. Soc., Chem. Commun.*, 1148.

Blake, P. C., Edelstein, N. M., Hitchcock, P. B., Kot, W. K., Lappert, M. F., Shalimoff, G. V., and Tian, S. (2001) *J. Organomet. Chem.*, **636**, 124–9.

Blume, M. (1966) *Phys. Rev.*, **141**, 517–24.

Blume, M. (1985) *J. Appl. Phys.*, **57**, 3615.

Blume, M. and Gibbs, D. (1988) *Phys. Rev. B*, **37**, 1779.

Boatner, L. A., Reynolds, R. W., Finch, C. B., and Abraham, M. M. (1972) *Phys. Lett. A*, **42**, 93–4.

Boatner, L. A., Reynolds, R. W., Finch, C. B., and Abraham, M. M. (1976) *Phys. Rev. B,* **13**, 953–8.

Boatner, L. A. and Abraham, M. M. (1978) *Rep. Prog. Phys.*, **41**, 87–155.

Boerrigter, P. M., Baerends, E. J., and Snijders, J. G. (1988) *Chem. Phys.*, **122**, 357–74.

Boeuf, A., Rustichelli, F., Fournier, J. M., Gueugnon, J. F., Manes, L., and Rebizant, J. (1979) *J. Phys. (Paris), Lett.*, **40**, L335–8.

Boeuf, A., Caciuffo, R. C., Fournier, J. M., Manes, L., Rebizant, J., Rustichelli, F., Spirlet, J. C., and Wright, A. (1983) *Phys. Status Solidi A*, **79**, K1–3.

Bombardi, A., Kernavanois, N., Dalmas de Réotier, P., Lander, G. H., Sanchez, J. P., Yaouanc, A., Burlet, P., Lelievre-Berna, E., Rogalev, A., Vogt, O., and Mattenberger, K. (2001) *Eur. Phys. J. B*, **21**, 547

Boudreaux, E. A. and Mulay, L. N. (1976) *Theory and Applications of Molecular Paramagnetism,* Wiley, New York.

Brandt, O. G. and Walker, C. T. (1967) *Phys. Rev. Lett.*, **18**, 11.

Brandt, O. G. and Walker, C. T. (1968) *Phys. Rev.*, **170**, 528–41.

Brennan, J. G., Andersen, R. A., and Zalkin, A. (1986) *Inorg. Chem*, **25**, 1761–5.

Brodsky, M. B. (1978) *Rep. Prog. Phys.*, **41**, 1547–608.

Brooks, M. S. S., Johansson, B., and Skriver, H. L. (1984) *in Handbook of the Physics and Chemistry of the Actinides* (ed. A. J. Freeman and G. H. Lander), North-Holland, Amsterdam, pp. 153–269.

Brown, D., Lidster, P., Whittaker, B., and Edelstein, N. (1976) *Inorg. Chem.*, **15**, 511–14.

Butler, J. E. and Hutchison, C. A. Jr (1981) *J. Chem. Phys.*, **74**, 3102–19.

Caciuffo, R. C., Lander, G. H., Spirlet, J. C., Fournier, J. M., and Kuhs, W. F. (1987) *Solid State Commun.*, **64**, 149.

Caciuffo, R. C., Amoretti, G., Santini, P., Lander, G. H., Kulda, J., and Du Plessis, P. D. V. (1999) *Phys. Rev. B*, **59**, 13892.

Carnall, W. T., Kanellakopulos, B., Klenze, R., and Stollenwerk, A. (1980) in *Proc. 10eme Journees des Actinides* (eds. B. Johansson and A. Rosengren), pp. 201–16.

Carnall, W. T. (1992) *J. Chem. Phys.*, **96**, 8713–26.

Carra, P. and Altarelli, M. (1990) *Phys. Rev. Lett.*, **64**, 1286.

Chan, S. K. and Lam, D. J. (1974) *in The Actinide Electronic Structure and Related Properties,* vol. 1 (ed. A. J. Freeman and J. B. Darby), Academic Press, New York.

Chang, A. H. H. and Pitzer, R. M. (1989) *J. Am. Chem. Soc.*, **111**, 2500

Chang, C. T., Haire, R. G., and Nave, S. E. (1990) *Phys. Rev. B Condensed Matter*, **41**, 9045–8.

Colarieti-Tosti, M., Eriksson, O., Nordström, L., Wills, J., and Brooks, M. S. S. (2002) *Phys. Rev. B*, **65**, 195102

Collins, S. P., Laundy, D., Tang, C. C., and Cernik, R. J. (1995) *J. Phys. Condensed Matter*, **7**, L223.

Cowley, R. A. and Dolling, G. (1968) *Phys. Rev.*, **167**, 464.

Cox, D. E. and Frazer, B. C. (1967) *J. Phys. Chem. Solids*, **28**, 1649.

Crosswhite, H. M., Crosswhite, H., Carnall, W. T., and Paszek, A. P. (1980) *J. Chem. Phys.*, **72**, 5103–17.

Cunningham, B. B. (1962) Thermodynamics of the Actinides. *Thermodynamics of Nuclear Materials. International Atomic Energy Agency Symposium held in Vienna, Austria, May 21–25, 1962. Proc. Ser. STI/PUB/58*, 61–70.

Dallinger, R. F., Stein, P., and Spiro, T. G. (1978) *J. Am. Chem. Soc.*, **100**, 7865

Dalmas de Réotier, P., Yaouanc, A., Van Der Laan, G., Kernavanois, N., Sanchez, J. P., Smith, J. L., Hiess, A., Huxley, A., and Rogalev, A. (1999) *Phys. Rev. B*, **60**, 10606.

Delamoye, P., Krupa, J. C., Kern, S., Loong, C. -K., and Lander, G. H. (1986) *J. Less Common Metals*, **122**, 59–63.

Dell, R. M. and Bridger, N. J. (1972) in *MTP International Review of Science, Inorganic Chemistry, ser. I, Lanthanides and Actinides,* vol. 7 (ed. K. W. Bagnall), Butterworths, London, pp. 211–74.

Denning, R. G. (1992) *Struc. Bonding* (*Berlin*), **79**, 215–71.

Dolling, G., Woods, A. B. D., and Cowley, R. A. (1965) *Can. J. Phys.*, **43**, 1397.

Dornberger, E., Kanellakopulos, B., Klenze, R., and Stollenwerk, A. H. (1980) Crystal field spectra and magnetic properties of neptuniumtetracyclopentadienide, $(C_5H_5)_4Np$, and triscyclopentadienylneptuniumchloride, $(C_5H_5)_3NpCl$, in *Proc. 10eme Journees des Actinides* (ed. B. Johansson and A. Rosengren), pp. 58–73.

Drifford, M., Rigny, P., and Plurien, P. (1968) *Phys. Lett.*, **27A**, 620.

Dunlap, B. D., Kalvius, G. M., Lam, D. J., and Brodsky, M. B. (1968) *J. Phys. Chem. Solids*, **29**, 1365.

Edelstein, N., Easley, W., and Mclaughlin, R. (1966) *J. Chem. Phys.*, **44**, 3130–1.

Edelstein, N. and Easley, W. (1968) *J. Chem. Phys.*, **48**, 2110.

Edelstein, N., Mollet, H. F., Easley, W. C., and Mehlhorn, R. J. (1969) *J. Chem. Phys.*, **51**, 3281–5.

Edelstein, N., Conway, J. G., Fujita, D., Kolbe, W., and Mclaughlin, R. (1970) *J. Chem. Phys.*, **52**, 6425–6.

Edelstein, N. (1971) *J. Chem. Phys.*, **54**, 2488–91.

Edelstein, N. and Karraker, D. G. (1975) *J. Chem. Phys.*, **62**, 938–40.

Edelstein, N., Streitwieser, A. J., Morrell, D. G., and Walker, R. (1976) *Inorg. Chem.*, **15**, 1397–8.

Edelstein, N. (1977) *Rev. Chim. Miner.*, **14**, 149.

Edelstein, N., Kolbe, W., and Bray, J. E. (1980) *Phys. Rev. B*, **21**, 338–42.

Eichberger, K. and Lux, F. (1980) *Ber. Bunsenges. Phys. Chem.*, **84**, 800–7.

Eisenstein, J. C. and Pryce, M. H. L. (1955) *Proc. R. Soc. A*, **A229**, 20–38.

Eisenstein, J. C. and Pryce, M. H. L. (1960) *Proc. R. Soc. Lond. A*, **A255**, 181–98.

Erdos, P., Solt, G., Zolnierek, Z., Blaise, A., and Fournier, J. M. (1980) *Physica*, **102B**, 164–70.

Evans, D. F. (1959) *J. Chem. Soc.*, 2003–5.

Faber, J., Lander, G. H., and Cooper, B. R. (1975) *Phys. Rev. Lett.*, **35**, 1770–3.

Faber, J. Jr and Lander, G. H. (1976) *Phys. Rev. B*, **14**, 1151–64.

Finazzi, M., Sainctavit, P., Dias, A. M., Kappler, J. P., Krill, G., Sanchez, J. P., Dalmas De Rotier, P., Yaouanc, A., Rogalev, A., and Goulon, J. (1997) *Phys. Rev. B*, **55**, 3010.

Flotow, H. E. and Tetenbaum, M. (1981) *J. Chem. Phys.*, **74**, 5269.

Folcher, G., Marquet- Ellis, H., Rigny, P., Soulie, E., and Goodman, G. (1976) *J. Inorg. Nucl. Chem.*, **38**, 747–53.

Fournier, J. M., Blaise, A., Muller, W., and Spirlet, J. C. (1977) *Physica B*, **86–88**, 30–1.

Fournier, J. M. (1985) Magnetic properties of actinide solids, in *Structure and Bonding 59/60: Actinides‐Chemistry and Physical Properties* (ed. L. Manes), Springer‐Verlag, Berlin, pp. 127–96.

Francis, R. J., Halasyamani, P. S., and O'Hare, D. (1998) *Chem. Mater.*, **10**, 3131–39.

Frazer, B. C., Shirane, G., Cox, D. E., and Olsen, C. E. (1965) *Phys. Rev A*, **140**, 1448–52.

Freeman, A. J. and Darby, J. B. J. (1974) *The Actinides: Electronic Structure and Related Properties,* vols. 1 and 2, Academic Press, New York.

Friedt, J. M., Litterst, F. J., and Rebizant, J. (1985) *Phys. Rev. B*, **32**, 257

Fuji, K., Miyake, C., and Imoto, S. (1979) *J. Nucl. Sci. Technol.*, **16**, 207–13.

Fujita, D. K. (1969) University of California Radiation Laboratory Report, UCRL-19507.

Fujita, D. K., Parsons, T. C., Edelstein, N., Noe, M., and Peterson, J. R. (1976) The magnetic susceptibility of ^{244}Cm metal and ^{249}Cf metal, in *Transplutonium Elements* (eds. W. Muller and R. Lindner), North‐Holland, Amsterdam, pp. 173–8.

Gajek, Z., Lahalle, M. P., Krupa, J. C., and Mulak, J. (1988) *J. Less Common Metals*, **139**, 351.

Gamp, E., Edelstein, N., Khan Malek, C., Hubert, S., and Genet, M. (1983) *J. Chem. Phys.*, **79**, 2023–6.

Gamp, E., Shinomoto, R., Edelstein, N., and McGarvey, B. R. (1987) *Inorg. Chem.*, **26**, 2177.

Giannozzi, P. and Erdos, P. (1987) *J. Magn. Magn. Mater.*, **67**, 75.

Gibbs, D., Hrashman, D. R., Isaacs, E. D., Mcwhan, D. B., Mills, D., and Vettier, C. (1988) *Phys. Rev. Lett.*, **61**, 1241.

Gourier, D., Caurant, D., Berthet, J. C., Boisson, C., and Ephritikhine, M. (1997) *Inorg. Chem.*, **36**, 5931–36.

Gourier, D., Caurant, D., Arliguie, T., and Ephritikhine, M. (1998) *J. Am. Chem. Soc.*, **120**, 6084–92.

Gruen, D. M. (1955) *J. Chem. Phys.*, **23**, 1708–10.

Handler, P. and Hutchison, C. A. Jr (1956) *J. Chem. Phys.*, **25**, 1210–13.

Hannon, J. P., Trammell, G. T., Blume, M., and Gibbs, D. (1988) *Phys. Rev. Lett.*, **62**, 2644.

Hauck, J. (1976) *Inorg. Nucl. Chem. Lett.*, **12**, 617–22.

Hayes, R. G. and Edelstein, N. (1972) *J. Am. Chem. Soc.*, **94**, 8688.

Heaton, L., Mueller, M. H., and Williams, J. M. (1967) *J. Phys. Chem. Solids*, **28**, 1651.

Hecht, H. G., Lewis, W. B., and Eastman, M. P. (1971) *Adv. Chem. Phys.*, **21**, 351.

Hendricks, M. E., Jones, E. R. Jr, Stone, J. A., and Karraker, D. G. (1971) *J. Chem. Phys.*, **55**, 2993–7.

Hendricks, M. E., Jones, E. R. Jr, Stone, J. A., and Karraker, D. G. (1974) *J. Chem. Phys.* **60**, 2095–103.

Hinatsu, Y., Miyake, C., and Imoto, S. (1981) *J. Nucl. Sci. Technol.*, **18**, 349–54.

Hinatsu, Y. and Edelstein, N. (1991) *J. Solid State Chem.*, **93**, 173.

Hinatsu, Y., Fujino, T., and Edelstein, N. (1992a) *J. Solid State Chem.*, **99**, 182–8.

Hinatsu, Y., Fujino, T., and Edelstein, N. (1992b) *J. Solid State Chem.*, **99**, 95–102.

Hinatsu, Y. (1994a) *J. Alloys Compd*, **203**, 251–7.

Hinatsu, Y. (1994b) *J. Solid State Chem.*, **109**, 1–6.

Holland-Moritz, E. and Lander, G. H. (1994) in *Handbook on the Physics and Chemistry of Rare Earths,* vol. 19 (eds. K. A. Gschneidner Jr, L. Eyring, G. H. Lander, and G. R. Choppin), North-Holland Physics, Amsterdam, pp. 1–121.

Howland, J. J. Jr and Calvin, M. (1950) *J. Chem. Phys.*, **18**, 239.

Hubert, S., Thouvenot, P., and Edelstein, N. (1993) *Phys. Rev. B*, **48**, 5751–60.

Huray, P. G., Nave, S. E., Peterson, J. R., and Haire, R. G. (1980) *Physica*, **102B+C**, 217–20.

Huray, P. G. and Nave, S. E. (1987) Magnetic studies of transplutonium actinides, in *Handbook on the Physics and Chemistry of the Actinides,* vol. 5 (eds. A. J. Freeman and G. H. Lander), North-Holland, Amsterdam, pp. 311–72.

Hutchison, C. A. Jr, Llewellyn, P. M., Wong, E., and Dorain, P. B. (1956) *Phys. Rev.*, **102**, 292.

Hutchison, C. A. Jr and Candela, G. A. (1957) *J. Chem. Phys.*, **27**, 707–10.

Hutchison, C. A. Jr and Weinstock, B. (1960) *J. Chem. Phys.*, **32**, 56–61.

Hutchison, C. A. Jr, Tsang, T., and Weinstock, B. (1962) *J. Chem. Phys.*, **37**, 555–62.

Ikushima, K., Tsutsui, S., Haga, Y., Ysauoka, H., Walstedt, R. E., Masaki, N. M., Nakamura, A., Nasu, S., and Onuki, Y. (2001) *Phys. Rev. B*, **63**, 104404.

James, R. W. (1958) *The Optical Principles of the Diffraction of X Rays*, G. Bell & Sons, London.

Johnston, D. A., Satten, R. A., Schreiber, C. L., and Wong, E. Y. (1966) *J. Chem. Phys.*, **44**, 3141.

Jones, E. R. Jr and Stone, J. A. (1972) *J. Chem. Phys.*, **56**, 1343.

Jones, E. R. Jr, Hendricks, M. E., Stone, J. A., and Karraker, D. G. (1974) *J. Chem. Phys.*, **60**, 2088–94.

Jones, W. M., Gordon, J., and Long, E. A. (1952) *J. Chem. Phys.*, **20**, 695.

Judd, B. R. (1963) *Operator Techniques in Atomic Spectroscopy,* McGraw-Hill, New York.

Kalina, D. G., Marks, T. J., and Wachter, W. A. (1977) *J. Am. Chem. Soc.*, **99**, 3877–9.

Kalvius, G. M., Ruby, S. L., Dunlap, B. D., Shenoy, G. K., Cohen, D., and Brodsky, M. B. (1969) *Phys. Lett. B*, **29**, 489.

Kalvius, G. M., Noakes, D. R., and Hartmann, O. (2001) (μ)SR studies of rare earth and actinide magnetic materials, in *Handbook on the Physics and Chemistry of Rare Earths,* vol. 32 (eds. K. A. Gschneidner Jr, L. Eyring, and G. H. Lander), North-Holland, Amsterdam.

Kanellakopulos, B., Dornberger, E., and Baumgartner, F. (1974) *Inorg. Nucl. Chem. Lett.*, **10**, 155–60.

Kanellakopulos, B., Blaise, A., Fournier, J. M., and Muller, W. (1975) *Solid State Commun.*, **17**, 713–15.

Kanellakopulos, B., Aderhold, C., Dornberger, E., Müller, W., and Baybarz, R. D. (1978) *Radiochim. Acta*, **25**, 85–92.

Kanellakopulos, B. (1979) Cyclopentadienyl compounds of the actinide elements, in *Organometallics of the f-Elements* (eds. T. J. Marks and R. D. Fischer), Reidel, Boston, pp. 1–35.

Kanellakopulos, B., Henrich, E., Keller, C., Baumgartner, F., Konig, E., and Desai, V. P. (1980a) *Chem. Phys.*, **53**, 197–213.

Kanellakopulos, B., Keller, C., Klenze, R., and Stollenwerk, A. H. (1980b) *Physica*, **102B**, 221–5.

Kanellakopulos, B., Klenze, R., and Stollenwerk, A. (1980c) Magnetic properties of the cubic octa-thiocyanato complexes, $(Et_4N)_4An(NCS)_8$, and of the tetra-chlorides, $AnCl_4$, of uranium and neptunium, in *Proc. 10eme Journees des Actinides* (eds. B. Johansson and A. Rosengren), pp. 217–31.

Karbowiak, M. and Drozdzynski, J. (1998a) *J. Alloys Compds*, **271–273**, 863–6.

Karbowiak, M. and Drozdzynski, J. (1998b) *J. Alloys Compds*, **275–277**, 848–51.

Karbowiak, M., Hanuza, J., Drozdzynski, J., and Hermanowicz, K. (1996) *J. Solid State Chem.*, **121**, 312–18.

Karbowiak, M., Drozdzynski, J., Hubert, S., Simoni, E., and Strek, W. (1998) *J. Chem. Phys.*, **108**, 10181–6.

Karraker, D. G., Stone, J. A., Jones, E. R. Jr, and Edelstein, N. (1970) *J. Am. Chem. Soc.*, **92**, 4841.

Karraker, D. G. (1971) *Inorg. Chem.*, **10**, 1564–6.

Karraker, D. G. (1973) *Inorg. Chem.*, **12**, 1105–8.

Karraker, D. G. (1975a) *J. Chem. Phys.*, **63**, 3174–5.

Karraker, D. G. (1975b) *J. Chem. Phys.*, **62**, 1444–6.

Karraker, D. G. and Dunlap, B. D. (1976) *J. Chem. Phys.*, **65**, 2032–3.

Karraker, D. G., and Stone, J. A. (1980) *Phys. Rev. B*, **22**, 111–14.

Keller, C. (1972) in *MTP International Review of Science, Inorganic Chemistry, ser. I, Lanthanides and Actinides,* vol. 7 (ed. K. W. Bagnall), Butterworths, London, pp. 47–85.

Kelly, P. J. and Brooks, M. S. S. (1987) *J. Chem. Soc., Faraday Trans. 2*, **83**, 1189–203.

Kern, S., Loong, C.-K., and Lander, G. H. (1985) *Phys. Rev. B*, **32**, 3051–7.

Kern, S., Morris, J., Loong, C. K., Goodman, G. L., Lander, G. H., and Cort, B. (1988) *J. Appl. Phys.*, **63**, 3598–600.

Kern, S., Loong, C.-K., Goodman, G. L., Cort, B., and Lander, G. H. (1990) *J. Phys. Condensed Matter*, **2**, 1933–40.

Kern, S., Robinson, R. A., Nakotte, H., Lander, G. H., Cort, B., Watson, P., and Vigil, F. A. (1999) *Phys. Rev. B*, **59**, 104–6.

Kolbe, W. and Edelstein, N. (1971) *Phys. Rev. B*, **4**, 2869–75.

Kolbe, W., Edelstein, N., Finch, C. B., and Abraham, M. M. (1972) *J. Chem. Phys.*, **56**, 5432–3.

Kolbe, W., Edelstein, N., Finch, C. B., and Abraham, M. M. (1973) *J. Chem. Phys.*, **58**, 820–1.

Kolbe, W., Edelstein, N., Finch, C. B., and Abraham, M. M. (1974) *J. Chem. Phys.*, **60**, 607–9.

Kolberg, D., Wastin, F., Rebizant, J., Boulet, P., Lander, G. H., and Schoenes, J. (2002) *Phys. Rev. B*, **66**, 214418.

Kopmann, W., Litterst, F. J., Klauss, H. H., Hillberg, M., Wagener, W., Kalvius, G. M., Schreier, E., Burghart, F. J., Rebizant, J., and Lander, G. H. (1998) *J. Alloys Compds*, **271**, 463–6.

Korobkov, I., Gambarotta, S., Yap, G. P. A., Thompson, L., and Hay, P. J. (2001) *Organometallics*, **20**, 5440–5.

Kostorz, G. E. (1979) Neutron scattering, in *Treatise on Materials Science and Technology*, vol. 15, Academic Press, New York.

Kot, W., Shalimoff, G., Edelstein, N., Edelman, M. A., and Lappert, M. F. (1988) *J. Am. Chem. Soc.*, **110**, 986.

Kot, W. K., Edelstein, N. M., Abraham, M. M., and Boatner, L. A. (1993a) *Phys. Rev. B*, **48**, 12704–12.

Kot, W. K., Edelstein, N. M., Abraham, M. M., and Boatner, L. A. (1993b) *Phys. Rev. B*, **47**, 3412–14.

Kot, W. K. and Edelstein, N. M. (1995) *New J. Chem.*, **19**, 641–54.

Lam, D. J. and Aldred, A. T. (1974) in *The Actinides: Electronic Structure and Related Properties*, vol. I, Academic Press, New York, pp. 109–79.

Lam, D. J. and Chan, S. K. (1974) *Phys. Rev. B*, **9**, 808–14.

Lämmermann, H. and Conway, J. G. (1963) *J. Chem. Phys.*, **38**, 259–69.

Lämmermann, H. and Stapleton, H. J. (1961) *J. Chem. Phys.*, **35**, 1514–16.

Lander, G. H., Brown, P. J., Spirlet, J. C., Rebizant, J., Kanellakopulos, B., and Klenze, R. (1985) *J. Chem. Phys.*, **83**, 5988–97.

Lander, G. H. and Aeppli, G. (1991) *J. Magn. Magn. Mater.*, **100**, 151–72.

Lander, G. H. (1993) in *Handbook on the Physics and Chemistry of Rare Earths,* vol. 17 (eds. K. A. Gschneidner Jr, L. Eyring, G. H. Lander, and G. R. Choppin), North-Holland Physics, Amsterdam, pp. 635–709.

Lander, G. H. (2002) *J. Magn. Magn. Mater.*, **242–245**, 3–8.

Langridge, S., Stirling, W. G., Lander, G. H., and Rebizant, J. (1994a) *Phys. Rev. B*, **49**, 12010–21.

Langridge, S., Stirling, W. G., Lander, G. H., and Rebizant, J. (1994b) *Phys. Rev. B*, **49**, 12022.

Langridge, S., Lander, G. H., Bernhoeft, N., Stunault, A., Vettier, C., Grübel, G., Sutter, C., Nuttall, W. J., Stirling, W. G., Mattenberger, K., and Vogt, O. (1997) *Phys. Rev. B*, **55**, 6392.

Lea, K., Leask, M., and Wolf, W. (1962) *J. Phys. Chem. Solids*, **23**, 1381–405.

Le Borgne, T., Riviere, E., Marrot, J., Thuery, P., Girerd, J. J., and Ephritikhine, M. (2002) *Chem. Eur. J.*, **8**, 774–83.

Leung, A. F. and Poon, Y. M. (1977) *Can. J. Phys.*, **55**, 937–42.

Lewis, W. B., Hecht, H. G., and Eastman, M. P. (1973) *Inorg. Chem.*, **12**, 1634–9.

Li, J. and Bursten, B. E. (1997) *J. Am. Chem. Soc.*, **119**, 9021–32.

Liu, G. K., Beitz, J. V., and Huang, J. (1993) *J. Chem. Phys.*, **99**, 3304–11.

Lovesey, S. W. and Collins, S. P. (1996) *X-ray Scattering and Absorption by Magnetic Materials,* Oxford Science Publications, New York.

Lukens, W. W. (1995) *Trivalent Metallocene Chemistry of Some Uranium, Titanium, and Zirconium Complexes*, Ph.D. Thesis, LBL-37646, University of California, Berkeley.

Lukens, W. W., Beshouri, S. M., Blosch, L. L., Stuart, A. L., and Andersen, R. A. (1999) *Organometallics*, **18**, 1235–46.

Mannix, D., Lander, G. H., Rebizant, J., Caciuffo, R., Bernhoeft, N., Lidstrom, E., and Vettier, C. (1999) *Phys. Rev. B*, **60**, 15187–93.

Marei, S. A. and Cunningham, B. B. (1972) *J. Inorg. Nucl. Chem.*, **34**, 1203–6.

McCart, B., Lander, G. H., and Aldred, A. T. (1981) *J. Chem. Phys.*, **74**, 5263–8.

McGarvey, B. R. (1998) *Inorg. Chim. Acta*, **272**, 43–54.

McGlynn, S. P. and Smith, J. K. (1962) *J. Mol. Spectrosc.*, **6**, 164.

McWhan, D. B., Vettier, C., Isaacs, E. D., Ice, G. E., Siddons, D. P., Hastings, J. B., Peters, C., and Vogt, O. (1990) *Phys. Rev. B*, **42**, 6007.

McWhan, D. B. (1998) *J. Alloys Compds*, **271–273**, 408.

Metoki, N., Haga, Y., Koike, Y., and Onuki, Y. (1998) *Phys. Rev. Lett.*, **80**, 5417.

Meyer, K., Mindiola, D. J., Baker, T. A., Davis, W. M., and Cummins, C. C. (2000) *Angew. Chem. Int. Ed. Engl.*, **39**, 3063–66.

Milman, V., Winkler, B., and Pickard, C. J. (2003) *J. Nucl. Mater.*, **322**, 165–79.

Miyake, C., Fuji, K., and Imoto, S. (1977a) *Chem. Phys. Lett.*, **46**, 349.

Miyake, C., Fuji, K., and Imoto, S. (1977b) *Inorg. Nucl. Chem. Lett.*, **13**, 53–5.

Miyake, C., Fuji, K., and Imoto, S. (1979) *Chem. Phys. Lett.*, **61**, 124–6.

Miyake, C., Takeuchi, H., Ohya-Nishiguchi, H., and Imoto, S. (1982) *Phys. Status Solidi (a)*, **74**, 173.

Miyake, C., Takeuchi, H., Fuji, K., and Imoto, S. (1984) *Phys. Status Solidi (a)*, **83**, 567.

Moore, J. R., Nave, S. E., Haire, R. G., and Huray, P. G. (1986) *J. Less Common Metals*, **121**, 187–92.

Moore, J. R., Nave, S. E., Hart, R. C., Wilmarth, W. R., Haire, R. G., and Peterson, J. R. (1988) *Phys. Rev. B Condensed Matter*, **38**, 2695–702.

Morss, L. R., Fuger, J., Goffart, J., and Haire, R. G. (1983) *Inorg. Chem.*, **22**, 1993–6.

Morss, L. R., Fuger, J., Goffart, J., Edelstein, N., and Shalimoff, G. (1987) *J. Less Common Metals*, **127**, 251.

Morss, L. R., Richardson, J. W. Jr, Williams, C. W., Lander, G. H., Lawson, A. C., Edelstein, N., and Shalimoff, G. (1989) *J. Less Common Metals*, **156**, 273–89.

Mortl, K. P., Sutter, J. P., Golhen, S., Ouahab, L., and Kahn, O. (2000) *Inorg. Chem.*, **39**, 1626–7.

Müller-Westerhoff, U. and Streitwieser, A. J. (1968) *J. Am. Chem. Soc.*, **90**, 7364–5.

Mulak, J. (1978) *J. Solid State Chem.*, **25**, 355–66.

Murasik, A. and Furrer, A. (1980) *Physica*, **102B+C**, 185–7.

Murasik, A., Fischer, P., and Szczepaniak, W. (1981) *J. Phys. C*, **14**, 1847–54.

Murasik, A., Fischer, P., Furrer, A., and Szczepaniak, W. (1985) *J. Phys. C: Solid State Phys.*, **18**, 2909–21.

Murasik, A., Fischer, P., Furrer, A., Schmid, B., and Szczepaniak, W. (1986) *J. Less Common Metals*, **121**, 151–5.

Murdoch, K. M., Edelstein, N. M., Boatner, L. A., and Abraham, M. M. (1996) *J. Chem. Phys.*, **105**, 2539–46.

Myers, R. J. (1973) *Molecular Magnetism and Magnetic Resonance Spectroscopy,* Prentice-Hall, New York.

Nakamoto, T., Nakada, M., Nakamura, A., Haga, Y., and Onuki, Y. (1999) *Solid State Commun.*, **109**, 77–81.

Nakamoto, T., Nakada, M., and Nakamura, A (2001) *Solid State Commun.*, **119**, 523–6.

Nave, S. E., Huray, P. G., and Haire, R. G. (1980) The magnetic susceptibility of sup 249/Bk metal. *Proc. Int. Conf. Crystalline Electric Field and Structural Effects in f-Electron Systems,* Plenum, 1980, pp. 269–74, New York.

Nave, S. E., Haire, R. G., and Huray, P. G. (1981) in *Actinides-1981, Abstracts,* Lawrence Berkeley Laboratory Report LBL-12441, pp. 144–6.

Nave, S. E., Haire, R. G., and Huray, P. G. (1983) *Phys. Rev. B*, **28**, 2317–27.

Nave, S. E., Moore, J. R., Spaar, M. T., Haire, R. G., and Huray, P. G. (1985) *Physica*, **130B+C**, 225–7.

Nave, S. E., Moore, J. R., Peterson, J. R., and Haire, R. G. (1987) *J. Less Common Metals*, **127**, 79–85.

Nellis, W. J. and Brodsky, M. B. (1974) *in The Actinides: Electronic Structure and Related Properties,* vol. II (eds. A. J. Freeman and J. B. J. Darby), Academic Press, New York, pp. 265–88.

Newman, D. J. (1971) *Adv. Phys.*, **20**, 197–256.

Normile, P. S., Stirling, W. G., Mannix, D., Lander, G. H., Wastin, F. J., Rebizant, J., Boudarot, F., Burlet, P., Lebech, B., and Coburn, S. (2002) *Phys. Rev. B*, **66**, 014405.

Osborn, R., Taylor, A. D., Bowden, Z. A., Hackett, M. A., Hayes, W., Hutchings, M. T., Amoretti, G., Caciuffo, R., Blaise, A., and Fournier, J. M. (1988) *J. Phys. C*, **21**, L931–7.

Osborne, D. W. and Westrum, E. F. (1953) *J. Chem. Phys.*, **21**, 1884.

Paixão, J. A., Detlefs, C., Longfield, M. J., Caciuffo, R., Santini, P., Bernhoeft, N., Rebizant, J., and Lander, G. H. (2002) *Phys. Rev. Lett.*, **89**, 187202–1–4.

Parry, J. S., Cloke, F. G. N., Coles, S. J., and Hursthouse, M. B. (1999) *J. Am. Chem. Soc.*, **121**, 6867–71.

Piehler, D., Kot, W. K., and Edelstein, N. (1991) *J. Chem. Phys.*, **94**, 942–8.

Pirie, J. D. and Smith, T. (1970) *Phys. Status Solidi*, **41**, 221.

Poirot, I., Kot, W., Shalimoff, G., Edelstein, N., Abraham, M. M., Finch, C. B., and Boatner, L. A. (1988) *Phys. Rev. B*, **37**, 3255–64.

Rahman, H. U. and Runciman, W. A. (1966) *J. Phys. Chem. Solids*, **27**, 1833–5.

Rahman, H. U. (1998) *Physica B*, **252**, 160.

Raison, P., Delapalme, A., Kiat, J. M., Schweiss, P., Kanellakopulos, B., Rebizant, J., Apostolides, C., Gonthier-Vassal, A., Lander, G. H., and Brown, P. J. (1994a) *Z. Kristallogr.*, **209**, 720.

Raison, P., Lander, G. H., Delapalme, A., Williams, J. H., Kahn, R., Carlile, C. J., and Kanellakopulis, B. (1994b) *Mol. Phys.*, **81**, 369.

Rajnak, K., Banks, R. H., Gamp, E., and Edelstein, N. (1984a) *J. Chem. Phys.*, **80**, 5951–62.

Rajnak, K., Gamp, E., Shinomoto, R., and Edelstein, N. (1984b) *J. Chem. Phys.*, **80**, 5942–50.

Raphael, G. and Lallement, R. (1968) *Solid State Commun.*, **6**, 383–5.

Reisfeld, M. J. and Crosby, G. A. (1965) *Inorg. Chem.*, **4**, 65.

Reynolds, J. G. and Edelstein, N. (1977) *Inorg. Chem.*, **16**, 2822–25.

Reynolds, J. G., Zalkin, A., Templeton, D. H., and Edelstein, N. (1977) *Inorg. Chem.*, **6**, 599–603.

Richardson, R. P. and Gruber, J. B. (1972) *J. Chem. Phys.*, **56**, 256–60.

Rigny, P. and Plurien, P. (1967) *J. Phys. Chem. Solids*, **28**, 2589.

Rigny, P., Dianoux, A. J., and Plurien, P. (1971a) *J. Phys. Chem. Solids*, **32**, 1175.

Rigny, P., Dianoux, A. J., and Plurien, P. (1971b) *J. Phys. Chem. Solids*, **32**, 1901–8.

Rosen, R. K., Andersen, R. A., and Edelstein, N. (1990) *J. Am. Chem. Soc.*, **112**, 4588–90.

Ross, J. W. and Lam, D. J. (1967) *J. Appl. Phys.*, **38**, 1451–3.

Rossat-Mignod, J., Lander, G. H., and Burlet, P. (1984) in *Handbook of the Physics and Chemistry of the Actinides* (eds. A. J. Freeman and G. H. Lander), North-Holland, Amsterdam, pp. 415–515.

Salmon, L., Thuery, P., Riviere, E., Girerd, J. J., and Ephritikhine, M. (2003) *Chem. Commun*, **21**, 762–3.

Santini, P., Lémanski, R., and Erdös, P. (1999) *Adv. Phys.*, **48**, 537–653.

Santini, P. and Amoretti, G. (2000) *Phys. Rev. Lett.*, **85**, 2188–91.

Santini, P. and Amoretti, G. (2002) *J. Phys. Soc. Jpn.*, **71**, 11.

Sarrao, J. L., Morales, L. A., Thompson, J. D., Scott, B. L., Stewart, G. R., Wastin, F., Rebizant, J., Boulet, P., Colineau, E., and Lander, G. H. (2002) *Nature*, **420**, 297–9.

Sasaki, K. and Obata, T. (1970) *J. Phys. Soc. Jpn.*, **28**, 1157.

Saxena, S. S., Agarwal, P., Ahilan, K., Grosche, F. M., Haselwimmer, R. K. W., Steiner, M. J., Pugh, E., Walker, I. R., Julian, S. R., Monthoux, P., Lonzarich, G. G., Huxley, A., Sheikin, I., Braithwaite, D., and Floquet, J. (2000) *Nature*, **406**, 587.

Schenk, H. J., Bohres, E. W., and Schwochau, K. (1975) *Inorg. Nucl. Chem. Lett.*, **11**, 201–6.

Schmid, B., Murasik, A., Fischer, P., Furrer, A., and Kanellakopulos, B. (1990) *J. Phys. Condensed Matter*, **2**, 3369–80.

Schoenes, J. (1980) *Phys. Rep.*, **63**, 301–36.

Schüssler-Langeheine, C., Weschke, E., Grigoriev, A. Y., Ott, H., Meier, R., Vyalikh, D. V., Mazumdar, C., Sutter, C., Abernathy, D., Grübel, G., and Kaindl, G. (2001) *J. Electron Spectrom. Related Phenom.*, **114–116**, 953.

Schütz, G., Wagner, W., Wilhelm, W., Zeller, R., Frahm, R., and Materlik, G. (1987) *Phys. Rev. Lett.*, **58**, 737.

Selbin, J., Ballhausen, C. J., and Durrett, D. G. (1972) *Inorg. Chem.*, **11**, 510.

Selbin, J. and Sherrill, H. J. (1974) *Inorg. Chem.*, **13**, 1235.

Seyferth, D. (2004) *Organometallics*, **23**, 3562–83.

Shinomoto, R., Gamp, E., Edelstein, N., Templeton, D. H., and Zalkin, A. (1983) *Inorg. Chem.*, **22**, 2351.

Shull, C. G. and Wilkinson, M. K. (1955) Oak Ridge National Laboratory, ORNL-1879, pp. 24–7.

Sidall, T. H., III. (1976) in *Theory and Applications of Molecular Paramagnetism* (eds. E. A. Boudreaux and L. N. Mulay), Wiley-Interscience, New York, pp. 317–48.

Siemann, R. and Cooper, B. R. (1979) *Phys. Rev. B*, **20**, 2869–85.

Skanthakumar, S., Williams, C. W., and Soderholm, L. (2001) *Phys. Rev. B Condensed Matter*, **64**, 144521/1–8.

Skold, K. and Price, D. L. (1987) *Neutron Scattering, Parts A, B, and C,* Academic Press, New York.

Soderholm, L., Edelstein, N., Morss, L. R., and Shalimoff, G. V. (1986) *J. Magn. Magn. Mater.*, **54–57**, 597–8.

Soderholm, L., Goodman, G. L., Welp, U., Williams, C. W., and Bolender, J. (1989) *Physica C*, **161**, 252–6.

Soderholm, L. (1992) *J. Alloys Compds*, **181**, 13–22.

Soderholm, L., Williams, C., Skanthakumar, S., Antonio, M. R., and Conradson, S. (1996) *Z. Phys. B*, **101**, 539–45.

Soderholm, L., Skanthakumar, S., and Williams, C. W. (1999) *Phys. Rev. B Condensed Matter*, **60**, 4302–8.

Solt, G. and Erdos, P. (1980) *J. Magn. Magn. Mater.*, **15–18**, 57.

Soulie, E. and Goodman, G. (1976) *Theor. Chim. Acta*, **41**, 17–36.

Soulie, E. and Goodman, G. (1979) *Erratum: Theor. Chim. Acta*, **51**, 259–60.

Soulie, E. and Edelstein, N. (1980) *Physica*, **102B**, 93–9.

Spirlet, M. R., Rebizant, J., Apostolidis, C., Dornberger, E., Kanellakopulos, B., and Powietzka, B. (1996) *Polyhedron*, **15**, 1503–8.

Squires, G. L. (1978) *Thermal Neutron Scattering,* Cambridge University Press, New York.

Stewart, J. L. (1988) *Tris[bis(trimethylsilyl)amido]uranium: Compounds with Tri-, Tetra-, and Pentavalent Uranium.* Ph.D. Thesis, LBL-25240, University of California, Berkeley.

Stewart, J. L. and Andersen, R. A. (1998) *Polyhedron*, **17**, 953–8.

Stollenwerk, A. H., Klenze, R., and Kanellakopulos, B. (1979) *J. Phys. (Paris), Colloq.*, **40** (C4), 179–80.

Stollenwerk, A. H. (1980) Institut für Heisse Chemie, Kernforschungszentrum Karls-ruhe, pp. 1–202.

Stone, J. A. and Jones, E. R. Jr (1971) *J. Chem. Phys.*, **54**, 1713–18.

Templeton, D. H. and Templeton, L. K. (1985) *Acta Crystallogr.*, **A41**, 133–42.

Thole, B. T., Van Der Laan, G., and Sawatzky, G. (1985) *Phys. Rev. Lett.*, **55**, 2086.

Thouvenot, P., Hubert, S., and Edelstein, N. (1994) *Phys. Rev. B*, **50**, 9715–20.

Troc, R., Suski, W., Franse, J. J. M., and Gersdorf, R. (1991) Actinide elements and their compounds with other elements, part 1, in *Landolt-Börnstein Group III: Condensed Matter Volume 19 Magnetic Properties of Metals Subvolume F1* (ed. H. P. J. Wijn), Springer-Verlag, Berlin.

Troc, R. and Suski, W. (1993) Actinide elements and their compounds with other elements, part 2, in *Landolt-Börnstein Group III: Condensed Matter Volume 19 Magnetic Properties of Metals Subvolume F2* (ed. H. P. J. Wijn), Springer-Verlag, Berlin.

Van Vleck, J. H. (1932) *The Theory of Electric and Magnetic Susceptibilities,* Oxford University Press, Oxford.

Warren, K. D. (1977) *Struct. Bonding*, **33**, 97–138.

Warren, K. D. (1983) *Chem. Phys. Lett.*, **99**, 427–31.

Watson, G. M., Gibbs, D., Lander, G. H., Gaulin, B. D., Berman, L. E., Matzke, H., and Ellis, W. (1996) *Phys. Rev. Lett.*, **77**, 751.

Watson, G. M., Gibbs, D., Lander, G. H., Gaulin, B. D., Berman, L. E., Matzke, H., and Ellis, W. (2000) *Phys. Rev. B*, **61**, 8966.

Wilkinson, M. K., Shull, C. G., and Rundle, R. E. (1955) *Phys. Rev.*, **99**, 627.

Willis, B. T. M. and Taylor, R. I. (1965) *Phys. Lett.*, **17**, 188.

Wulff, M. and Lander, G. H. (1988) *J. Chem. Phys.*, **89**, 3295.

Wybourne, B. G. (1965) *Spectroscopic Properties of Rare Earths,* Interscience Publishers, New York.

Zimmermann, M. V., Nelson, C. S., Hill, J. P., Gibbs, D., Blume, M., Casa, D., Keimer, B., Murakami, Y., Kao, C. C., Venkataraman, C., Gog, T., Tomioka, Y., and Tokura, Y. (2001) *Phys. Rev. B*, **64**, 195133.

Zolnierek, A., Solt, G., and Erdos, P. (1981) *J. Phys. Chem. Solids*, **42**, 773–6.

Zolnierek, Z., Gajek, Z., and Khan Malek, C. (1984) *Physica*, **125B**, 199–214.